Loughborough University

Pilkington Library

Author/Filing Title ..... APTE .....

.....

Vol. No. ..... Class Mark ..... T .....

Please note that fines are charged on ALL overdue items.

FOR REFERENCE ONLY

0402799690

LASER BEAM CHARACTERISATION FOR INDUSTRIAL APPLICATIONS

By

Paul Apte

Doctoral Thesis

Submitted in partial fulfilment of the requirements
for the award of

Doctor of Philosophy of Loughborough University

June 2003

© by Paul Apte (2003)

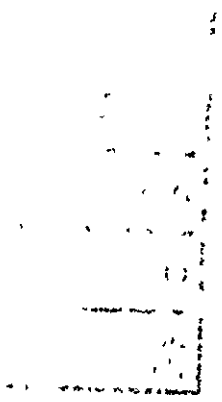

Loughborough University
Pilkington Library
Date Dec 03
Class
Acc No. 040279969

ABSTRACT

This thesis describes the theory, development and applications of laser beam characterisation for industrial laser materials processing systems. Descriptions are given of novel forms of beam diagnostic systems and their integration into highly automated industrial tools. Work is also presented that has contributed to the new ISO standard on beam characterisation. Particular emphasis is given to excimer laser applications and UV micromachining.

There are many laser applications that involve using both the near and far field intensity distributions of the beam. The irradiance distribution of a laser beam can be characterised by the spatial distribution of the irradiant power density (peak or time averaged power/area) with lateral displacement in a particular plane normal to the direction of propagation. Characterising the size and shape of these distributions is becoming increasingly important for a growing number of industrial and scientific laser applications. The development and application of laser beam diagnostic systems for industrial systems and real world measurement problems is described.

International standards are currently being derived that address the measurement and testing of beam divergence, size, irradiance and phase distribution. Descriptions are given of experiments performed to support these emerging standards, together with new approaches to noise reduction and profile measurement. A commercial beam diagnostic system developed by the author is described along with a number of key applications for excimer laser beam profiling. In particular the first use of in chuck beam profiling for characterising excimer lasers and the design of systems for measuring high aspect ratio line beam profiles is reported.

Laser based micromachining using excimer lasers has been well established in many industrial processes, covering a broad range of applications from drilling ink jet printer nozzles to annealing amorphous silicon flat panel displays. Descriptions are given of several new machining systems and applications.

Keywords: Laser, Excimer, Beam characterisation, Micromachining, Beam propagation

TABLE OF CONTENTS

ABSTRACT 2

CONTENTS 4

1. GENERAL INTRODUCTION 10

1.1 Background 10
1.2 Laser materials processing 11
1.3 The importance of beam profile 12
1.4 The development of beam diagnostics 12
1.5 Laser beam characterisation 16
1.6 laser beam propagation 17
1.7 Industrial systems 18
1.8 Contents of Thesis 19
1.9 References 21

2. LASERS AND BEAM PROPAGATION 24

2.1 Introduction 24
2.2 Laser development 24
2.3 Laser resonators and modes 25
2.4 Mode stability 27
2.5 Gaussian beam propagation 27
2.6 Beam quality and M^2 28
2.7 Near field intensity distributions 32
2.8 Beam quality and laser processing 33
2.9 Summary 34
2.10 References 34

3. CHARACTERISING LASER BEAM INTENSITY DISTRIBUTIONS 37

3.1 Introduction 37
3.2 Formal definitions 38
3.2.1 Local irradiance 38
3.2.2 Definition of moments 39
3.2.3 Spatial moments 39
3.2.4 Derivation of beam widths 40
3.2.5 Enclosed power radii 41
3.2.6 Beam uniformity 42
3.2.7 Threshold power density 42
3.3 Numerical implementations 43
3.3.1 Calculation of moments 43
3.3.2 Calculation of enclosed power 44
3.3.3 Beam uniformity 44
3.4 Practical measurement problems 45
3.4.1 Base line correction 45
3.4.2 Sampling window truncation 46
3.4.3 Energy fraction truncation 47
3.5 Experimental setup 47
3.6 Discussion 48
3.7 Polynomial shape fitting 51
3.7.1 Polynomial fits 51
3.8 Experimental results of fitting techniques 52
3.8.1 Linear fits 52
3.8.2 Higher order fits 54
3.8.3 Gaussian fits 57
3.9 Discussion of fitting techniques 57
3.10 Conclusions 58
3.11 References 58

4. TESTING OF THE DRAFT ISO STANDARDS FOR BEAM PROPAGATION AND INTENSITY PROFILE MEASUREMENT **60**

4.1 Introduction **60**

4.2 Testing the draft ISO standard for beam propagation **60**

4.2.1 Calculating beam widths using moments 61

4.2.2 Truncated and reduced moments 62

4.2.3 Histogram analysis for baseline offset 62

4.2.4 Calculation of a moment histogram 63

4.2.5 Experimental arrangement 64

4.2.6 Beam analysis software 65

4.2.7 Calculation of moment tables 65

4.2.8 Computation of beam waist loci and M^2. 66

4.2.9 Results and analysis 67

4.2.10 Beam waist and location 67

4.2.11 M^2 calculations 67

4.2.12 Beam diameter 68

4.2.13 Discussion 71

4.3 Testing the draft ISO standard for power and energy density distribution **72**

4.3.1 Experimental setup 72

4.3.2 Simulation 73

4.3.3 Test sources 74

4.3.4 Analysis algorithms 75

4.3.5 Background correction 75

4.3.6 Optimisation and checking 76

4.3.7 Choice of integration limits 77

4.3.8 Beam shape measurements 81

4.3.9 Calibration 82

4.3.10 Discussion 83

4.4 General conclusions **90**

4.5 References **91**

5. THE CHARACTERISATION OF EXCIMER LASER BEAMS 93

5.1 Introduction 93

5.2 Beam sampling techniques for excimer lasers 93

5.2.1 Fluorescent converters 94

5.2.2 Material tests 94

5.2.3 Pellicle beam splitters 97

5.2.4 Performance of pellicle splitters 98

5.2.5 Through mirror beam sampling 99

5.2.6 Performance of through mirror sampling 100

5.2.7 Comments 101

5.3 Data acquisition and system integration 102

5.3.1 Introduction 102

5.3.2 Workstation integration 102

5.4 The characterisation of excimer laser line beam profiles 103

5.4.1 Background 104

5.4.2 Applications 104

5.4.3 Experimental setup 105

5.4.4 Energy monitoring 106

5.4.5 Synchronisation and image processing 107

5.4.6 Workpiece embedded beam diagnostics 108

5.4.7 Data processing and visualisation 109

5.4.8 Beam analysis algorithms 111

5.4.8.1 Threshold Uniformity 111

5.4.8.2 Plateau uniformity and edge steepness 112

5.4.9 Experimental results 113

5.4.10 Pulse to pulse variations 114

5.4.11 Results from an α Silicon annealing tool 114

5.4.12 Discussion 117

5.5 Industrial beam diagnostics 117

5.6 Conclusions 121

5.7 References 122

6. EXCIMER LASER SYSTEMS & APPLICATIONS **123**

6.1 Introduction **123**
6.2 Excimer laser Micromachining **123**
6.2.1 Applications 125
6.2.2 Micro via fabrication 127
6.2.3 Inkjet printer nozzle drilling 128
6.2.4 Biomedical devices 129
6.3 The M8000 Micromachining system **131**
6.3.1 System Architecture 131
6.3.2 MEMS fabrication 132
6.3.3 Overlay mask scanning 134
6.4 The GWS200 FBG writing system **136**
6.4.1 Introduction 136
6.4.2 System description 137
6.4.3 Control software 138
6.4.4 Integrated beam profiler 141
6.4.5 Exposure Dose controller 142
6.4 6 Calibration 144
6.4.7 Fibre load and tensioning 146
6.4.8 Process screen 147
6.4.9 Summary 148
6.6 Conclusions **149**
6.7 References **149**

7. INDUSTRIAL MICROMACHINING SYSTEMS **152**

7.1 Introduction **152**
7.2 The M5000 FPD processing system **152**
7.2.1 System Architecture 153
7.2.2 Beam diagnostics and control 156
7.2.3 Applications 157
7.2.4 Ablating Polyimide for LCD production 161

7.2.5 Industrial trials 163
7.2.6 Applications in the electronics industry 166
7.2.7 Discussion 167
7.3 The M9000 Micro fabrication tool 168
7.3.1 Micro via and Interconnect patterning 169
7.3.2 Sync Scan 171

7.4 The M9000S solar cell scribing tool 173
7.4.1 Description 173
7.4.2 Scribing Silicon 174
7.4.3 Control System 175
7.4.4 Optical system 175
7.4.5 System diagnostics 180
7.4.6 Dust extract and assist gas 182
7.4.7 Translation stages 182
7.4.8 Auto Loader systems 183
7.4.9 Process Optimisation 184
7.4.10 Summary 184
7.5 Conclusions 184
7.6 References 185

8.GENERAL CONCLUSIONS 186

8.1 Future outlook 188
8.2 A history of beam diagnostics development 189

ACKNOWLEDGEMENTS 191

PUBLICATIONS AND CONFERENCE PRESENTATIONS 192

CHAPTER 1

GENERAL INTRODUCTION

1.1Background

On entering this field some 15 years ago little was known about the spatial profile and propagation characteristics of laser sources outside of the research lab. Today advanced beam characterization equipment is becoming a standard addition to many industrial laser machines and now laser beam profilers are as commonplace as laser power meters in a service engineer's toolkit. The driving force behind this transformation has been the need to accurately quantify how laser energy is coupled to the work piece and its subsequent material interaction; these processes can be very sensitive to spatial beam profile. As laser materials processing have been driven into mainstream applications ranging from robotic seam welding for the automotive industry to corneal sculpting, it has an increasing influence on our daily lives in a world dependent upon high technology. Perhaps few people realize that the latest generation of microprocessors that power their PC's can only be fabricated using laser based Deep UV lithography, that the photographic print quality of low cost inkjet printers would not be possible without UV laser micro machined printer heads, or that several hundred thousand people in the world have greatly improved eyesight thanks to UV laser corneal sculpting. The success of all these applications on an economic industrial scale relies crucially on the ability to measure and control the spatial profile of the laser beam.

The laser was invented some 40 years ago [1] and has been used as a serious industrial tool for only about the past 30 years, finding its first industrial use in the automobile industry in 1969 [2]. During this time great advances have been made both in the design of lasers and their range of applications. Like many new technologies the first industrial systems were quite simple, and once set up the laser system would require adjustment only at service intervals by specialist staff. However in modern industrial laser systems the laser is treated just as another manufacturing tool. Hence the requirements placed upon modern laser systems in terms of operating reliability,

stability and quality are greater than ever before. To this end there is a need for sophisticated beam characterisation techniques, process control and monitoring for both for the set up, maintenance and on line operation of industrial laser systems.

1.2 Laser Materials Processing

Resistor trimming was one of the first large scale applications for solid state Nd:Yag lasers [3]. It was a major leap forward for the electronics industry, leading to the low cost fabrication of Analogue to Digital and Digital to Analogue converters that form a key component of digital electronic systems. Laser marking using Nd:Yag and CO_2 lasers has an enormous range of applications, and is now widespread from marking aircraft cables, Silicon wafers, surgical implements, and keyboards [4].

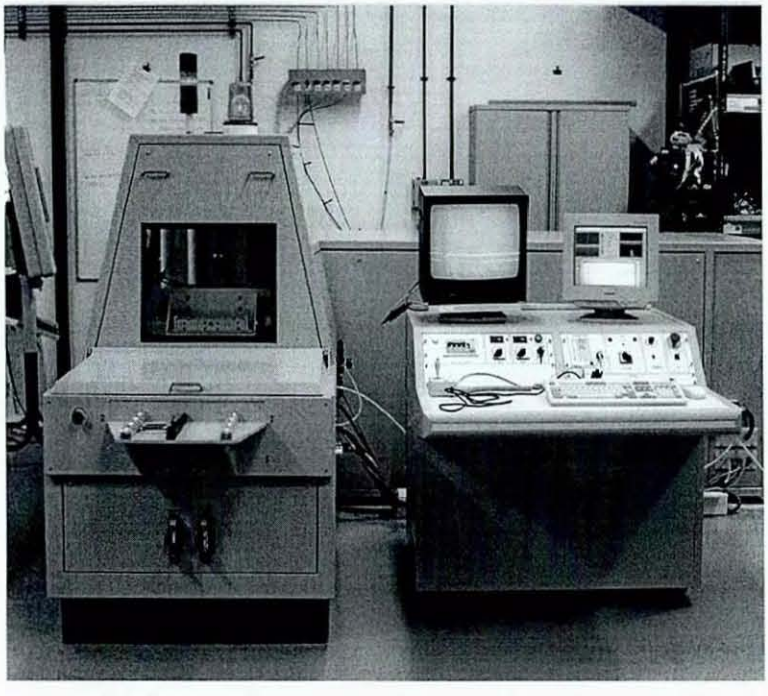

Fig 1.1 Excimer laser Tool for processing Multi Chip modules used in super computers.

Laser soldering involves using fast galvanometer beam deflection with two separate heads working independently to increase speed [5]. Of course CO_2 laser cutting is widely used in the sheet metal industry, and a wide range of materials can be cut, e.g. a 3kW TEM_{00} CO_2 laser can cut in excess of 28mm of steel [6]. Furthermore laser spot welding is used extensively in applications as diverse as car body fabrication to making razors [7].

Excimer lasers were invented in 1975 [8] and their application in laser ablation soon followed [9]. They now have diverse applications such as Silicon annealing for TFT display fabrication, the drilling of ink jet printer nozzles, DUV lithography, biomedical devices and via hole drilling [10]. Figure 1.1 shows an excimer laser tool designed to process multi chip modules for super computers, and figure 1.2 shows an example of excimer laser ablation.

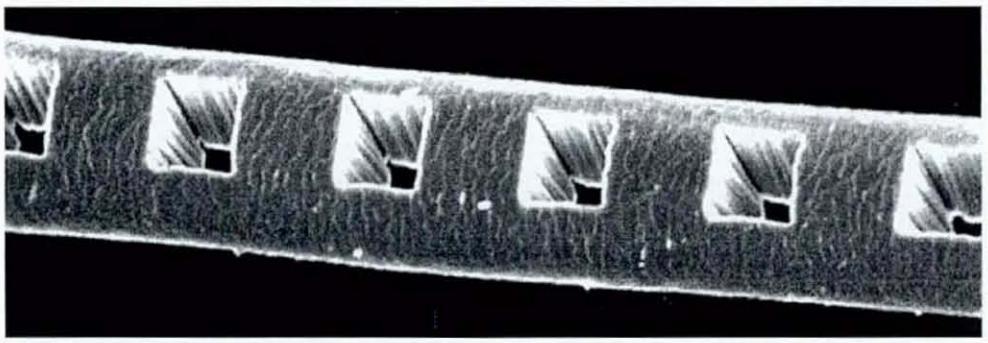

Fig 1.2. Human hair (supplied by the author), micromachined by excimer laser with 40 um square apertures

1.3 The importance of beam profile

The beam intensity distribution (spatial beam profile) is a major variable for many processes. This is in part due to the non-linear properties of laser materials interaction, beam uniformity being critical to ablation and annealing process and beam shape to cutting and drilling applications [11] . Allied to beam profile is the determination of propagation constants that allow the prediction of the beam intensity profile along the path of the beam. This can also have a critical effect on the shape of the beam waist and hence depth of focus which in turn affects keyhole formation and cut quality [12].

1.4 The development of beam diagnostics

Early attempts at measuring high power laser beam profiles involved taking surface and volumetric burn imprints in various materials including paper and brick [13]. Further enhancements led to the use of acrylic blocks for assessing CO_2 laser beam profiles, though care had to be exercised because of the production of toxic fumes.

An example of a profile recorded in acrylic is shown in figure 1.3. Incandescent mode plates made from graphite and other special materials and coatings have also been used to visualise beam profiles.

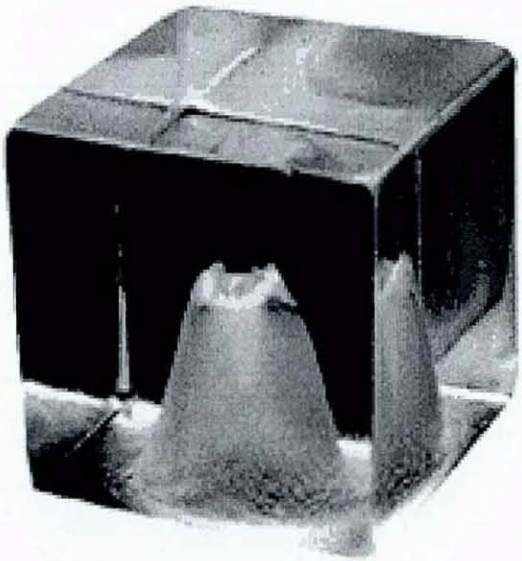

Fig 1.3. An acrylic burn. A technique still used for evaluating high power CO_2 laser beam profiles

With the development of suitable photo diodes and pyroelectric detectors, electronic methods were developed in conjunction with mechanical scanners such as Nipkow disks [14] and spinning needles [15]. These devices use a single point detector and typically produce a readout on an oscilloscope, with little in the way of data analysis or visualisation. An example is shown in figure 1.4.

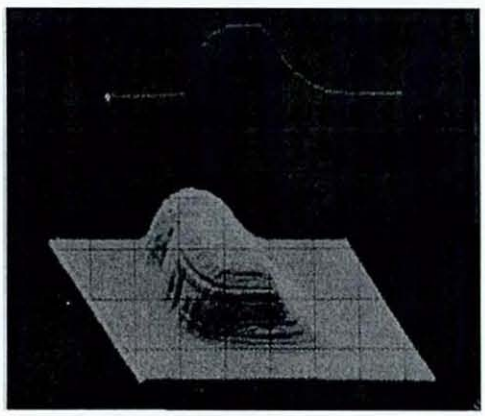

Fig 1.4. 3D plot of laser beam profile on an Oscilloscope, from an Exitech P256D system. The world's first commercially available UV laser beam profiler.

The availability of Silicon photodiode arrays and CCD cameras in the early 1980's revolutionized real time spatial beam profiling for visible and UV beams. A full two-dimensional intensity map of the beam profile could be acquired within 20 ms using such devices [16]. Coupled to newly developed video digitising electronics and frame

grabbers, computer analysis of beam profiles was now possible. The arrival of relatively low cost personal computers and software development platforms enabled the development of the first commercial instruments. Figures 1.5 a & b, show examples of instruments developed by the author. Figure 1.6 shows a beam sampling unit for excimer lasers.

Fig 1.5a

The Exitech P256 NG, PC based Laser beam profiling system.

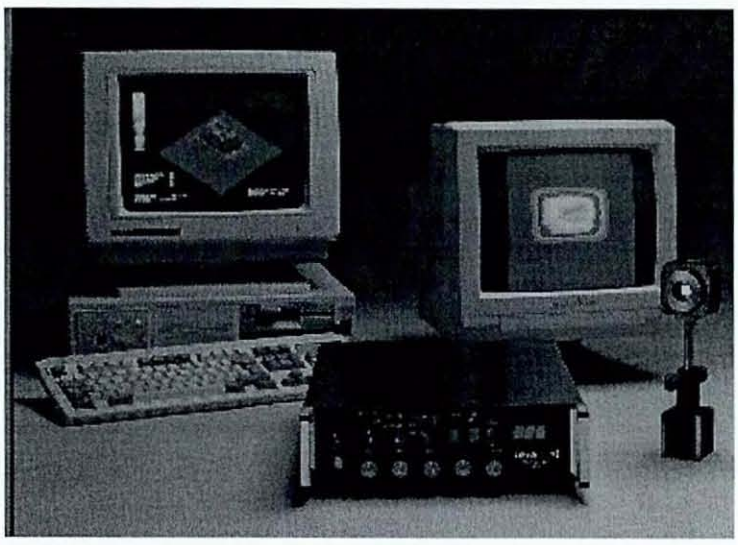

Fig 1.5b

The Exitech P256D. The first commercially available UV Laser beam profiling system.

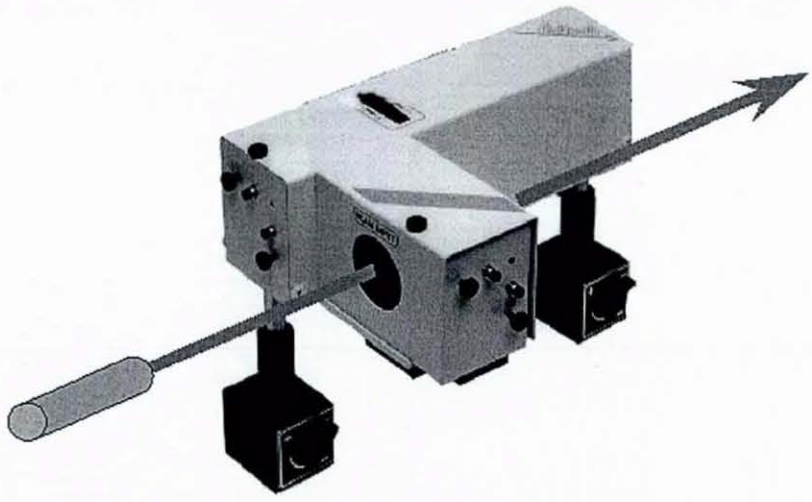

Fig 1.6. Exitech beam sampling interface unit for excimer lasers

These instruments would typically provide effective beam visualization (2D false colour maps, Isometric 3D intensity plots), as shown in figure 1.7.

Fig 1.7

3D Intensity plot of a Gaussian laser beam profile, taken with P256 software developed by the author.

These devices were further enhanced by the development of 2D pyroelectric arrays [17], which allowed for the first time, real time profiling of CO_2 lasers at 10.6 um.

The latest systems now use high dynamic range CCD detectors with extended spectral responses. The improvement in availability of low cost IR sensitive arrays such as bolometer devices now enable the integration of beam diagnostics into CO_2 laser tools.

1.5 Laser beam characterisation

This subject has grown in prominence over the past few years and is now a well developed field with yearly conferences to discuss new developments. The subject draws a mix of both academia and industry. There are at least 7 optical parameters that describe a beam [18]. The key parameters of interest in materials processing relate to the intensity distribution and pointing stability. Of these typically the beam uniformity (of a top hat profile) will be of greatest importance for excimer laser applications, where as for a Nd:Yag laser used for drilling, the beam shape will be of greater importance.

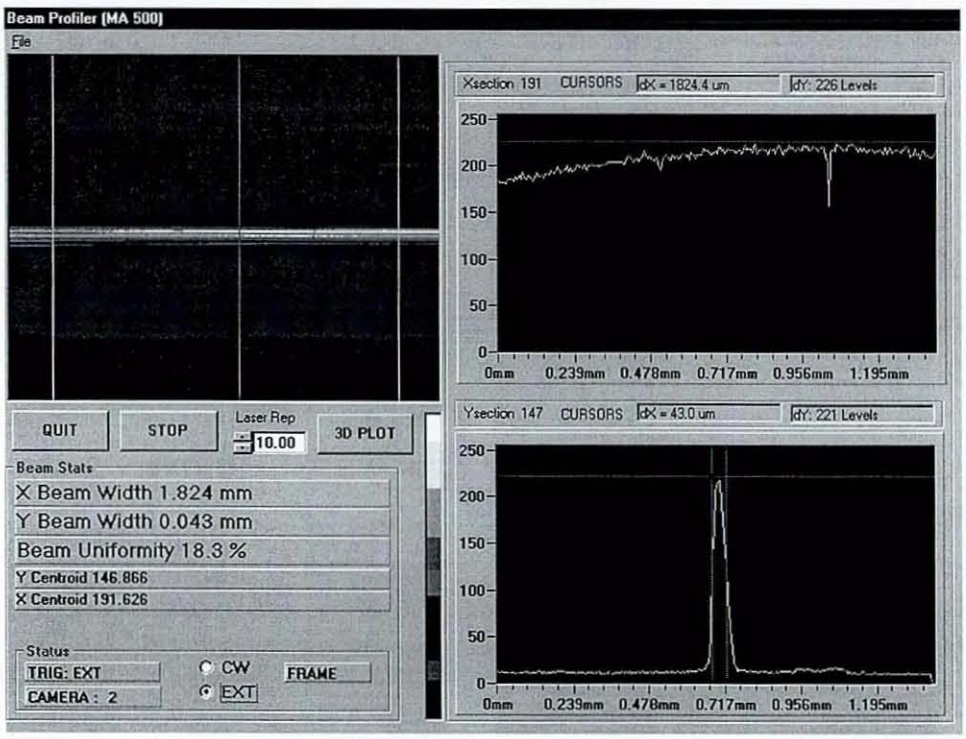

Figure 1.8. Beam analysis software.

An evolving ISO standard is under development [19] that deals with both intensity profile and propagation parameters. An example of the latest beam analysis software, developed by the author is shown in figure 1.8.

1.6 Laser beam propagation

Although the near field intensity distribution is the most important parameter affecting materials processing tasks the behaviour of this distribution through the beam waist can also affect processing results particularly when cutting or drilling.

A full analysis of the parameters involved in characterizing a beam waist would be somewhat unwieldy and complicated; however the universal propagation constant M^2 proposed by Siegman [20] goes a long way to redress this problem. Using this single measure of beam quality any laser beam can be compared to an ideal Gaussian beam of the same diameter and wavelength. So successful has been this measure that it is now adopted by most laser manufacturers and forms part of the emerging ISO standard. However the M^2 definition is not without its limitations ([21] Lawrence), in particular it has difficulty in dealing with beams with hard edge diffraction (such as laser diodes) or for beams with very low coherence (such as excimer lasers). For these lasers alternative measures of beam quality are now under development. Beam diagnostic systems developed by the author for these applications are shown in figures 1.10 a & b.

It is because the parameters best used to characterise a beam are both application and laser specific that much development work still remains in this field and will continue to do so for the foreseeable future.

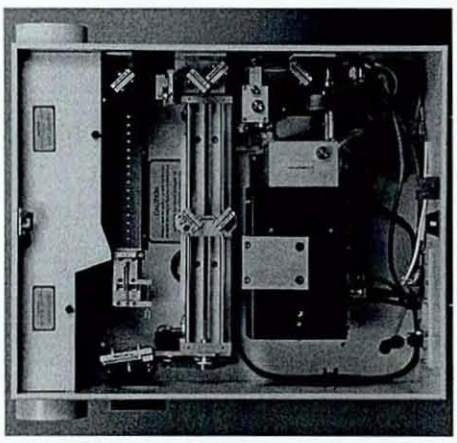

Fig 1.10 a. Beam propagation analyser For high power (2kW) CO_2 lasers

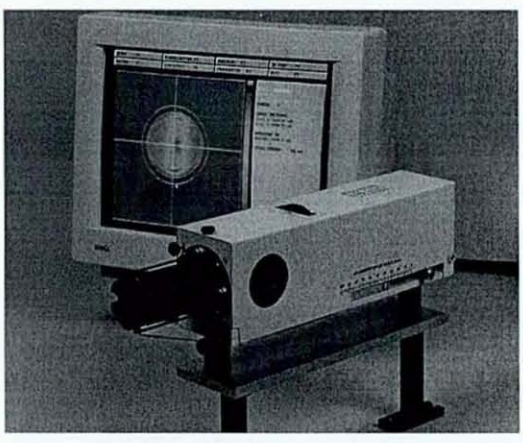

Fig 1.10 b. Beam sampling unit for high power (1 kW) Nd:Yag lasers

1.7 Industrial systems

Some of the first integrated beam diagnostic systems were implemented in Exitech micromachining systems in 1992 [22] by the author. Advanced applications include focal plane diagnostics for ink jet nozzle drilling systems, Nd:Yag beam shape monitoring for laser marking systems and excimer line beam diagnostics for amorphous Silicon annealing [23], as shown in figure 1.11.

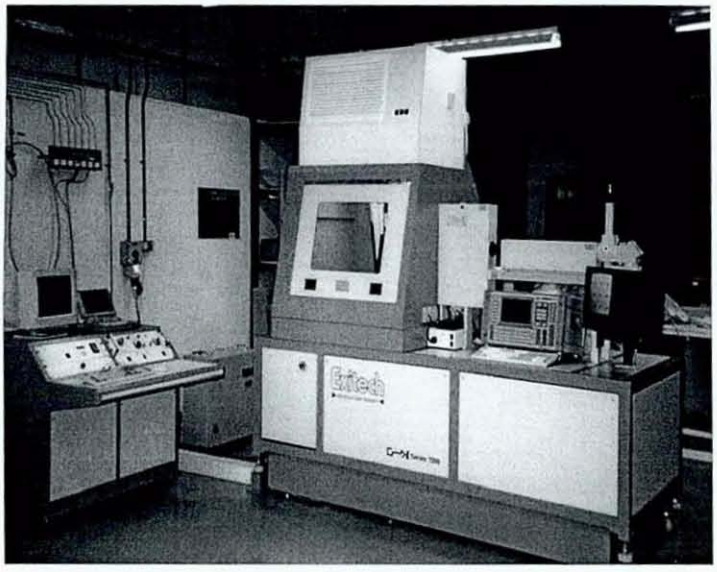

Fig 1.11

Experimental tool for excimer laser annealing of amorphous Silicon.

The marking of ceramic substrates is a typical high value item example, where on-line beam monitoring provides assurance that the laser system is operating to specification, ensuring consistent production quality and low reject rates, see figure 1.12.

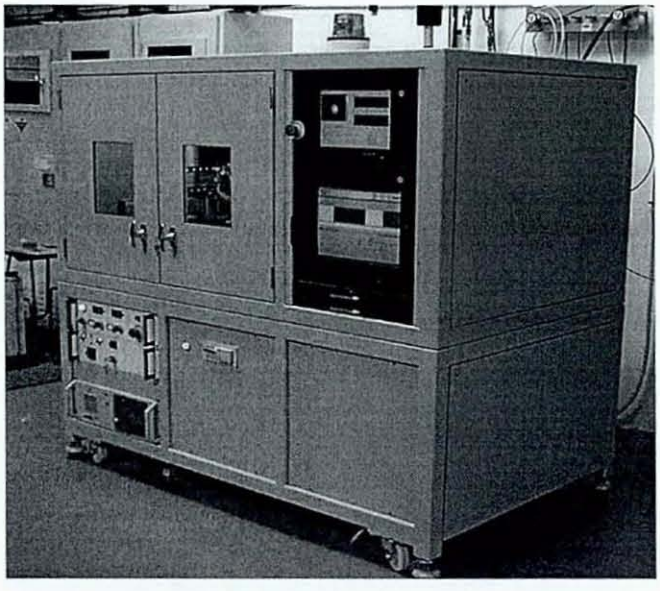

Fig 1.12

Machine for marking Ceramic chip substrates using a 3rd harmonic Nd:Yag laser, with integrated beam monitoring.

Surface treatment applications using excimer lasers also require beam monitoring. Effective laser cleaning requires accurate knowledge of exposure fluence and beam uniformity in order to achieve uniform results. A laser tool for this application is shown in figure 1.13.

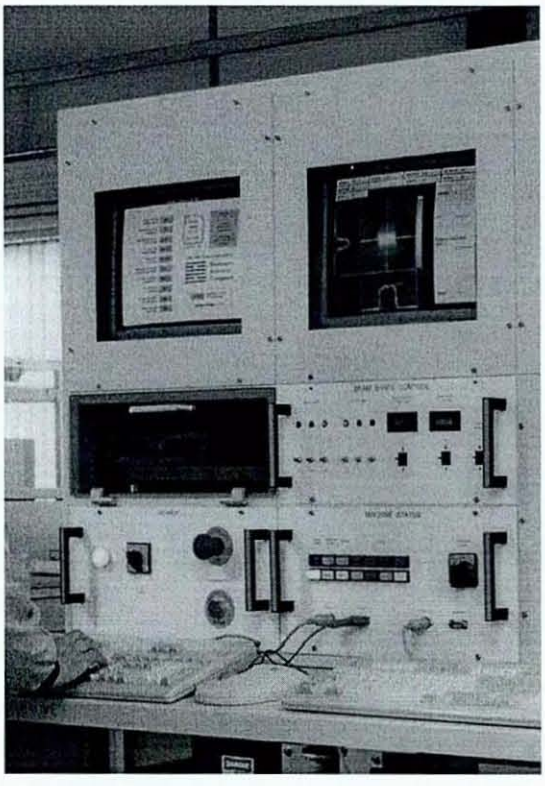

Fig 1.13.Tool for excimer laser cleaning of Silicon wafers, showing integrated beam profiler.

1.8 Contents of Thesis

This thesis summarises a varied body of work that includes conference papers presented over several years, covering both laser beam diagnostics and laser micromachining. In this context it presents a broad range of topics related to laser micromachining systems and the control systems required to maintain consistent results in production environments. It is split into eight chapters including this introduction.

The second chapter briefly describes the history of laser development, resonator design and theories on beam propagation. This then leads on to a description of how the beam quality factor "M^2" is derived and measured in practise.

The third chapter concentrates on the analysis of laser beam shape and beam diameter, introducing the important concepts of the second moment definition of beam width and how the novel use of truncated moments is useful in practical applications for the suppression of measurement errors.

The fourth chapter describes experiments conducted to verify the proposed ISO standards on laser beam propagation and profile intensity distribution measurements, specifically the measurement of "M squared" for ideal and non-ideal laser sources. A number of measurement examples are illustrated on three different types of laser and then the results are presented as example beam analysis test reports. The concept of threshold beam uniformity is first introduced, a measurement now included in the ISO standard for beam profile analysis.

The fifth chapter describes the implementation of excimer laser beam diagnostics for materials processing applications It discusses the best choice of detector and beam sampling optics, digitisation electronics and integration into a workstation control system and describes the algorithms involved in beam characterisation. Attention is also given to the practicalities of implementing such schemes on real hardware. The author has developed beam analysis systems used in over 300 practical applications world wide, many of them to support new and novel processes. A description is then given of a system designed to measure excimer line beam profiles for Silicon annealing applications. This includes the first use of an in-chuck profiling system for excimer lasers using CCD cameras, which has proved a significant development for enhancing the performance of high precision laser processing machines.

The sixth chapter describes a range of excimer and UV laser micromachining and processing applications. Examples are given as to how laser systems for micromachining have been designed and implemented in practise using a number of novel techniques. A quite different system is also described for the writing of fibre Bragg gratings using an excimer laser; this is an application that not only greatly benefits from integrated beam profiling and control systems, but would be impossible to reliably implement without this technology.

The seventh chapter describes the further development and applications of some novel industrial laser systems for micromachining. These include descriptions of a combined linear stage and galvanometer scanner machine architecture that has been developed for micromachining applications. This new machine architecture has been the subject of several conference papers and magazine articles. Specific applications include the patterning of high density interconnects in Copper films using galvanometer scanners and the grooving of mono-crystalline Silicon wafers for solar cell applications.

The conclusions summarise the results of this work, emphasising its relevance to real industrial applications and production processes. A table is presented showing the history of development of beam diagnostic systems by the author. It highlights a number of first uses of the techniques described in this thesis.

1.9 References

1). T H Maiman, "Stimulated optical radiation in Ruby" Nature, 187,493, (1960)

2). W M Steen, "Laser material processing",p5, Springer Verlag , London (1991)

3). A B May, "Laser processing in manufacturing" Chapter 5, p96 , Chapman & Hall (1993)

4). A B May, "Laser processing in manufacturing" Chapter 5, p102 , Chapman & Hall (1993)

5). A B May, "Laser processing in manufacturing" Chapter 5, p108 , Chapman & Hall (1993)

6). J Powell, "CO_2 laser cutting" Springer Verlag, London (1993)

7). A Chesnaukas and S Llewellyn , "Laser welding makes it a close shave", Industrial Laser review, May, 4-5 (1990)

8). JJ Ewing and K Brau, "Laser action on the bands of KrF and XeCl ", Appl.Phys Letts, 27,350 (1975)

9). R Srinivasan and V Mayne-Banton, "Self-developing photoetching of polyethylene terephthalate films by far ultraviolet excimer laser radiation", Appl Phys Letts 41, 576, (1982)

10). M C Gower , " Excimer laser micromachining: a 15 year perspective", SPIE proceedings LAMOM (1999)

11). G Herziger, M Scholl and P Loosen, "Beam shape characterisation for materials processing", Proc of the 2nd workshop on Laser beam characterisation. H Weber et al. Berlin (1994)

12). B A Ward, "An experimentalists approach to laser beam characterisation and the emerging measurement standards", Proc of the 2nd workshop on Laser beam characterisation, H Weber et al. Berlin (1994)

13). C Courtney and W M Steen, Applied Physics A (Germany), p303-7 November (1978)

14). G Sepold et al. "Proc of the International conference on welding research in the 1980's" A-29,3,Osaka, October (1980)

15). G C Lim, and W M Steen, "The measurement of the temporal and spatial power distribution of a high powered CO_2 laser beam", Optics and Laser Technology, p149-153, June (1982)

16). E A Teppo, "Diagnostic tools for laser beam characterisation" Proc of Laser beam characterisation workshop, Madrid (1993)

17). C B Roundy, "Instrumentation for laser beam profile measurement ". Proc of Laser beam characterisation workshop, Madrid (1993)

18). A E Siegman."Lasers" University Science Books,Mill Valley CA, (1986)

19). ISO/TC/SC9/WG1/CD 11 146,"Optics and optical instruments, Test Methods for laser beam parameters: Beam widths, divergence angle and beam propagation factor."

20). AE Siegman,"New developments in laser resonators", Proc SPIE Vol 1224 "Optical Resonators" (1990)

21). GN Lawrence, "Beyond beam divergence", Proc SPIE Vol 2375 "Beam Control, Diagnostics, Standards and Propagation" (1995)

22). P Apte, M Gower and P T Rumsby, " Characterising beam quality for laser processing". Proc of laser beam characterisation workshop, Madrid (1993)

23). P Apte, M Gower and P Rumsby, "The measurement and characterisation of high aspect ratio line focus beam profiles for excimer laser applications", Proceedings of the 4th Workshop on laser beam characterisation, Munich (1997)

CHAPTER 2

CHARACTERISING LASERS AND BEAM PROPAGATION

2.1 Introduction

In 1917 Albert Einstein published a now famous paper that described the relationship between atomic energy levels and the wavelength of light [1] and from this work he postulated that the process of stimulated emission must exist. However it was not until 1960 with the invention of the Ruby laser by T.H.Maiman [2] that the full potential of Einstein's theory was realised. Since then many new types of laser have been developed using new materials and principles of operation. Some of the best known types of laser are the Helium Neon (HeNe), Neodymium YAG (Nd:Yag) ,Carbon Dioxide (CO_2) , excimer laser and semiconductor diode laser. Almost every day new applications for laser radiation are being discovered or developed. The basic construction and operation of most types of laser is relatively simple. However in modern industrial and scientific laser systems considerable engineering sophistication and theoretical know how lie behind these seemingly simple designs.

2.2 Laser Development

The first recognizable form of laser was invented Maiman [3] at the Hughes Research Laboratories in 1960. As always in science a number of key advances during the 19^{th} and 20^{th} centuries contributed greatly to its development. In the mid-nineteenth century the behaviour of light was quite successfully described using Maxwell's Equations. These are still used to explain macroscopic behaviour, but fail to explain interactions on an atomic scale. In particular, these equations predicted the occurrence of the so-called ultraviolet catastrophe in black body spectra which was not observed in practice.This was finally resolved by the German physicist Max Planck, who postulated a quantum theory of light [4] .This simple but elegant approach removed the ultraviolet

catastrophe and brought prediction and observation once more into agreement. In 1913, the Danish physicist Neils Bohr extended Planck's ideas to atomic energy structure and was able to explain the absorption and emission spectra of atoms in terms of transitions between atomic energy levels.

Then in 1917 Albert Einstein's important work was published on the interaction between atomic energy levels and light [5], which led to the prediction of a hitherto unobserved effect. This effect, now called Stimulated Emission, is central to the operation of all laser devices. By the early 1930s stimulated emission was actually observed in a gas discharge by the German physicist Ladenburg [6]. However the potential of Stimulated Emission was not at that time realized as many technical barriers existed to impede the fabrication of a laser device.

However by the mid 1950's the first device was reported utilizing stimulated emission by Gordon, Zeiger and Townes (1955) [7]. This device achieved Microwave Amplification by Stimulated Emission of Radiation (hence the acronym MASER). Following several years of intense debate concerning the possibility of this microwave effect occurring at optical or visible wavelengths, the matter was finally put to rest in 1960 with the invention of the ruby laser by Theodore Maiman. Once the principle had been established there followed a decade of intense activity during which most of the laser types we know today were established. In particular, the Helium Neon laser was investigated and developed by Javan *et al.* (1961) [8], Neodymium:YAG by Geusic *et al.* (1964) [9], and Carbon Dioxide by Patel (1964) [10]. The only major industrial type to be developed outside that decade was the excimer laser [11] in 1976. Since then many new laser types have been discovered. The Semiconductor laser diode [12] was discovered in the 1960's but has only recently found major applications in both telecommunications and materials processing.

2.3 Laser Resonators and modes

The simplest laser resonator consists of two plane mirrors facing each other along a common axis. If we combine two waves travelling in opposite directions along the resonator axis, stable resonance patterns or standing waves occur whenever the

separation of the mirrors is an integral number of half wavelengths. The number of half wavelengths is the axial mode number of the resonator. For such a plane cavity the variation is purely axial, and the modes are known as axial modes. However such resonators are seldom used as they are lossy and difficult to align.

Most practical resonators have curved mirrors. In a simple case, both mirrors are sufficiently concave to counteract natural diffraction spreading. This also relaxes mirror alignment since for small offsets there is always one point on each mirror aligned with the other. A side effect of mirror curvature is that the number of standing waves depends on the exact path traversed so that, in addition to the axial modes, there are also off-axis or transverse modes. For circular geometries these modes are described mathematically by the Laguerre - Gaussian distribution function [13].

These are usually described as Transverse Electromagnetic or TEMplq for short, followed by up to three suffix digits (plq). The three digits refer to the degree of mode structure, thus TEM_{00} is purely axial, TEM_{10}, has a simple two spot structure in the x direction, and in general TEM_{nn} has an n + 1 spot structure. Likewise the second digit refers to structure in the y direction. Both x and y structures can be combined, as for example TEM_{31}. Figure 2.1 shows an example of these modes. The x - y type description is relevant to lasers where optical asymmetries define an x direction. In many lasers such asymmetries are weak, and the modes have a circular symmetry.

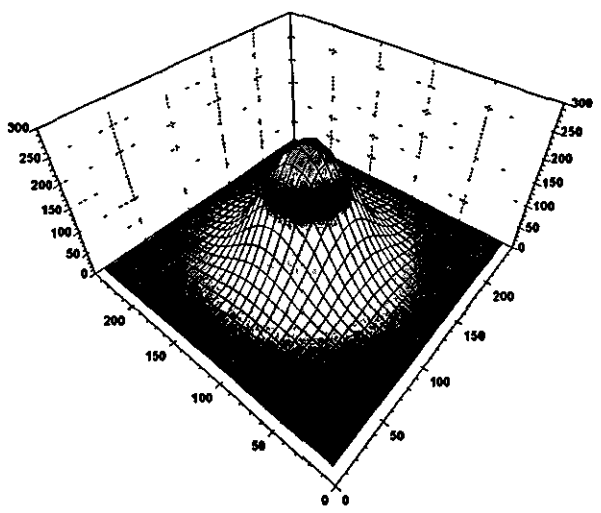

Fig. 2.1 TEM_{00} Gaussian mode

For example, TEM_{01} consists of a hollow annular ring centred on the axis. It is not unusual for lasers to operate in several modes at once, and in this context the phrase 'combination of low order transverse modes' is often encountered. An authoritative description of the theory of laser modes and resonators is given by Siegman [14].

2.4 Mode stability

Mode stability within a curved mirror resonator was thoroughly investigated early in the course of laser development. A concise and useful description is the stability diagram of Fox and Li (1961) [15] where hyperbolic curves are used to represent the limits of mode stability. In the region between these curves and the axes, the mirrors refocus light periodically and the volume occupied, the so-called mode volume, remains fixed and well defined. Resonators lying within these areas are called stable resonators. Resonators lying beyond the curves, or in the other quadrants, are called unstable resonators. These have their own, totally different type of mode structure in which successive reflections never retrace their previous paths. Nd:Yag and excimer lasers use stable resonators almost exclusively whereas CO_2 lasers use both types. Stable resonators are ideal for cases where light is extracted through one partially transmitting mirror.

2.5 Gaussian beam propagation.

The propagation of Gaussian beams is decribed by the well known equation (2.1). Here ω is the radial distance from the axis at which the field amplitude has dropped to $1/e^2$ of its peak axial value. Hence the cross sectional beam intensity profile at any point in the beam has a Gaussian intensity profile, the width of which changes with distance along the z axis. This is the essential form of the Gaussian beam propagation equation as shown graphically in fig 2.2.

Crucially the minimum beam radius ω_0 or waist occurs at the point where the phase front is planar.

$$\omega^2(z) = \omega_0^2\left[1+\{\frac{\lambda z}{\pi\,\omega_0^2}\}^2\right] \qquad \text{Equ 2.1}$$

If the axial origin is taken at this waist then the variation in the wavefront radius of curvature with distance z can be expressed as Equ 2.2a

$$R(z) = z + \frac{z_R^2}{z} \qquad \text{Equ 2.2a}$$

Here Z_R is the Rayleigh length defined in equation 2.2 b

$$z_R = \left(\frac{\pi\omega_0^2}{\lambda}\right) \qquad \text{Equ 2.2b}$$

The half angle angle divergence of this beam is given by

$$\Theta_D = \sqrt{\frac{\lambda}{\pi\, z_R}} \qquad \text{Equ 2.3}$$

This is the smallest angular spread that a beam with waist ω_0 can have.

It is important to note that the product of the beam waist half width and the divergence half angle ($\omega_0.\Theta_D$) is only a function of the wavelength of the laser beam, it is independent of the the Rayleigh length and the distance from the beam waist. This product is an invariant of propagation. Hence as TEM_{00} guassian beam propagates through an optical system the width/divergence product does not change.This forms the basis for the beam quality standard described in the next section.

2.6 Beam quality and M^2.

The concept of M^2 was developed by Siegmann [16] in the 1980's. The concept defines a number for the focussing ability of a laser beam and allows a direct calculation of the minimum spot size achievable with any laser and optical setup without prior knowledge of other laser parameters. The M^2 value represents the ratio of beam waist diameters achievable at focus for a "perfect" gaussian beam and a real gaussian beam of the same diameter. Hence the theoretical maximum value is $M^2 = 1$ for a "perfect" laser; however in reality values of 1.1 or higher are typical of a good TEM_{00} laser.

The derivation of M^2 is thoroughly dealt with in ref [17], and of more concern to an industrial user is a simple method for measuring it. But essentially it is described by equation 2.4.

$$M_x^2 = 4\pi \sigma_{xmin} \sigma_{sx} \qquad \text{Equ 2.4}$$

where σ_{xmin} is the minimum value of second moment beam radius along the x direction, and σ_{sx} is the standard deviation of the spatial frequency distribution of the beam along the x direction.

This can be done relatively simply for laser beams without hard edge diffraction by taking beam diameter measurements using the second moment algorithm (described in section 3.3) at different points through the waist produced at the focus of a simple lens [18]. This method is described as follows.

From the coefficients of fit of the beam propagation hyperbola (A,B,C).

$$\mathbf{d^2 = A + B.z + C.z^2} \qquad \text{Equ 2.5}$$

where **d** is the beam diameter and **z** is the detector position.

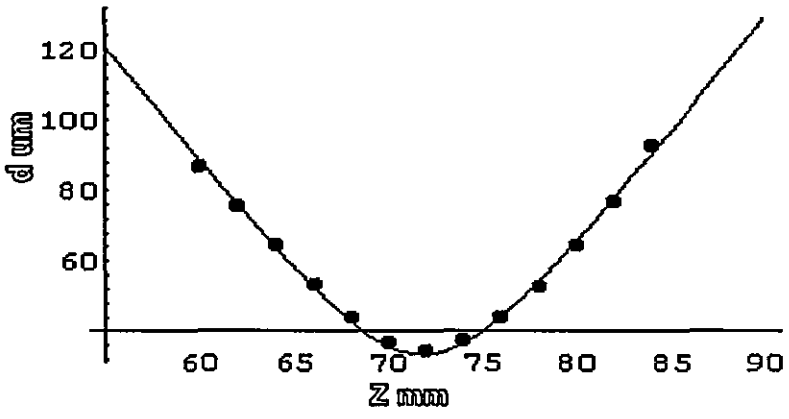

Fig 2.2 Least Squares Hyperbolic fit

Figure 2.2 shows points fitted to real data taken from a HeNe laser with a nominal TEM_{00} mode using the least squares method. A number of standard numerical libraries exist for this purpose.

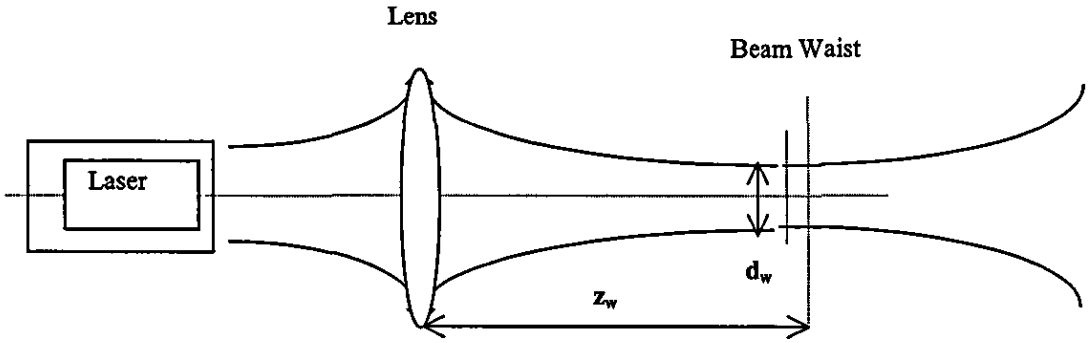

Fig 2.3 The beam waist generated by a lens focussing a TEM_{00} laser beam.

The waist size, position and M^2 can be then calculated as follows from the coefficients of the quadratic fit to the propagation hyperbola as shown in figure 2.3.

Waist position.

$$z_w = (-B)/(2.C) \qquad \text{Equ 2.6}$$

Waist Size.

$$d_w = \sqrt{(A - (B^2)/(4.C))} \qquad \text{Equ 2.7}$$

and

$$M^2 = (\pi/4) . (n/\lambda). \sqrt{(A.C - (B^2)/4)} \qquad \text{Equ 2.8}$$

Here **n** is the refractive index of air (1.000001) and λ is the laser wavelength.
These algorithms have been implemented in software by the author as part of the Exitech P256 beam diagnostic system.

An example of real hardware for a beam propagation analyzer is shown in figure 2.4. This unit was developed for a high power CO_2 laser installed in a large Trumpf laser cutting machine.

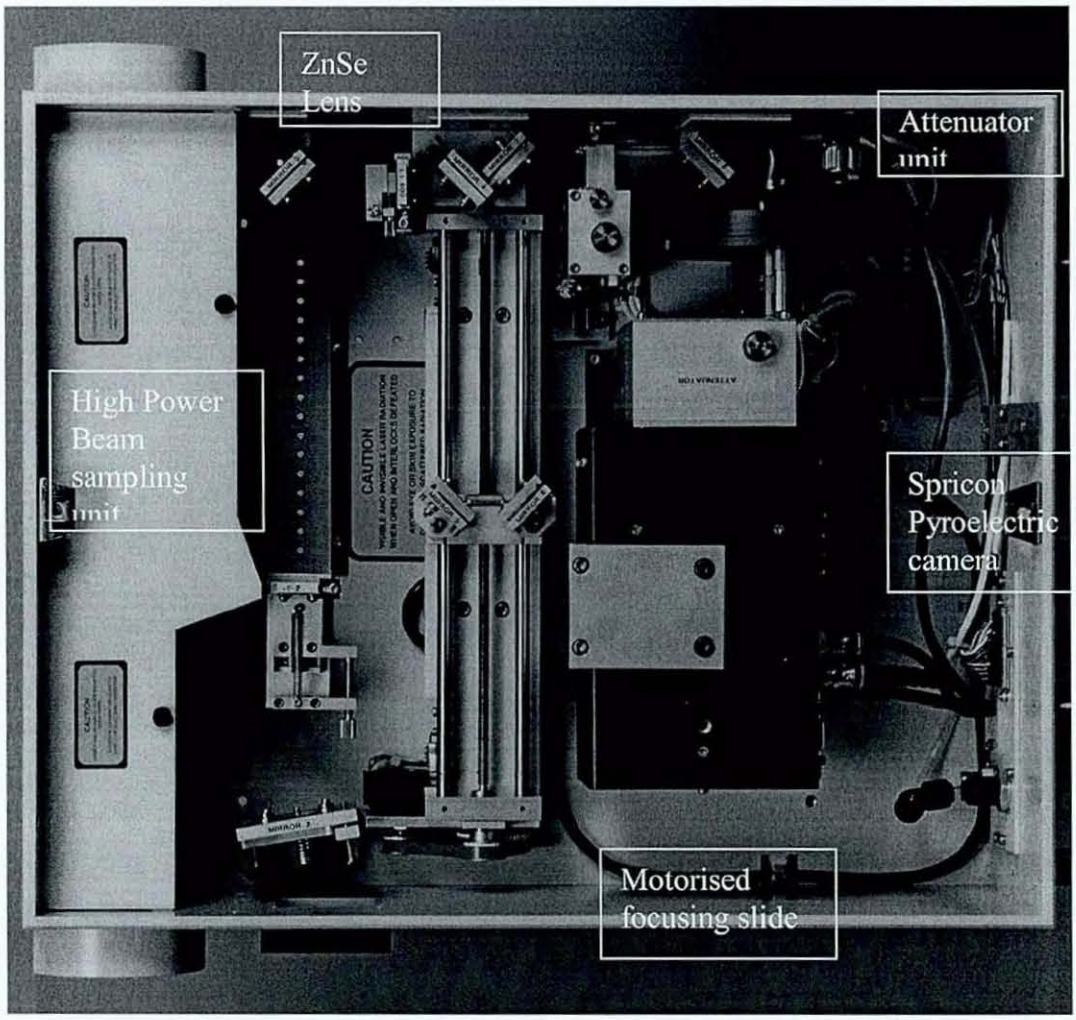

Fig 2.4 : A beam propagation analyser designed for a high power (3kW) CO_2 laser. Developed by the author it was one of the first instruments of its kind.

The latest generation of propagation analysers use Shack-Hartmann or Shearing interferometers and sophisticated image processing techniques to measure the laser beam wavefront directly [19]. Thus in principle they can fully characterise the propagation characteristics of a beam.

2.7 Near field intensity distributions.

The majority of Nd:Yag and CO_2 laser processes use the focussed beam, whereas the near field intensity distribution is of particular importance for excimer laser materials processing for which the near field is almost exclusively used. The intensity distribution

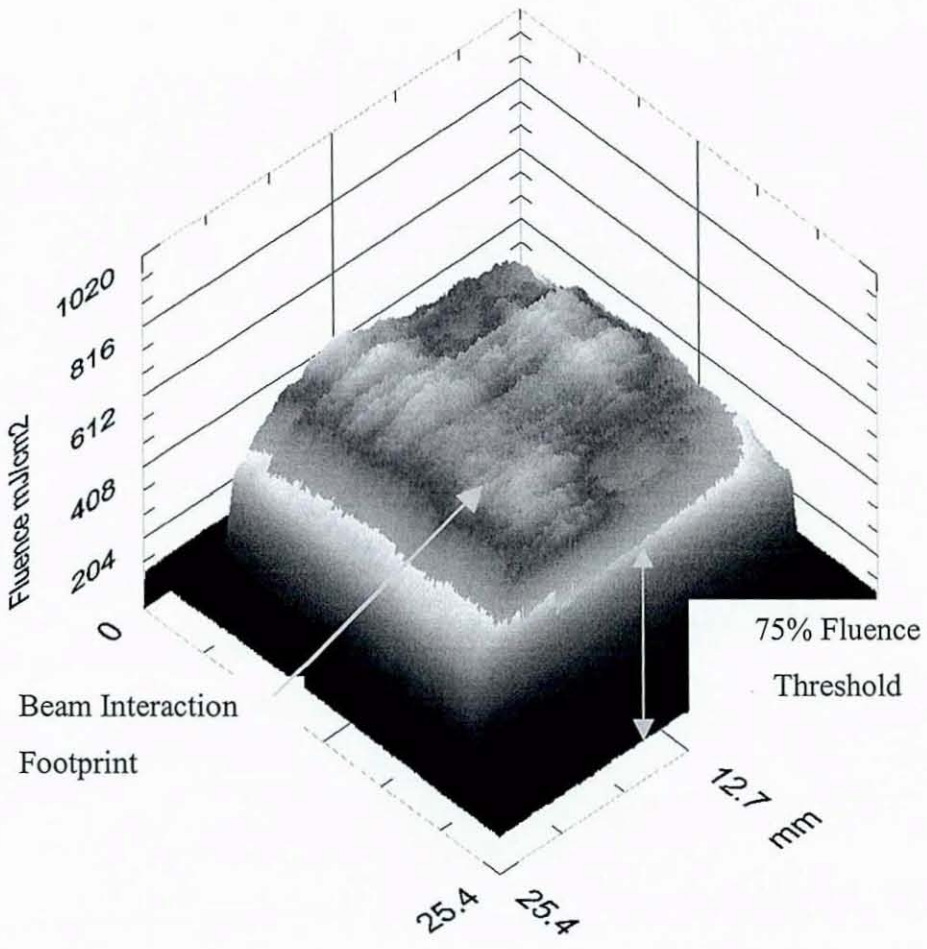

Fig 2.5 . The near field beam interaction footprint of a homogenised excimer laser beam used for Silicon annealing.

can be measured directly by using suitable beam sampling optics and imaging devices. The author has helped pioneer the use of 2D matrix array cameras in this application, as further described in chapter 3.

An example of the near field beam profile is shown in figure 2.5. This illustrates the concept of interaction footprint which is described in further detail in Chapter 3.

2.8 Beam Quality and laser processing.

It is well known that beam parameters have a profound effect on a lasers ability to process materials. In scribing , cutting and welding applications the spot size and mode quality have a direct effect on process speeds [20]. This is also true of excimer laser processing, where beam uniformity is of critical importance to a number of applications including Silicon annealing and and ink jet nozzel drilling [21]. These effects are described in more detail in later chapters of this thesis.

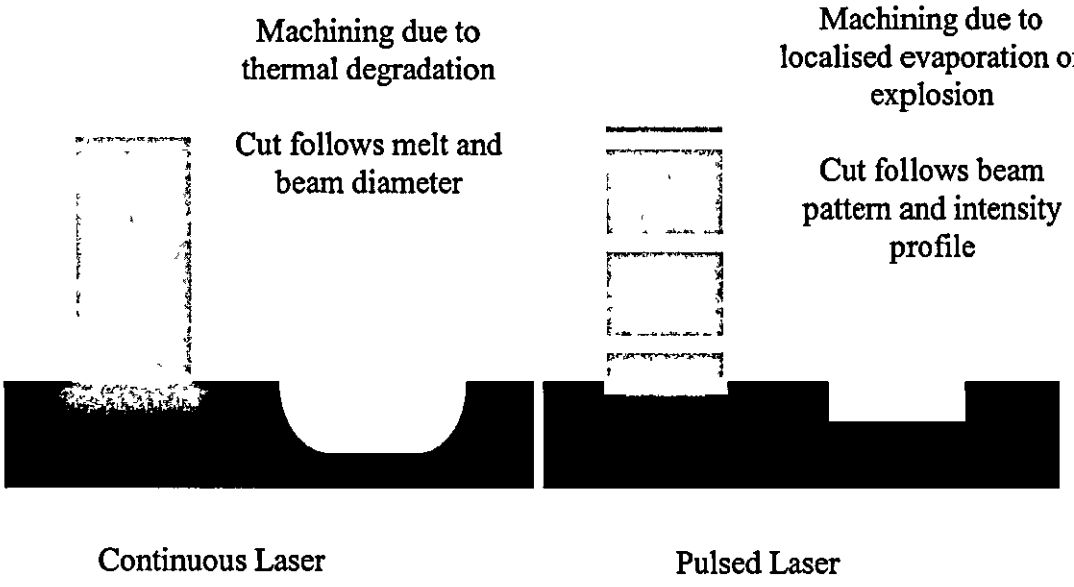

Fig 2.6 Basic laser material interaction

However Figure 2.6 shows in very simple terms the interaction between the laser beam and the workpiece. For a continuous laser , such as a CO_2 laser in a metal cutting application, the focussed laser spot will generate a local melt pool. The size and quality of the cut is sensitive to both the laser spot diameter at the material surface and the properties of the focussed beam waist (and hence beam quality).

For a pulsed laser application such as the excimer patterning of polymer, the beam is not focussed and the material is locally ablated by the high instantaneous power of the beam. This results in the processed surface being very sensitive to the fluence profile of the laser beam at the material surface as no time averaging occurs. However the propagation properties of the beam are less important as the beam is not being used at focus.

There are exceptions to these cases. For example when drilling inkjet printer nozzels , or other high aspect ratio structures by excimer laser, the propagation properties of the beam are also important, as the beam profile is subject to change as the laser ablates along the length of the structure. Conversely when writing tracks on layers of thin photo resist using CW Ar^+ lasers for CD mastering applications, the intensity profile of the beam is of great importance.

2.9 Summary

Clearly the laser is a very useful tool for many production processes, however laser energy needs to be carefully characterised and controlled if the full benefit of this technology is to be realised. How some of the beam parameters described in this chapter are measured and characterised is the subject of the next three chapters. The last two chapters of the thesis describe practical applications and production laser machine tools which incorporate some of these ideas.

2.10 References

1). A Einstein, Phys. Zeit. 18, 121, (1917)

2). A G Fox and T Li, Bell systems technical Journal, 40, 453, (1961)

3). T H Maiman, "Stimulated Optical radiation in Ruby" Nature, 187,493, (1960)

4). M Planck, Ann. Phys. 1,69, (1900)

5). A Einstein , Mitt.Phys.Ges. Zurich 1618, p47, (1916)

6). R Landenburg , " Research on the anomolous dispersion of gases", Phys. Z, 48,15, (1928)

7). J P Gordon, Zeiger and C Townes, Phys Rev, 95,282, (1955)

8). A Javan, Bennet and Herriott, Phys Rev Letts, 6, 106,(1961)

9).J E Geusic, Marcos and Van Uitert, "Laser Oscillations in Nd doped Yttrium Aluminium , Yttrium Gallium and Gadolinium garnets",App Phys Letts, 4, 182, (1964)

10). C K N Patel, "Continuous wave laser action on vibrational and rotational transitions of CO_2", Phys Rev, 136A, 1187, (1964)

11). J J Ewing and K Brau, "laser action on the bands of KrF and XeCl" , Appl.Phys Letts, 27,350,(1975)

12). R N Hall, Fenner, Kingsley, Soltys and Carlson, "Coherent light emission form GaAs junctions", Phys Rev Letts, 9,366, (1962)

13). A E Siegman,"Lasers" University Science Books,Mill valley CA, (1986)

14). A E Siegman,"Lasers" University Science Books,Mill valley CA, (1986)

15). A G Fox and T Li, Bell systems technical Journal, 40, 453, (1961)

16). A E Siegman,"New developments in laser resonators", Proc SPIE Vol 1224 "Optical Resonators" , (1990)

17). M W Sasnett, "Propagation of multimode laser beams – the M^2 factor", "The Physics and Technology of Laser Resonators", Adam Hilger, (1989)

18). B A Ward, "An experimentalists approach to laser beam characterisation and the emerging measurement standards", Proc of the 2nd workshop on Laser beam characterisation, H Weber et al. Berlin (1994)

19). J Snyder, "Laser wavefront analysis with dynamic shearing interferometer", Proc SPIE Vol 2375 "Beam control,Diagnostics,Standards, and Propagation", (1995)

20). P Loosen, K Du, C Maier, O Marten and M Scholl, "Laser beam characterisation and measurement techniques", Proc of Laser beam characterisation workshop, Madrid (1993)

21). K Mann et al, "Monitoring and shaping of excimer laser beam profiles", Proc SPIE Vol 1834,184, (1992)

CHAPTER 3

CHARACTERISING LASER BEAM INTENSITY DISTRIBUTIONS

3.1 Introduction

The irradiance distribution of a laser beam can be characterised by the spatial distribution of the irradiant power density (peak or time averaged power/area) with lateral displacement in a particular plane normal to the direction of propagation. In general, the irradiance distribution will change along the direction of propagation of the beam.

Characterising the size and shape of these distributions is becoming increasingly important for a growing number of industrial and scientific laser applications. Indeed the measurement of other important beam parameters relating to divergence and propagation depend critically upon the accurate determination of beam size. International standards are currently being derived that address the measurement and testing of beam divergence, size, amplitude and phase distribution [1].

Some of the current methods used for beam amplitude characterisation usually use the normal (Gaussian) spatial energy distribution as their model and standard statistical methods to characterise the beam. This approach is driven by pragmatism and computational convenience, as such distributions are relatively simple to analyse. While for many applications it is assumed that the laser has a Gaussian beam profile, in practise this is often not the case.

For this reason if general methods are to be found for beam amplitude characterisation, they should be capable of being applied to all types of laser beam, or at least within clearly defined limits The methods discussed in this chapter apply to 2D spatial intensity profiles measured using a CCD camera and analysed using RISC and CISC

based micro processors on a personal computer. This type of hardware is now widely available at a reasonable cost but suffers from a relatively limited dynamic range (200:1) compared to single point scanning detectors (> 1000:1). Of particular concern are errors due to baseline offset and noise, which can lead to very severe errors in the computation of moment and integrated energy. Methods for reducing these errors are discussed.

Shape fitting techniques using polynomials and other algorithms are also discussed. While these techniques are not strictly part of the ISO measurement standard they may have uses in assisting the alignment and setup of beam delivery optics.

3.2 Formal Definitions

The nomenclature and parameters used below are consistent with those defined in the ISO 11 145 document, "Terminology, symbols and units of measure for the specification and testing of lasers and laser subassemblies".

3.2.1 Local irradiance

Cartesian axes x, y, z are assumed with the x and y axes being transverse to the beam propagation direction along the z-axis. The electric field vector of an electromagnetic wave oscillating at frequency ω at position (x, y, and z) can be described by

$$\varepsilon(x,y,z) = \frac{1}{2}\varepsilon_0(x,y,z)e^{i[\omega t-\{k_x x+k_y y+k_z z\}+\varphi(x,y,z)]} \qquad \text{Equ (3.1)}$$

Where ε(x, y, z) is the wave amplitude, φ (x, y, z) the phase and $k_x k_y$ and k_z the appropriate wave vectors. From this definition the local irradiance at position (x, y, z) in SI units is given by

$$E(x,y,z) = \frac{nc\,\epsilon_0}{2}\varepsilon_0^2(x,y,z) \qquad \text{Equ (3.2)}$$

where n is the refractive index of the material at (x, y, z), c is the velocity of light in vacuum and ϵ_0 is the free space permitivity.

Hence for a laser beam travelling in the z direction the peak power density at location x_p , y_p are defined as

$$E_p = E(x_p, y_p) \qquad \text{Equ (3.3)}$$

such that E (x_p, y_p) > E (x, y) for all positions (x, y) through which the beam passes.

3.2.2 Definition of moments

The total laser power P_H contained in the beam at z is given by the zero order mixed moment of the distribution:

$$P_H = \int\int E(x,y)\,dx\,dy \qquad \text{Equ (3.4)}$$

For a detector of finite aperture the detector area defines the limits of integration. When using a CCD array detector these limits are defined by the rectangle (x_1, y_1, x_2, y_2) in the x, y plane. Where x_1, y_1 is the coordinate defining the top left hand corner of the rectangle, and x_2, y_2 define the bottom right hand corner.

3.2.3 Spatial Moments

The Nth order spatial moments are given by direct analogy to methods used to analyse statistical distributions. The properties of beam amplitude distributions can be quantified by taking moments of the power density distribution. The Nth order moment of E (x, y) is defined as

$$< x^n y^n >= \frac{1}{P_H} \int_{y1}^{y2} \int_{x1}^{x2} x^n y^n E(x,y)\,dx\,dy \qquad \text{Equ (3.5)}$$

Treating the x and y axis independently, the 1st linear moment corresponds to the position of the beam centroid or centre of gravity (x_c, y_c).

$$x_c = \frac{1}{P_H} \int\int xE(x,y)\,dx\,dy \qquad \text{Equ (3.6a)}$$

$$y_c = \frac{1}{P_H}\iint yE(x,y)\,dx\,dy \qquad \text{Equ (3.6b)}$$

Higher order moments are best expressed as centred moments relative to the centroid position. Hence

$$< x^n y^n >_c = \quad < (x - x_c)^n (y - y_c)^n > \qquad \text{Equ (3.7)}$$

The centred linear second moments are therefore

$$< x^n >_c = \frac{1}{P_H}\iint (x - x_c)^n E(x,y)\,dx\,dy \qquad \text{Equ (3.8a)}$$

$$< y^n >_c = \frac{1}{P_H}\iint (y - y_c)^n E(x,y)\,dx\,dy \qquad \text{Equ (3.8b)}$$

The third linear moment ... $< x^3 >$, skewness and the fourth moment ... $< x^4 >$, Kurtosis follow in the same way. These higher order moments can be scaled to dimensionless quantities S_n by dividing by powers of the second moment.

$$S_{xn} = \frac{< x^n >_c}{(< x^2 >_c)^{\frac{n}{2}}} \qquad S_{yn} = \frac{< y^n >_c}{(< y^2 >_c)^{\frac{n}{2}}} \qquad \text{Equ (3.9 a,b)}$$

These are the so-called scaled cumulants and have applications in measuring the symmetry and "sharpness" of intensity profiles [2].

3.2.4 Derivation of Beam Widths

For Gaussian statistically normal intensity distributions the second moment is equivalent to the variance of the distribution. The standard deviation σ is the square root of the second moment.

$$\sigma_x^2 = \quad < x^2 >_c \qquad \sigma_y^2 = \quad < y^2 >_c \qquad \text{Equ (3.10a)}$$

The Beam widths $d_{\sigma x}$, $d_{\sigma y}$ are defined as four times the standard deviations

$$d_{\sigma x} = 4\sigma_x \qquad d_{\sigma y} = 4\sigma_y \qquad \text{Equ (3.10b,c)}$$

For a Gaussian beam amplitude distribution $d_{\sigma x}$ and $d_{\sigma y}$ correspond to the separation of the $1/e^2$ cut positions of a Gaussian beam and contains 95.45% of the total power of the distribution.

3.2.5 Enclosed Power Radii

The enclosed power concept defines a beam radius R_{86} within which 86% of the total laser power is contained.

Using Polar co-ordinates, and taking the beam centroid (x_c, y_c) as the origin,

$$r = \sqrt{(x - x_c)^2 + (y - y_c)^2} \qquad \text{Equ (3.11a)}$$

$$\theta = \tan^{-1}\frac{(y - y_c)}{(x - x_c)} \qquad \text{Equ (3.11b)}$$

For beam distributions that have a rotationally invariant beam width the enclosed power can be defined as:

$$(1 - \frac{1}{e^2}).P_H = \int_0^{+2\pi}\int_0^{+R_{86}} E(r,\theta)\, dr\, d\theta \qquad \text{Equ (3.12)}$$

where R_{86} is the 86% enclosed power radius. The enclosed power diameter is defined as:

$$d_{86} = 2R_{86} \qquad \text{Equ (3.13a)}$$

For a Gaussian beam the d_{86} diameter corresponds to the distance between the 1/e (36%) intensity cut points, and in terms of the moment radius.

$$d_\sigma = \sqrt{2}d_{86} \qquad \text{Equ (3.13b)}$$

3.2.6 Beam Uniformity

To define beam uniformity the average irradiance is defined such that

$$E_{ave} = \frac{\int_{y1}^{y2}\int_{x1}^{x2} E(x,y)\,dx\,dy}{\int_{y1}^{y2}\int_{x1}^{x2} dx\,dy} \qquad \text{Equ (3.14a)}$$

Then the beam uniformity U corresponds to the standard deviation of the irradiance distribution.

$$U = \frac{1}{E_{ave}}\sqrt{\frac{\int_{y1}^{y2}\int_{x1}^{x2}(E(x,y)-E_{ave})^2\,dx\,dy}{\int_{y1}^{y2}\int_{x1}^{x2} dx\,dy}} \qquad \text{Equ (3.14b)}$$

By analogy to the spatial intensity distribution, U^2 is the second moment of the irradiance distribution.

3.2.7 Threshold Power Density

For practical measurements of distribution parameters, a threshold irradiance E_T is defined such that the moment and uniformity integrals are carried out only for locations (x, y) where $E(x, y) > E_T$.

E_T is expressed as the factor η of the peak irradiance of the distribution.

$$E_T = \eta E_p \qquad \text{Equ (3.15)}$$

3.3 Numerical Implementations

The integrals defined in section 3.2 can readily be solved numerically for a set of digitised input data within certain restrictions that limit the dynamic range, resolution and integration area in the (x, y) plane.

The algorithms described below are implemented assuming a 256 x 256 square grid of data points, digitised to 256 grey levels (8 bits). Each data point corresponds to a pixel of the CCD imaging device. An important point to note is that CCD cameras respond only to the total energy deposited on each pixel during the integration time of the camera, and not the instantaneous irradiance. For CW sources the incident power density corresponds directly to the responsivity of the detector in terms of (Volts/Watts)/cm^2, while for pulsed laser sources the energy density corresponds to the detector responsivity in (Volts/Joule)/cm^2.

3.3.1 The Calculation of moments

If the output of the detector in Volts at (x, y) is defined as A(x, y) and R is the responsivity of the CCD detector array in (Volts/Watt)/cm^2 , then the moments of the power density distribution being measured can be expressed as;

Zero order (Total Laser power P_H)

$$P_H = \sum_{0}^{255}\sum_{0}^{255} A(x,y).R^{-1} \qquad \text{Equ (3.16a)}$$

First order linear moments (Beam centroid)

$$x_c = \frac{1}{P_H}\sum_{0}^{255}\sum_{0}^{255} x.A(x,y).R^{-1} \qquad y_c = \frac{1}{P_H}\sum_{0}^{255}\sum_{0}^{255} y.A(x,y).R^{-1} \qquad \text{Equ (3.17 a,b)}$$

Second order centred linear moments (variance)

$$< x^2 >_c = \frac{1}{P_H}\sum_{0}^{255}\sum_{0}^{255} (x - x_c).^2 A(x,y)\, R^{-1} \qquad \text{Equ (3.18a)}$$

$$< y^2 >_c = \frac{1}{P_H} \sum_0^{255} \sum_0^{255} (y - y_c).^2 A(x,y).R^{-1} \qquad \text{Equ (3.18b)}$$

The Beam diameters are then given by

$$d_{ox} = 4\sqrt{< x^2 >_c} \qquad d_{oy} = 4\sqrt{< y^2 >_c} \qquad \text{Equ (3.19 a,b)}$$

Higher order moments can be defined in a similar way.

3.3.2 Calculation of enclosed Power.

In all but well defined irradiance distributions the power content radii cannot be computed directly and must be found by radially integrating the distribution about the centroid until a radius R_{86} is found that encloses 86% of the beam power. For radially symmetric gaussian-like beams this radius will be found at the E_p/e intensity cut point (36% of peak).

$$P(r) = \sum_0^{2\pi} \sum_0^{r} A(r,\theta).R^{-1} \qquad r = \sqrt{(x - x_c)^2 + (y - y_c)^2} \qquad \text{Equ (3.20a,b,c)}$$

$$\theta = \tan^{-1} \frac{(y - y_c)}{(x - x_c)}$$

r is increased until $P(r) = 0.86P_H$

3.3.3 Beam Uniformity.

The Beam uniformity U is calculated as the standard deviation of the power density histogram distribution

$$U = \frac{1}{A_{ave}} \sqrt{\frac{1}{(256)^2} \sum_0^{255} \sum_0^{255} (A(x,y) - A_{ave})^2} \; . \qquad \text{Equ (3.21a)}$$

where

$$A_{ave} = \frac{1}{(256)^2}\sum_{0}^{255}\sum_{0}^{255} A(x,y) \qquad \text{Equ (3.21b)}$$

These integrations are usually performed only for pixels above the threshold power density ηE_p, the value of η is chosen empirically to simulate the derived beam interaction footprint, and is usually above 0.5 for distributions with $U \leq 0.1$. This concept of beam interaction footprint is particularly useful for characterising excimer laser beams.

3.4 Practical Measurement problems.

When analysing beam profile data taken from CCD arrays a number of measurement errors can substantially affect the accuracy of results [3], in particular noise, baseline offset and beam sampling distortion. The main source of noise is the CCD array readout itself, which can add several counts to the rms noise figure of the system; this degrades the dynamic range of the measuring system.

Accurate determination of the base line offset is critical to beam width measurements, especially when measuring Gaussian-like beams that have very broad low amplitude wings. The base line offset of a typical CCD camera will drift with time over several counts dependent upon ambient temperature, and can severely affect the consistency of results.

Finally beam sampling distortion introduced by beam splitters, imaging optics and attenuating filters can have a serious effect on measurement accuracy. Such components can introduce geometric distortions of the beam profile, while dust and aperturing effects can generate diffraction and interference patterns that increase the optical noise on the profile and further degrade the dynamic range.

3.4.1 Base Line correction

The simplest method of base line correction is to shield the CCD array from any stray source of illumination and by means of viewing a line intensity profile of the array

signal, manually adjust the base line to zero. The presence of noise can complicate this procedure so it is usual to make a 'best guess' of the correct setting. This technique can now be automated using digital image processing. By means of frame averaging the effects of noise can be almost completely eliminated and an appropriate base line found by taking the mean of the image intensity histogram. The value derived is then subtracted from the profile data to correct it.

For CW laser beams the technique of frame averaging can also be used to improve measurement accuracy. The signal to noise will improve as $\sqrt{n}$ where n is the number of frames averaged, up to the fundamental level imposed by the digitisation process itself, which for an 8 bit digitiser is 48dB.

For pulsed laser sources the use of frame integration is not usually appropriate. Moreover the base line is liable to drift over time due to thermal effects, and requires constant recalibration

An alternative approach is to use histogram analysis of the beam intensity distribution to determine the base line. This can be carried out continuously for all profile data and provides a potential method for tracking the base line in real time.

3.4.2 Sampling window truncation.

The use of sampling windows to truncate the range of input data is a common technique in digital signal processing where the so called "Hamming" window is used to limit the spectral range when performing Fast Fourier transforms on continuous data. Similarly a Gaussian sample window [4] can be used to limit the area of integration. When analysing diffracted beams this method conveniently windows out diffraction side lobes that would otherwise contribute to the moment integrals.

The optimum size and shape of the sampling window has to be found empirically depending upon the characteristics of the beam being analysed. This somewhat arbitrary approach could present difficulties in the formulation of a standard that includes this method.

3.4.3 Energy fraction truncation.

This involves setting a threshold power density E_T, which is expressed as the factor η of the peak power density of the distribution, and then only integrating pixels which have a higher power density than E_T .

This technique has been tested for computing excimer laser beam uniformity and enclosed power, because it gives an accurate representation of the "beam interaction footprint" [5] .For such calculations the threshold clip level is usually set to 50% or higher. Within the limitations of the method it provides a good representation of many practical laser power distributions, in applications where the interaction footprint is important.

3.5 Experimental setup

Measurements were made on an optical bench using an Exitech beam diagnostic system with specially modified software that included custom algorithms to change the threshold clip levels of the beam analysis calculations. The system was used with a windowless Pulnix TM 6 CCD camera .The image from the camera was sampled at 256 x 256 square pixel resolution and digitised to 8 bits (256 grey levels). The equivalent re-sampled pixel size was 15.8 um. The laser beam was sampled directly by the detector after suitable attenuation provided by 2mm thick glass ND filters.

Two different test lasers were used, a 1mW HeNe laser at 633nm and a 5mW laser diode at 680nm.The HeNe produced an excellent TEM_{00} Gaussian beam. The laser diode produced a highly structured beam with circular diffraction rings. By varying the diode current above and below laser threshold the beam symmetry could be changed. This is because at currents below the lasing threshold the device behaves as a light emitting diode and emits a different intensity profile. The CCD camera and test lasers were mounted on a sliding rail allowing the separation between them to be varied from 10cm to over 1m, and thus changing the beam size on the detector. The digitised profile images were processed on a 486 PC using algorithms written in Turbo Pascal. Beam analysis results were then displayed in 256 colours on the computer's VGA screen.

Flexible software enabled the resolution, background level and threshold clip level to be varied for all of the algorithms during on line beam analysis. Fig 3.1 shows an example of the software.

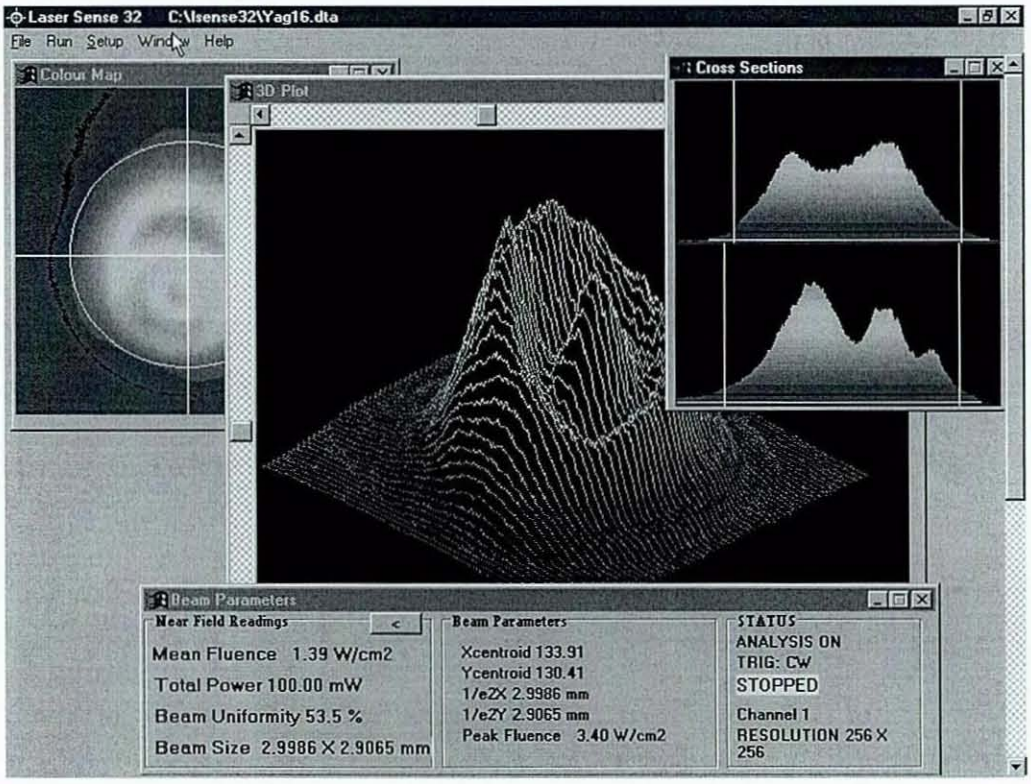

Fig 3.1. Multimode Spectron Nd:Yag beam profile

3.6 Discussion

Preliminary experimental results indicated the need for some form of sample window truncation before accurate measurements could be made of the beam diameter using momentum methods. Without truncation the value of the second moment beam diameter can vary dramatically with changes in background level and noise. Typically there can be a greater than 50% variation in computed diameter with a 5% variation in background level. Using energy fraction truncation variations can be reduced to within 3% or less with a 5% variation in background.

The accuracy of results are dependent upon the clip level chosen. Using a value corresponding to the E_p/e^2 threshold level (13.5%) a constant error in the calculation of the whole beam width is introduced. that is found to vary according to the beam shape.

By plotting the variation of second moment beam width against clip level a distinctive beam signature is produced that depends upon beam shape.

It was clear that further experimental work was required to determine the optimum algorithms for beam amplitude characterisation.

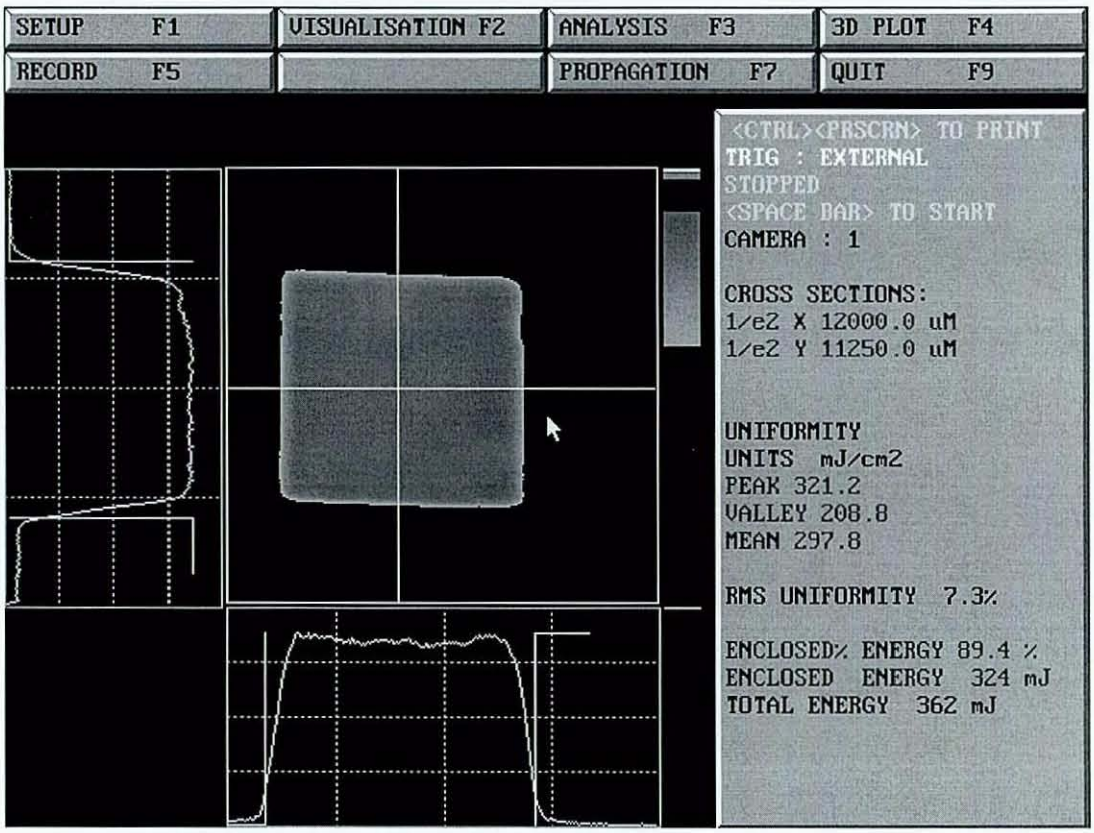

Fig 3.2 Display from the Exitech Laser Sense beam diagnostic system, showing threshold uniformity and beam interaction footprint of an homogenised excimer laser beam.

The author developed the software shown in figures 3.1 and 3.2. It computes a number of key parameters, including threshold beam uniformity, enclosed energy and beam widths, implementing the ISO compliant algorithms discussed in this chapter. Apart from offering useful visualisations of beam shape using false colour intensity maps and three dimensional surface plots, it provides qualitative data to assist in the alignment and setup of beam delivery systems.

Figures 3.3 and 3.4 show 3D plots of intensity profiles of laser beams taken using the Hardware described in section 3.5. The plotting and visualisation software is part of the Exitech P256C beam analysis system developed by the author

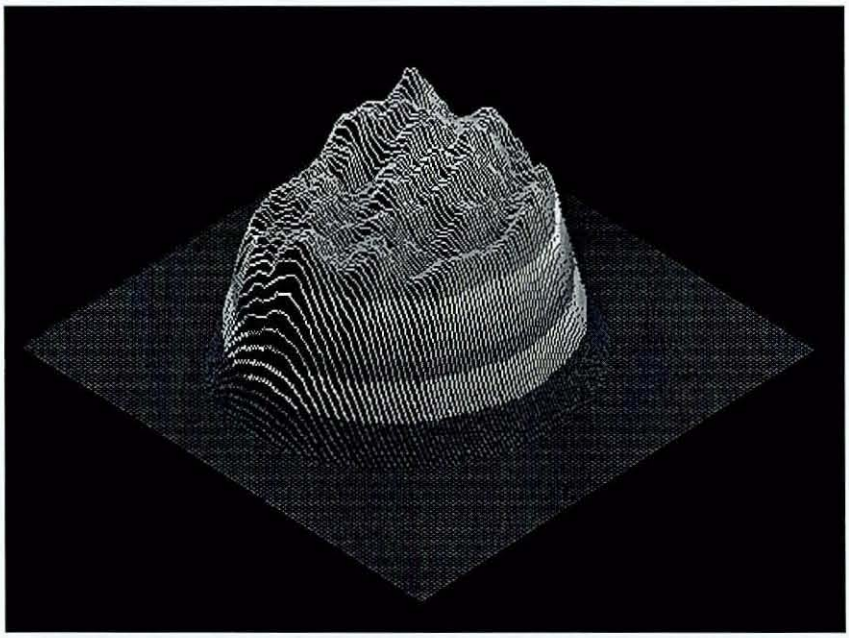

Fig 3.3. Near field profile, Spectron SL404 Nd:YAG laser 1.064 um, multimode, 10 mJ per pulse.

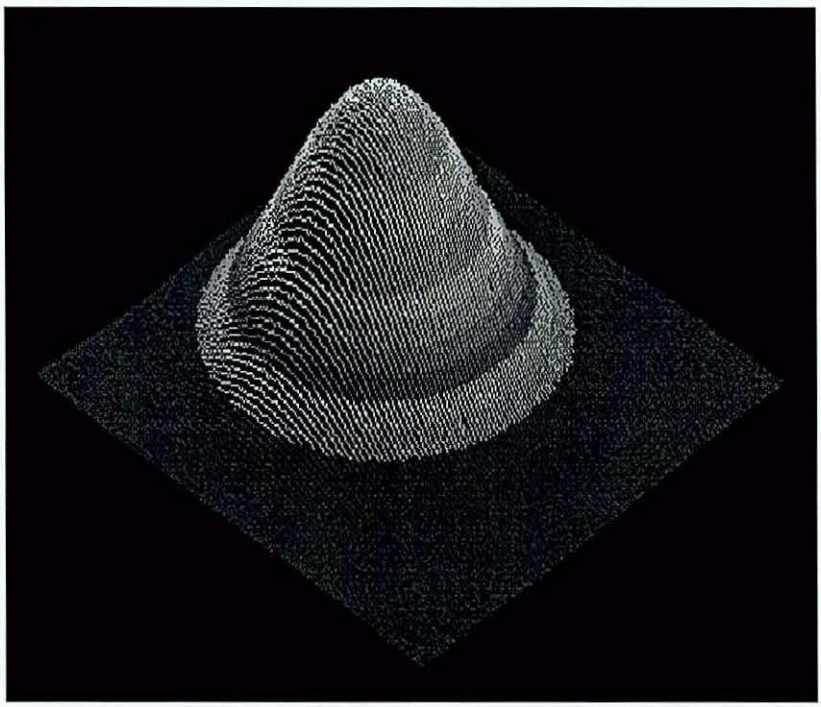

Fig 3.4 Near field profile, Metrologic HeNe laser 633nm, 5mW CW Gaussian beam profile

3.7 Polynomial shape fitting techniques

Polynomial fit techniques can serve as a useful measure of beam symmetry in laser materials processing applications. Work has been done on using both Gaussian fits, Hermite polynomials [6] and higher order moments such as kurtosis [7] to characterize beam shape and it effects on laser material interaction. This is also particularly applicable to the analysis of excimer laser beams, where by linear fitting to sections of the intensity profile, a slope angle can be determined, which can act as a useful aid to the alignment of optical systems.

It is can also be of use in the measurement of symmetry of the mode patterns of lasers in the near and far field, where it can act as a tool for optical alignment. Another use is to separate the measurement of "surface uniformity" of an excimer beam, from its alignment symmetry.

3.7.1 Polynomial fits

In order to fit an n^{th} order polynomial function to a line intensity profile of the laser beam, a standard set of fitting algorithms is used. These algorithms find the coefficients that best represent the polynomial fit of the data points (x, y) using the least squares method. The fitting algorithms input a sequence of y values and output a sequence of z values. Element z_i of the output array z is obtained by using the following formula:

$$z_i = \sum_{k=0}^{order} coef_k x_i^k \quad i = 0,1,...n-1 \qquad \text{Equ 3.22}$$

The mean squared error (mse) is obtained using the following formula:

$$mse = \sum_{i=0}^{n-1} |z_i - y_i|^2 / n \qquad \text{Equ 3.23}$$

Here order is the polynomial order, and n is the number of sample points.

The algorithm used to find the best curve fit is based upon the Least Squares method. A commercial software package by National instruments provided the software analysis libraries used to do this. These libraries were integrated into the beam analysis code used for these experiments and are described in more detail in reference [8].

3.8 Experimental results of fitting techniques

3.8.1 Linear fits

These fitting algorithms were applied to a number of different laser beam intensity profiles namely a raw excimer beam, a homogenized excimer beam and a multimode Nd:Yag beam. The first case considered is using a first order linear fit. The slope angle of the fit can be used as a measure of beam symmetry and is particularly useful as an aid to excimer beam alignment. Figures 3.5 a & b show the intensity profile of a cross section of a 248nm excimer beam. A linear fit has been applied to all points above 50% of peak intensity; because the beam is misaligned the profiles are not symmetric and exhibit slope angles of 16.1 degrees and –18.6 degrees respectively.

Although to a human engineer viewing these results this may seem obvious, this quantitative data could be used by an automatic control system to adjust the alignment of the beam.

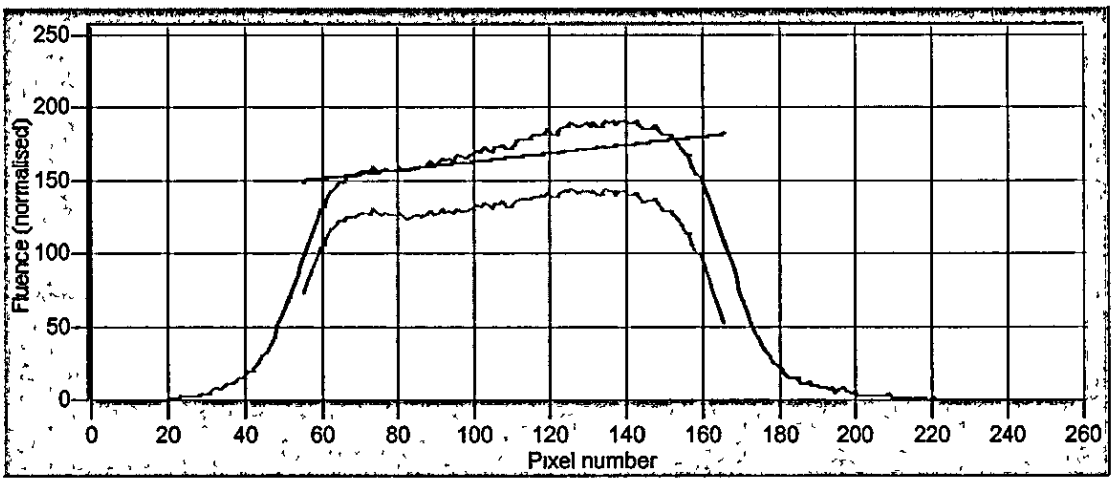

Fig 3.5b : Linear fit to misaligned excimer beam. Slope angle 16.1 deg

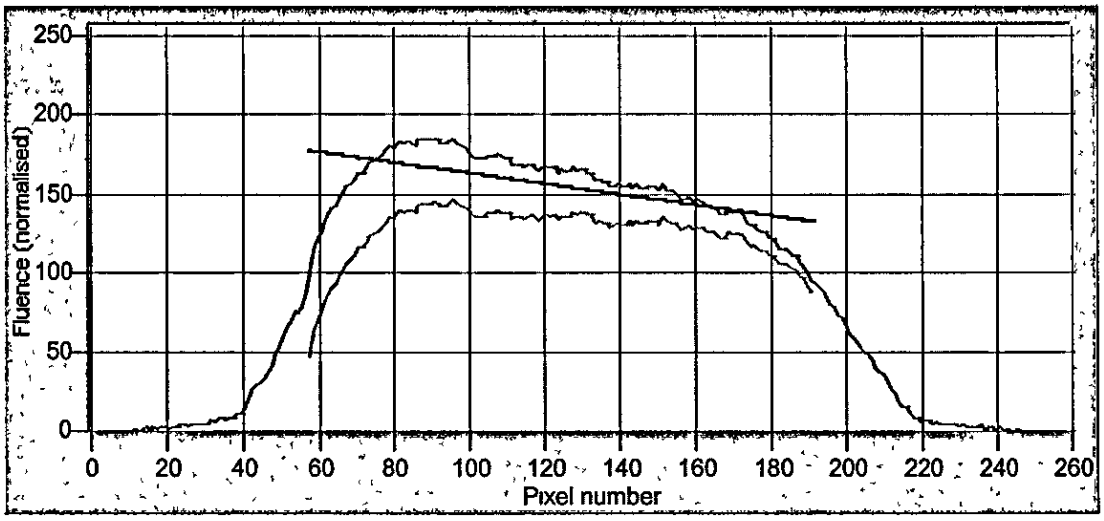

Fig 3.5a: Linear fit to misaligned excimer beam, slope angle –18.6 deg

Figure 3.6, shows the result when fitting to a well aligned homogenised excimer beam, the linear fit slope angle is 0.2 degrees, indicating a "Flat top" and high beam symmetry.

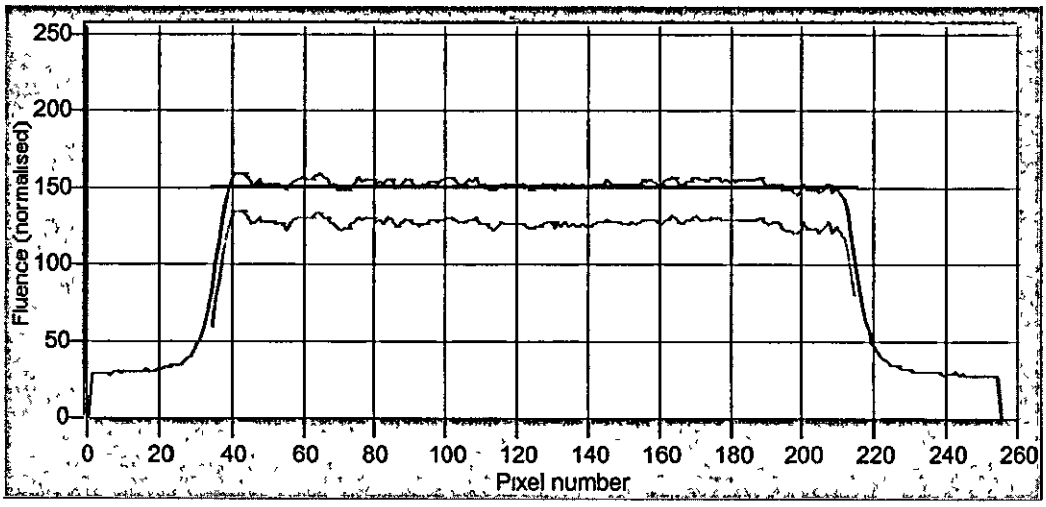

Fig 3.6: Linear fit to a well aligned "top hat" homogenised beam. Slope angle 0.2 deg, indicating good beam symmetry.

These techniques are already employed in beam analysis software installed in a variety of excimer laser production tools.

3.8.2 Higher order polynomial fits

The order of fit to use has been determined purely on an empirical basis, but for most cases a 6^{th} or 7^{th} order fit appears to give good results. Once the best curve has been fitted, the difference between fit and real data can be calculated. This data represents the "surface uniformity" of the beam, namely higher order noise and artefacts that are separate from the mode structure of the beam and may be introduced by the optics and coatings in the beam path.

Figure 3.7 shows a sixth order polynomial fit applied to the intensity profile of a TEM_{01} HeNe beam at 50% cut points. The fit follows the profile closely; the difference between the interpolated fit data and the actual data is also plotted as a second line (offset for clarity) below the main plot, and yields "surface uniformity" of approximately 1.8% rms with a normalised mse of 2.4.

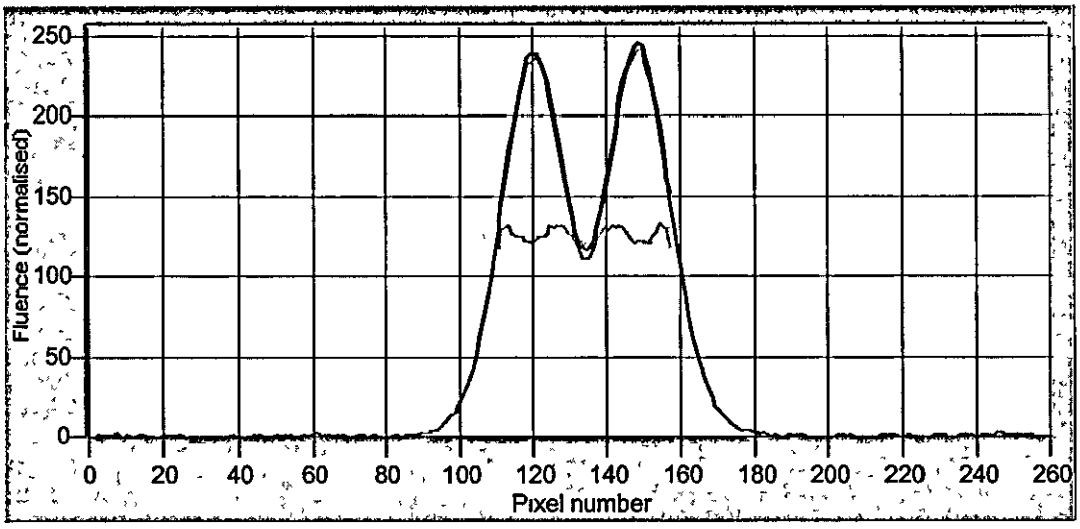

Fig 3.7.Sixth order polynomial fit to a TEM_{01} HeNe beam.

Figure 3.8 shows a sixth order fit applied to a typical KrF excimer beam profile. The difference between the interpolated data and the real data is plotted and gives a surface uniformity figure of 2.1% rms with a normalised mse of 6.74. The difference between the interpolated fit data and the actual data is shown as a second line offset for clarity below the intensity plot, and corresponds to the surface uniformity.

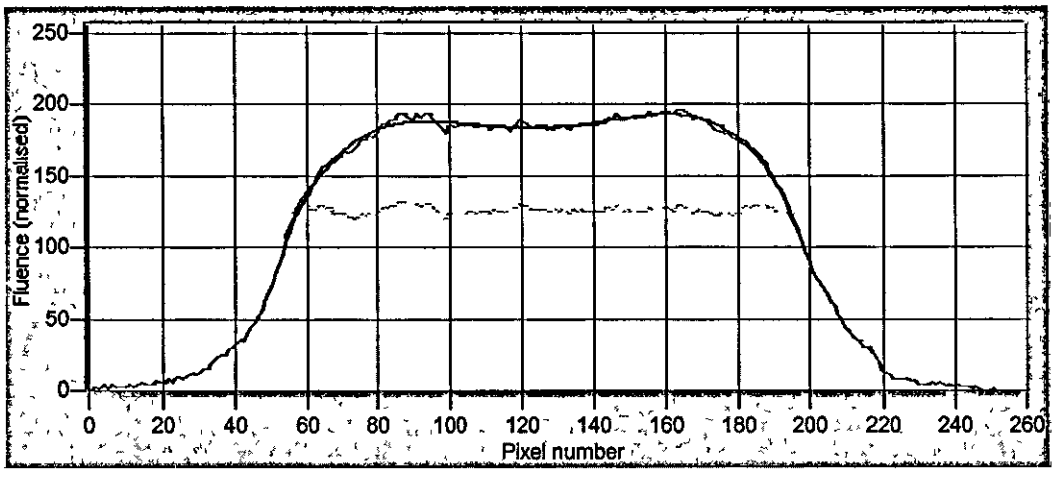

Fig 3.8. Sixth order polynomial fit to the cross section of a raw KrF excimer laser profile.

Figure 3.9 shows the beam profile of the excimer laser used in this test. Excimer beams often have fine surface structure superimposed upon the main beam profile. Whereas the beam shape can be homogenised to provide a flat top profile as in fig 3.6, this process will not change the fine surface structure. Using the results of the polynomial fit is a possible method for quantitatively measuring this structure independent of the actual beam shape.

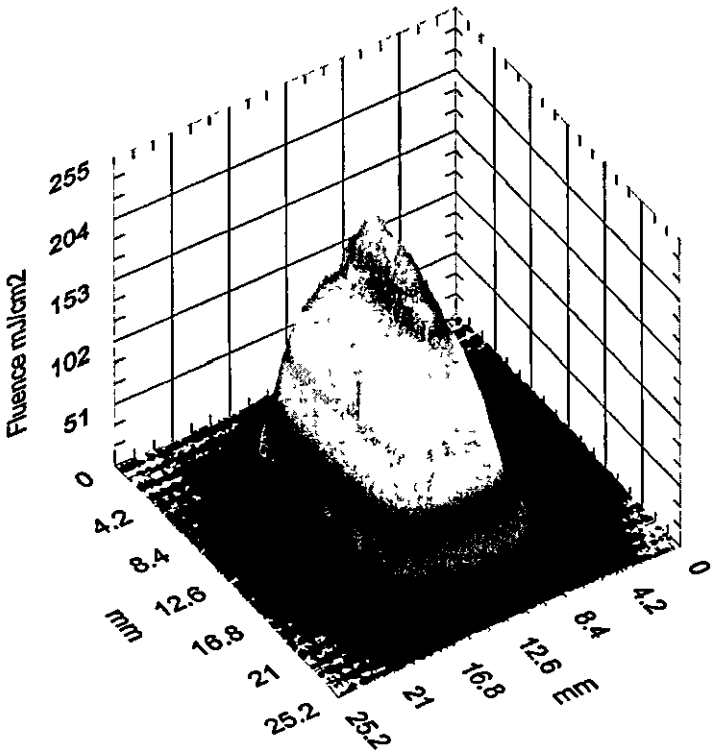

Fig 3.9. Fluence plot of a KrF excimer laser used for micromachining applications.

These algorithms are not specifically included in the ISO standards, but further research and testing would be of value.

3.8.3 Gaussian fits

Using Gaussian fits to quantify beam quality and symmetry is well known and many commercial beam diagnostic systems offer this feature [9]. This type of fit offers a useful visual indication of beam symmetry and shape. However care must be taken not to interpret results as an indicator to absolute mode quality and hence beam quality (as given by M^2). This measurement technique should be used only to characterise near field profiles. Figure 3.10 shows an example of Gaussian fitting software.

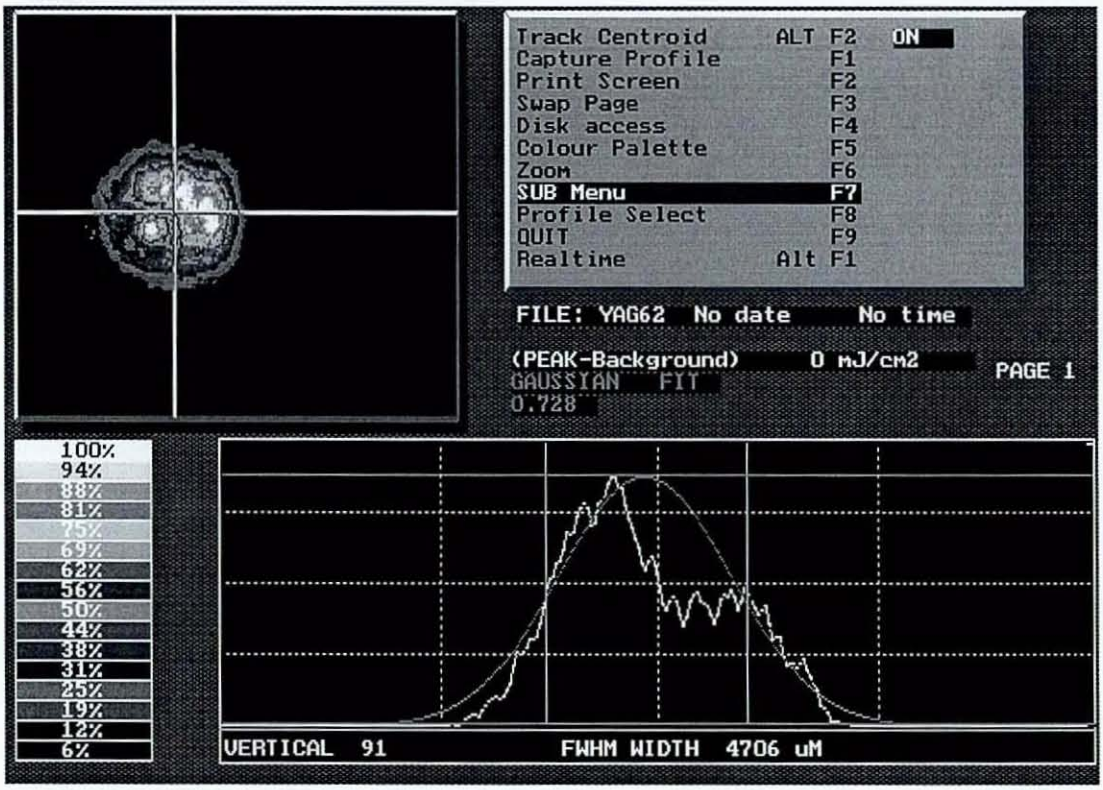

Fig 3.10: Example display of Gaussian shape fitting software written by the author.

3.9 Discussion of fitting techniques

Using shape fitting algorithms are of benefit when aligning optical systems as they can give a meaningful measure of beam symmetry. They are not a replacement for true

beam propagation measurements such as the evaluation of M^2 . In the past Gaussian fits have been used as a measure of beam quality for TEM_{00} beams, these can yield misleading results. There is scope for further work on this topic, particularly as an aid to automatic beam alignment.

3.10 Conclusions

In this chapter a variety of methods for the measurement of beam shape have been described. Of particular note is the development of the concept of threshold beam uniformity, which is explored in further chapters and has now become part of the ISO standard for laser beam characterisation.

Polynomial shape fitting techniques have potential in aiding automatic beam alignment and characterisation systems. By providing a quantitative measure of beam symmetry and by revealing beam surface structure they may be used to measure degradation arising from optics and coatings in beam delivery systems.

A number of newer image analysis techniques warrant further study. The use of Fourier transform and wavelet methods could be useful for analysing noise due to optical interference in the beam profile. Fractal analysis is already used in the evaluation of surface texture; it may be of some use in analysing intensity profiles. Advances in the processing power of desktop computers, enable ever more complex analysis algorithms to be used.

3.11 References

1. Draft ISO 13 694-1 standards document "Test Methods for laser beam parameters: Amplitude and phase distribution Part 1: Amplitude."

2. P Loosen et al, "Laser Beam Characterisation and Measurement techniques", Proceedings from the workshop on laser beam characterisation, Madrid (1993)

3). B Eppich, "Reliability of Beam Parameter Measurements with CCD cameras"

Proceedings from the workshop on laser beam characterisation, Madrid (1993)

4). P Loosen et al, "Laser Beam Characterisation and Measurement techniques" Proceedings from the workshop on laser beam characterisation, Madrid (1993)

5). P Apte, M C Gower, "Computational methods for beam amplitude characterisation", Proceedings of the 2nd Workshop on laser beam characterisation, H Weber et al eds, FestKorper Laser Institut, Berlin, (1994)

6). G Dumitru, D G Sporea and C Timus, "Computation of the 3D energy density profile using a linear array of pyroelectric detectors", Proceedings of the 4th workshop on laser beam characterization, Munich (1997)

7). M Scholl, G Herziger, "Kurtosis as a tool parameter for laser welding", Proc SPIE 2375, 130-141, (1995)

8). National Instruments Component Works Analysis Library V3.0, (2000)

9). Coherent Instruments, "Beam View V2.3", Operating manual, (2000)

CHAPTER 4

TESTING OF THE DRAFT ISO STANDARDS FOR BEAM PROPAGATION AND INTENSITY PROFILE MEASUREMENT

4.1 Introduction

International standards are currently being derived that address the measurement and testing of beam divergence, size, amplitude and phase distribution of laser beams. Descriptions are given of experiments performed to support these emerging standards, together with new approaches to noise reduction and profile measurement. Experiments are carried out to test some of the recommendations on beam characterisation as described in the ISO standards documents; CD 11 146,'Optics and optical instruments, Test Methods for laser beam parameters: Beam widths, divergence angle and beam - propagation factor, and CD 13694,'Optics and optical instruments, Test Methods for laser beam parameters: Power (Energy) Density distribution.' These documents have been developed to meet the growing need to provide calibration references and standardised algorithms for commercial beam profiling equipment. The results from these trials were presented at international conferences and have played a part in the development of the standards.

4.2 Testing the draft ISO standard for beam propagation measurement.

There has been much theoretical study and modelling of Gaussian beam propagation using ideal Gaussian beams, and a consistent and useable measure of beam quality has been proposed by Siegman [1] based on the invariance of the space beam width product. The strength of using this approach to characterise the propagation of laser beams is that it may then in theory be extended to characterise a wide range of beams. The method

relies on the Fourier transform relationship between the intensity distribution of a beam and it's spatial intensity distribution at the focus of a lens.

According to this theory the propagation constants of any beam can be derived so long as the beam width is calculated using the square root of the variance of the spatial intensity distribution, the so-called second moment definition. Beam widths calculated in this way then conform to the hyperbolic propagation law. Hence fitting the beam width to a hyperbola yields results for the size and location of the beam waist from which the propagation constants can be derived. Although theoretically elegant this approach suffers from a number of drawbacks that hinder its practical implementation.

A particular problem is the calculation of moment integrals in the presence of optical and electrical noise. Due to the square law weighting of the integral, small variations in intensity far from the beam centroid can give large errors in the calculation of beam widths. Moreover for beams containing a large diffracted component the moment integrals can oscillate unpredictably in both the near and far fields unless suitable windowing or truncation of the integral is performed.

The approach adopted in this experiment is to limit the range of integration by introducing variable intensity clip levels to reduce the area of integration. The effect of clipping on the calculation of propagation constants is then tested for three different laser beams using a reference lens placed at different distances from the laser aperture.

4.2.1 Calculating beam widths using moments

If the output of the detector in Volts at (x,y) is defined as A(x,y) and R is the responsivity of the CCD detector array in (Volts/Watt)/cm^2 and assuming that the profile data is digitised as a 256 x 256 square pixel array, then the moments of the power density distribution being measured can be expressed as:

Zero order (Total Laser power P_H)

$$P_H = \sum_{0}^{255}\sum_{0}^{255} A(x,y)\,R^{-1} \qquad \text{Equ (4.1a)}$$

First order linear moments (Beam centroid)

$$x_c = \frac{1}{P_H}\sum_{0}^{255}\sum_{0}^{255} x.A(x,y).R^{-1} \qquad y_c = \frac{1}{P_H}\sum_{0}^{255}\sum_{0}^{255} y.A(x,y).R^{-1} \qquad \text{Equ (4.1b,c)}$$

Second order centred linear moments (variance) Equ (4.2 a,b)

$$< x^2 >_c = \frac{1}{P_H}\sum_{0}^{255}\sum_{0}^{255}(x - x_c).^2 A(x,y).R^{-1} \qquad < y^2 >_c = \frac{1}{P_H}\sum_{0}^{255}\sum_{0}^{255}(y - y_c).^2 A(x,y).R^{-1}$$

The Beam diameters are then given by

$$d_{ox} = 4\sqrt{< x^2 >_c} \qquad d_{oy} = 4\sqrt{< y^2 >_c} \qquad \text{Equ (4.3 a, b)}$$

Higher order moments can be defined in a similar way.

All of these summations are carried out over the full dynamic range of the detector. Calculations using real beams are highly sensitive to the effects of baseline offset and background noise. In order to overcome these problems limits are imposed on the range of integration.

4.2.2 Truncated and Reduced Moments

Of great importance to the computation of moment integrals is the proper selection of baseline offset and spatial limits of integration in a self-consistent manner. Several authors [2] & [3] have evaluated and compared moment and 'power in bucket' methods of calculating beam widths using somewhat arbitrarily set integration limits and clip levels. For practical instrumentation these procedures must be carried out automatically and consistently. For this reason it is necessary to develop and test algorithms for automatic baseline compensation and integral truncation.

4.2.3 Using Histogram analysis to find baseline offset.

The basic histogram summation is as follows

$$H[I] = \sum_y \sum_x I(x,y) \qquad \text{Equ (4.3)}$$

Where $I(x,y)$ is the local intensity at each pixel site and H[I] is the beam intensity histogram..

Reducing the summation to an intensity histogram is computationally convenient because several parameters may be derived from it without re-computation. From analysis of the beam intensity histogram H[I] the background count level can be calculated by examining the first peak count of the histogram. Assuming that the beam profile does not fill more than about 80% of the detector area the lowest peak count can be used as a reliable measure of background.

Due to noise and sensor fixed pattern non uniformities, the background peak will never be a singularity but a truncated Gaussian-like distribution which can present difficulties in precise background determination and can particularly influence results when using area summation algorithms that are sensitive to noise. Under such circumstances it may be desirable to set a fixed offset clip level above the background distribution [4], thus ensuring unambiguously that there is no false contribution due to background noise in the moment integrations.

Once the background I_B has been determined, the total integrated power can be calculated by summing the histogram as

$$P_H = \sum_{Background}^{Peak} H[I]R^{-1} \qquad \text{Equ (4.5)}$$

With this method the total beam power above a defined clip level can be calculated.

4.2.4. Calculation of a Moment Histogram.

Similarly the moment integral may be reduced in a similar fashion to a histogram such that :

$$Mx^n[I] = \sum_y \sum_x I(x,y)\,(x-x_c)^n \qquad \text{Equ (4.6)}$$

Then in order to calculate the reduced moment

$$< x^n >_{clipc} = \frac{\sum_{Clip}^{Peak} Mx^n[I]}{\sum_{Clip}^{Peak} H[I]} \qquad \text{Equ (4.7)}$$

Other moments and higher orders can be evaluated in a similar manner. In this form the values of second moment radius for different levels of clip can be easily evaluated without need to completely re perform the integral each time.

4.2.5 Experimental arrangement.

The laser source, reference lens and CCD camera were mounted on a 100 cm long optical rail. The laser and lens were kept at fixed positions and the CCD detector moved for each measurement run. Suitable ND attenuating filters were placed in a holder directly in front of the CCD detector. Care was taken to keep all optical components scrupulously clean and free from aberration. Plano convex lenses of 50 mm diameter fabricated in fused silica were used to generate beam waists in accordance with the recommended ISO procedure. The measurement runs were performed for two different lens positions for each laser.

The tests were carried out using a windowless Cohu 4712 CCD camera with agc disabled, for low noise and high linearity of response. Three sources were tested. A 1 mW Metrologic 633 nm TEM_{00} HeNe laser ,a 5 mW PMS multiline (594,605,611 nm) TEM_{01} (donut mode) HeNe laser and a laser diode (680 nm) with collimating optic.

A video digitiser of 8 bit (256 grey level) resolution and high linearity of better than 1 least significant bit was used to acquire the profile image. The image was digitised into an array of 256 x 256 square pixel resolution. Although this digitisation effectively under samples the full camera resolution, which is approximately double this value, for the purposes of this experiment the resolution is adequate and computationally convenient.

4.2.6 Beam Analysis software

Data acquisition and analysis was carried out using a 486 computer running Exitech and Profile 256™ Beam analysis software (see figure 4.1). Custom procedures were written in Turbo Pascal to calculate tables of moment widths at different clip levels.

Particular care was taken to avoid the effects of rounding errors and numerical overflow, because during moment calculations numerical values can become very large and this can cause some subtle compiler errors. Finally the data was formatted and imported into a scientific Mathematics package (Mathematica) for Hyperbolic fitting and the calculation of propagation constants.

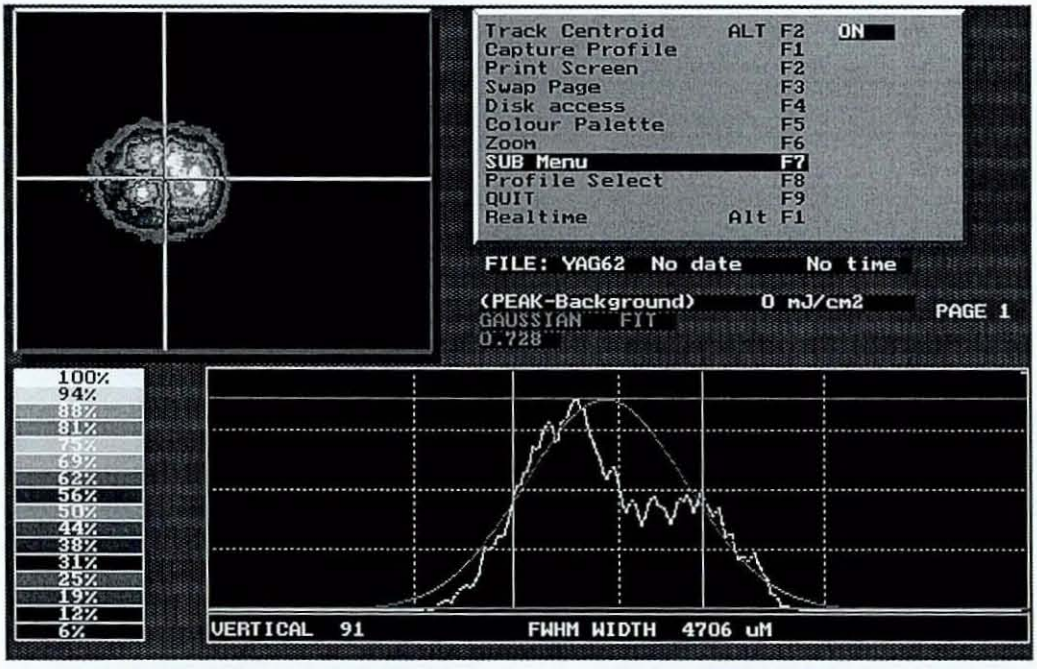

Fig 4.1: Beam Analysis system

4.2.7 Calculation of Moment tables.

The calculation speed of second moments at different clip levels can be greatly improved by computing moment tables. This procedure involves using an algorithm that sorts the results of the moment integrals into a table according to their intensity.
In this case using 8 bit data the result is a table of 256 values. Once the table has been calculated, lists of beam diameters can be calculated for each different clip level.

4.2.8 Computation of Beam waist Loci and M^2

These lists of data were imported into a mathematics package (Mathematica). This package then performed quadratic fitting of the data to yield the coefficients of the beam propagation hyperbola. Figure 4.2 shows an example of the hyperbolic fit for the TEM_{00} HeNe laser. The coefficients used for fitting were then used to derive beam parameters in accordance with ISO recommended procedure [5], an explanation of which was given in chapter 2, section 2.6.

This procedure yielded values for beam waist location, beam waist diameter,M^2 , laser waist location and laser diameter at waist.

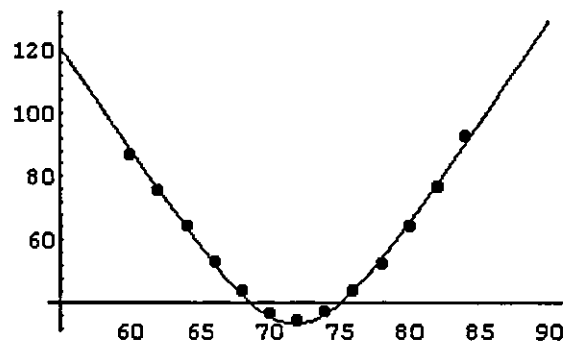

Fig 4.2 Least Squares Hyperbolic fit

The beam parameters were then tabulated and plotted as graphs showing their variation with increasing clip level. Each increase in clip level corresponds to one digitiser count. This was done for all three types of laser beam studied.

Typical sets of data are presented on the following pages (Figures 4.3 and 4.4). The data for the Laser diode beam is not presented. For this beam there was great difficulty in obtaining any accurate hyperbolic fits due to the presence of diffraction maxima around the beam waist. Alternative techniques for analysing this type of beam are currently being investigated.

4.2.9 Results and Analysis

A study of the graphs in figures 4.3 and 4.4 reveals some interesting characteristics. The graphs of waist size and location appear to converge to a relatively stable value at higher clip levels exhibiting a 'knee' at lower values of clip level. This behaviour corresponds to the effective background of the detector system. The transition to a stable value is very pronounced due to the noise sensitivity of the second moment beam width calculation.

The effective background levels for each beam profile were also calculated using Histogram analysis. These were 3 levels (digitiser counts) for the TEM_{01} data and 7 levels for the TEM_{00} data. The convergence point for the plots was generally several clip levels higher than the background calculated using histogram analysis.

4.2.10 Beam waist minimum diameter and location.

The beam waist diameter and location (at focus) plots for both HeNe lasers are shown in figures 4.3 c,e and 4.4 b,c. For both cases the value for waist location converges quickly to a stable number that then varies less than one percent with increasing clip level. This is not a surprising result because the calculated location is dependent upon relative beam width and not on the absolute value. The effect of increasing clip level for Gaussian beams is to change the absolute beam width but not it's relative value.

The result for the measured beam diameter shown in figures 4.3d and 4.4d does not converge as quickly and exhibits variations in the region of ten percent per level near background, and reduces to about three percent per level well above background.
Both sets of data show a sharp 'knee' above the clip level corresponding to the true background count.

4.2.11 M^2 calculations.

The M^2 plots for both HeNe lasers are shown in figures 4.3b and 4.4a. As can be seen, the calculated value for M^2 steadily decreases with increasing clip level by several percent. This variation is greater than that displayed by the beam width and location plots. Interestingly the value for the TEM_{00} laser drops below unity at a clip level of 10, which demonstrates the sensitivity of this parameter to small errors in the beam width measurement.

4.2.12 Beam diameter

The calculation of second moment beam diameter were performed for both HeNe lasers and the results plotted in figures 4.3d and 4.4d.The behaviour of these plots follows closely that of the corresponding beam width and location plots, demonstrating a sharp knee in the curve then fast convergence to a relatively stable value at higher clip levels.

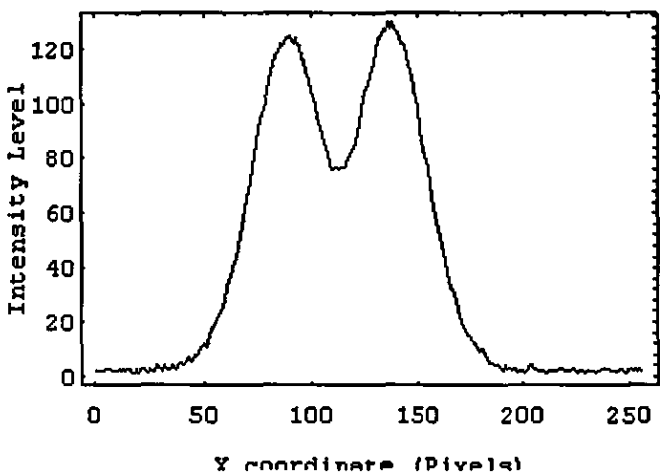

Fig 4.3a
HeNe, mixed mode TEM_{00} TEM_{01}.

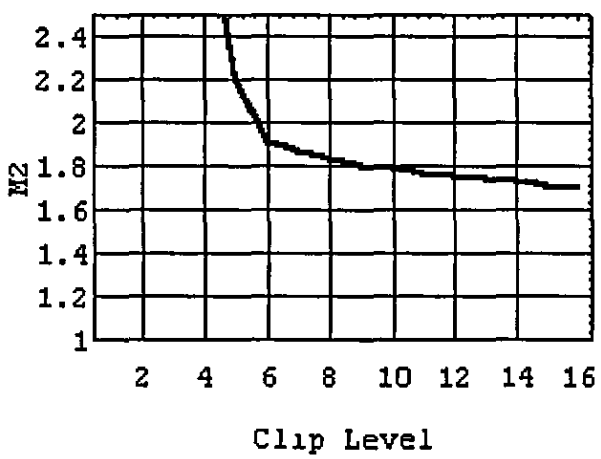

Fig 4.3b
Mixed mode.
The variation of M^2 with clip level

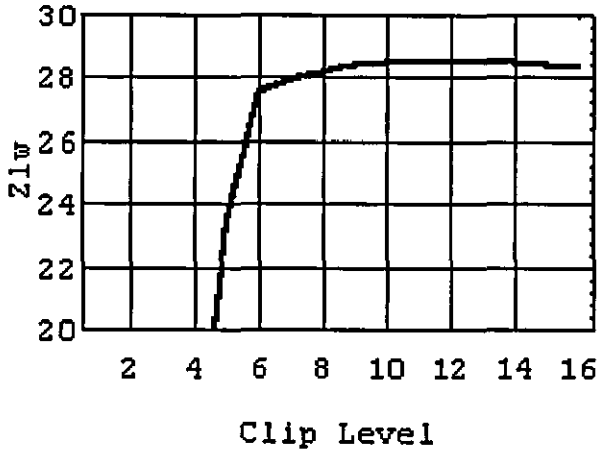

Fig 4.3c
Mixed mode.
The variation of minimum Beam Waist diameter with clip level

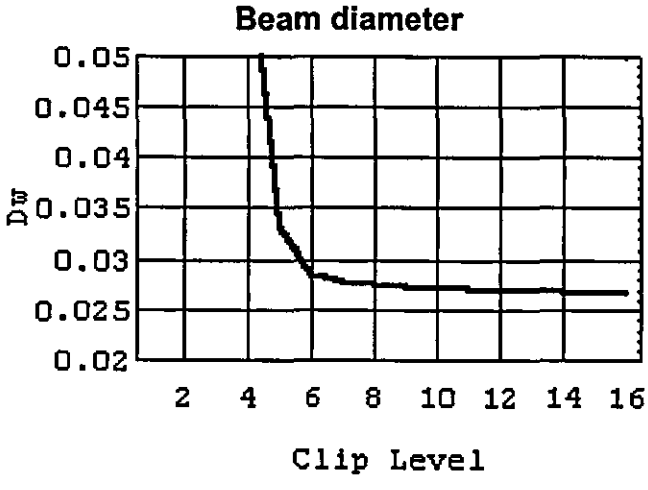

Fig 4.3d
Mixed mode.
The variation of 2nd moment Beam diameter with clip level

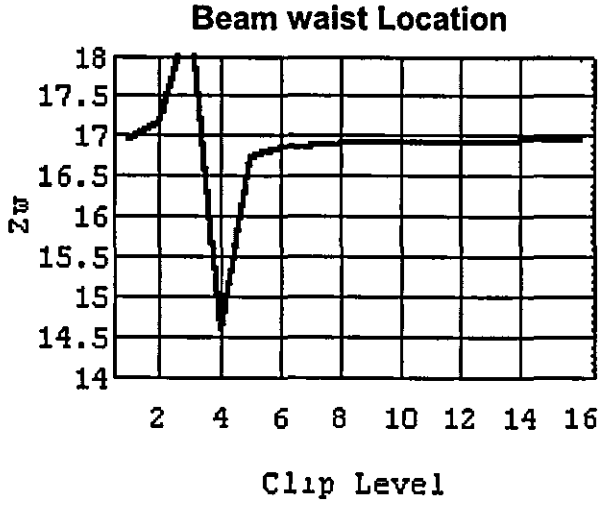

Fig 4.3e
Mixed mode.
The variation of Beam waist location with clip level

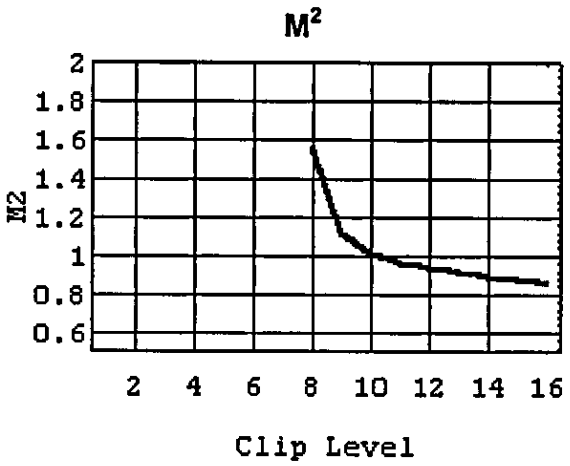

Fig 4.4 a
Single mode.
HeNe,TEM_{00}
The variation
of M^2 with
clip level

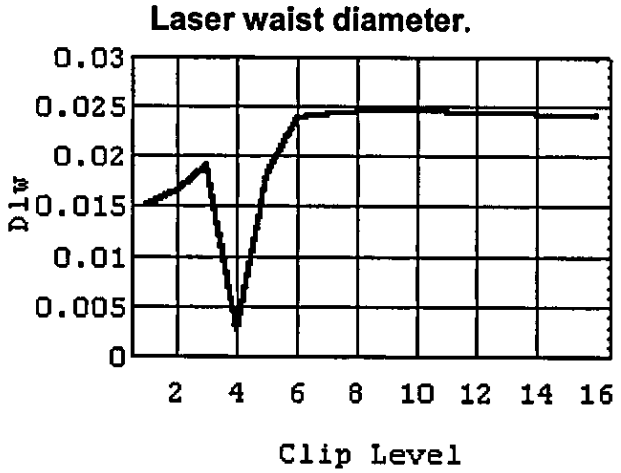

Fig 4.4 b
Single mode.
The variation
of minimum
Beam waist
diameter with
clip level

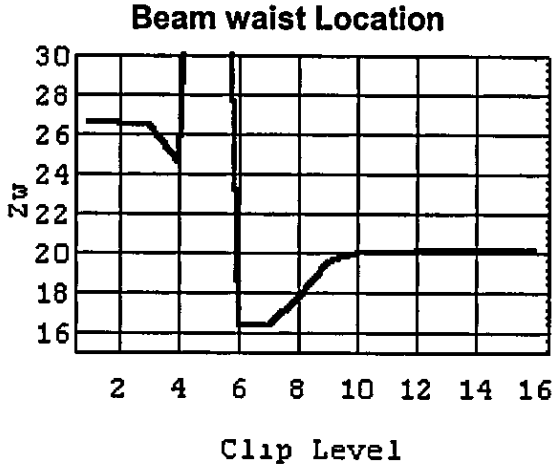

Fig 4.4 c
Single mode.
The variation
Beam waist
location with
clip level

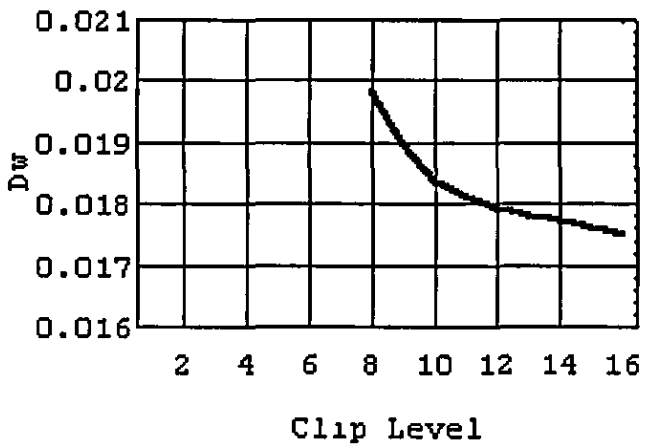

Fig 4.4 d
Single mode.
The variation
of 2nd moment
Beam diameter
with clip level

4.2.13 Discussion

Histogram analysis can be used to find the background level of beam profile data but care must be taken in interpreting the background energy distribution and setting correct clip levels. Significant variations in the calculated values of beam parameters were observed at clip levels close to the estimated detector background level. Clip level noise suppression is useable for Gaussian-like beam profiles, but results are inconsistent for non-Gaussian beams particularly those that contain diffractive components.

There is a need to explore other window truncation algorithms such as Gaussian windowing and perform further extensive experimental testing. Currently we are repeating these experiments using lower noise CCD cameras and higher dynamic range digitisers.

4.3 TESTING THE DRAFT STANDARD FOR LASER BEAM POWER AND ENERGY DENSITY DISTRIBUTION

This section presents results on the experimental testing of characterisation methods for laser beam power and energy density distribution as described in draft ISO standards ISO 11146 and 13694 .The tests were carried out using various laboratory and industrial laser sources. The accurate and repeatable measurement of distributions is of particular concern. Attention has been paid to background compensation and noise reduction methods. Tests were made to calculate beam uniformity, goodness of fit, beam size and the higher order moments of beam profile data derived from various CCD array detectors. These methods are evaluated in the context of their usefulness for on line monitoring, final laser test, and laser R&D.

Tests were initially performed on a HeNe source, an industrial excimer workstation, and an industrial YAG laser. Inexpensive beam analysis hardware, typical of that available to an industrial user was used to obtain the results.

Some seventeen laser parameters as specified in the standards documents were measured simultaneously on line. Temporal variations of these parameters over a period of time were then monitored. The data series were stored for each parameter, from which the mean, minimum, maximum and standard deviation were computed. These results were then put into spreadsheet format and charted in the form of a typical laser test report.

4.3.1 Experimental setup

The detector system consisted of a windowless Pulnix TM6ex CCD camera coupled to a stack of neutral density filters to provide secondary beam attenuation. Primary attenuation was achieved by the use of beam splitters. Since the active detector area uses only 4mm x 4mm it was necessary in some cases to reduce the beam size using imaging optics. A typical beam analysis system layout used to collect test data is shown in figure 4.5

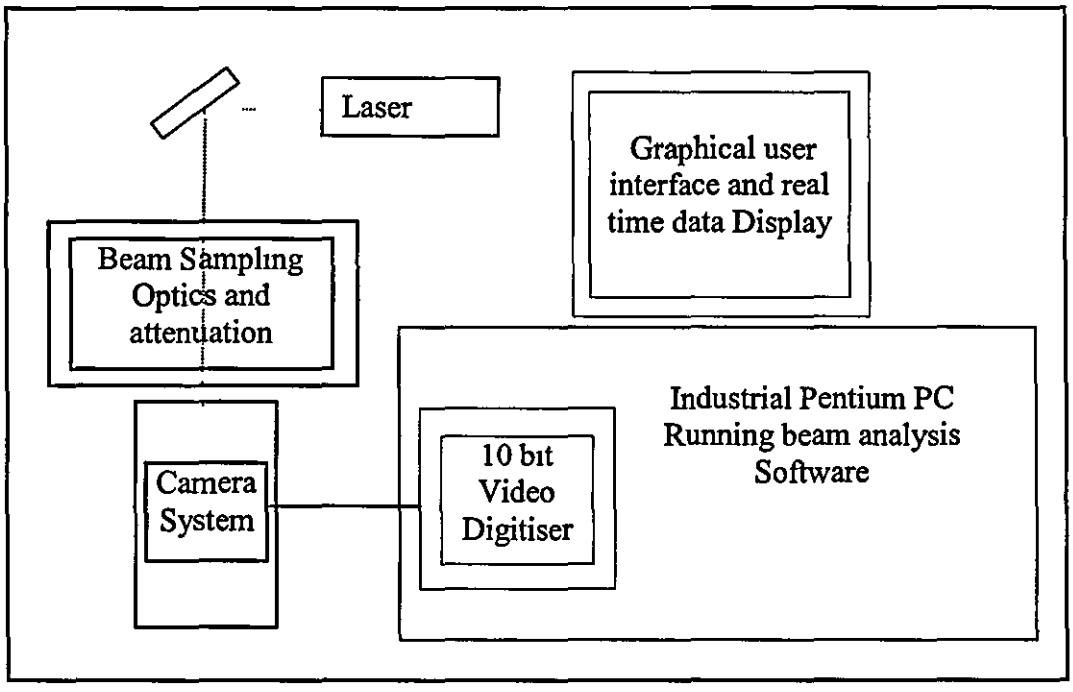

Figure 4.5. Experimental setup

The image profiles from the camera were digitised using a specially developed video digitiser card, which can digitise to both 8 bit (256 grey level) and 10 bit (1024 grey level) resolutions. However the limiting factor to dynamic range is camera noise, so the 10 bit facility was not used for the main tests. The digitised profile data was analysed using custom developed Exitech Laser Sense beam analysis software. This has been written using a new 32 bit Pascal compiler (Borland Delphi) which greatly facilitates the development of image analysis algorithms by providing a flat address space, easy manipulation of huge array structures and optimised code compilation. Running under MS Windows, beam analysis data could be exported directly to spreadsheets for further statistical analysis and to charting packages for data presentation.

The software was chosen to reflect the power of the computer platforms now available to new industrial users at reasonable cost without redress to specialist computing facilities.

4.3.2 Simulation

In order to aid the development of beam analysis algorithms it is very important to test their accuracy using simulated 'reference' beam profiles. To this end a beam profile simulation program was developed that generates test beam profiles in the same data file format used by the analysis software. The data format is 8 bit at 256 x 256 pixel resolution.

Beam profiles can be generated with Gaussian or Tophat profiles. Parameters that can be varied include amplitude, diameter, edge steepness and noise. Moreover complete profile sequences may be automatically generated in which only one parameter is varied. These simulated beam profile sequences were then imported into the beam analysis software package and analysed. The results of the beam analysis sequence were then stored in spreadsheet format for plotting and further statistical analysis.

Using this test method beam width calculation algorithms could be tested for their accuracy over a wide range of beam diameters, or background compensation methods could be tested for their sensitivity to noise.

4.3.3 Test sources.

Once the algorithms had been proven using simulated data further tests were made using both a laboratory and high power industrial laser source. Two very different laser sources were chosen, with the aim of illustrating the usefulness of the range of analysis algorithms in the draft ISO standard.

For the lab tests a Metrologic 2 mW HeNe laser with a nominal TEM_{00} mode at 633 nm was used. The digitiser was run in high-resolution full frame 512 x 512 pixel mode, although beam analysis was performed only upon a 256 x 256 pixel window centred upon the beam.

The industrial laser source used for on line monitoring was a Lambda Physik LPX 210i excimer laser, operating at 248 nm with a KrF gas mix. A combination of beam splitters, imaging optics and Inconel coated filters were used to attenuate the beam and

reduce it in size by a factor of 10 so it could be analysed with a UV sensitive COHU 6712 CCD camera. The digitiser was run in 256 x 256 pixel single field mode, synchronised to the laser trigger. The laser beam was analysed both before and after beam homogenisation.

4.3.4 Analysis algorithms.

The beam analysis equations used are outlined in refs [6], [7] and [8] and the draft ISO standards ISO 11146 and 13694. As outlined in the draft standards algorithms to implement these equations were then developed to calculate the following beam parameters.

Beam Power :

1. Beam Power (P)
2. Effective Power (P_n)
3. Average Power Density (H_n)

Beam Location :

4. Maximum Location (X_{max},Y_{max})
5. Centroid Location (X_c,Y_c)

Effective Beam sizes :

6. Azimuth angle (Φ)
7. Widths (d_{nx},d_{ny})
8. Diameter(d_n)
9. Area (A_n)
10. Irradiation area (A'_n)

Temporal statistics :

19.Time Average

20.Std deviation

Beam shape (Footprint) :

11. Ellipticity(ξ_η)
12. Flatness Factor (F_n)
13. Uniformity (U_n)
14. Plateau Uniformity (U_p)
15. Fractional Power (f_n)
16. Edge Steepness (s,0.1 - 0.9)
17. Goodness of Fit C
18. Roughness of Fit R

4.3.5 Background correction

It is very important to correct for the effects of digitiser baseline offset and background light before performing any beam analysis calculations. This is particularly so for calculations involving weighted integral sums such as power and moment calculations. The following methods can be used: The analysis system should store a darkfield map of the detector with the laser shutter closed. This map should then be subtracted pixel by pixel from the beam profile data.

Average background determination:

Average at least ten readings taken at evenly spaced intervals over the area of the darkfield map of the detector. This value should then be subtracted as a fixed offset from the beam profile data.

Histogram analysis:

This procedure can be performed directly upon the beam profile data without the need to store a background map. The most frequently occurring value in the profile data below the mean is found and taken as the background reference. This method only works well if the detector area is filled by no more than about 50 % by the beam otherwise the background count becomes difficult to distinguish.

4.3.6 Optimisation and checking.

The accuracy of the computed background level can be checked using linear programming techniques. The simplest method is to compute the ratio of whole beam integrals for two different window sizes. If the background correction is exactly correct then this ratio will be close to one. In practical situations, due to noise and detector non uniformity the ratio should fall within the minimum acceptable measurement uncertainty for the application.

If the background level is non uniform or is changing with time then it is not possible to fully correct it using the methods so far described. In these cases limits need to be placed upon the range of integration.

4.3.7 Choice of integration Limits.

Once the background level has been corrected there can still remain problems due to detector noise and optical background noise. Because these sources of error affect the calculation of beam widths and the higher order moments, they are of fundamental importance.

One computational approach to this problem is to introduce a clip level or integration threshold (n) [9]. This is defined as a percentage of the maximum energy density (Emax). All beam analysis integrations are then performed only on pixels with intensities (> nEmax). The effect of this threshold method for integration truncation is to transform statistical errors into systematic errors, which are more easily quantifiable. Moreover the value of neta can be chosen to reflect an application specific value like a material ablation or marking threshold.

For example in the annealing of amorphous silicon wafers by excimer laser, the user would typically set n to >80 %. On the other hand if the application is to measure the spot size of a Nd:Yag laser for cutting the user might choose n < 5%. The effect of clip threshold on the measurement error of the second moment diameter of a Gaussian beam is shown in figure 4.7.

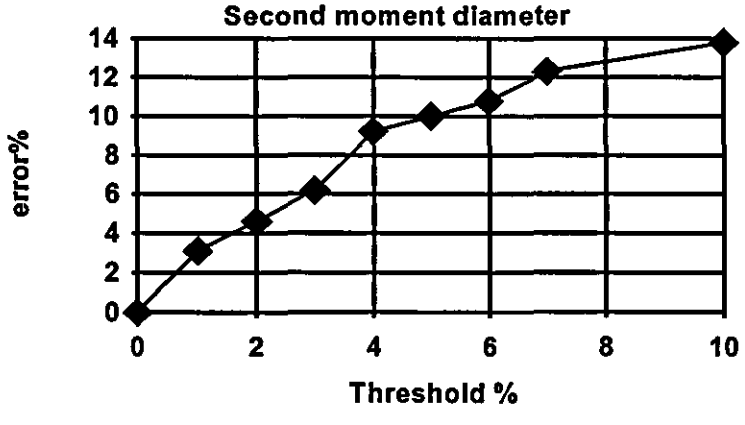

Fig 4.7
The variation of error in the second moment beam width versus threshold level for a real Gaussian beam .

The following figures 4.8 a,b,c show results of tests on the variation with threshold level of three key beam profile parameters, beam diameter, and effective beam energy and irradiation area.

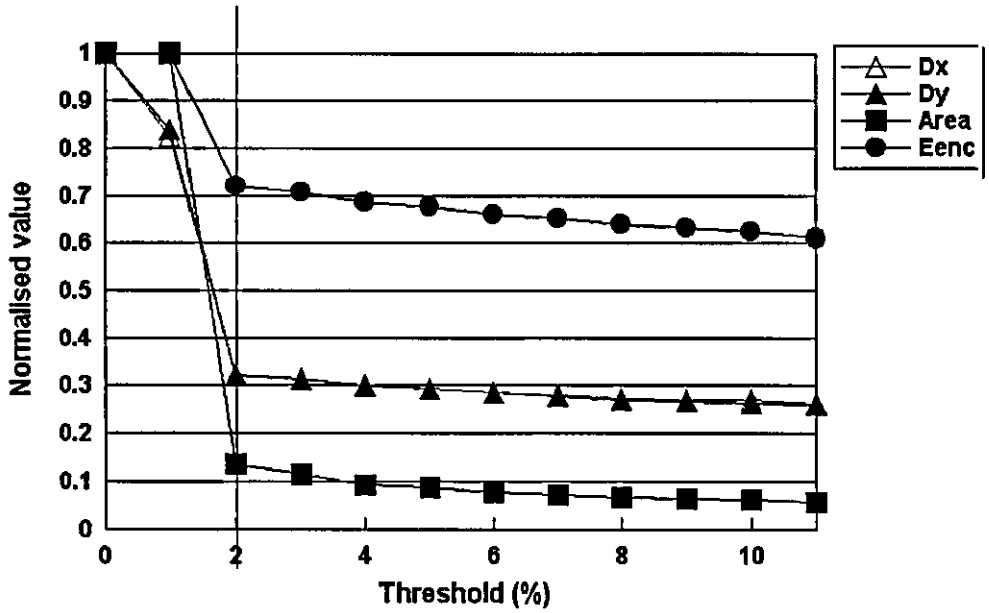

Fig 4.8(a)
The variation of key parameters with threshold level for a real Gaussian beam. Note the sharp 'knee' in the curves at the background level. The plot data for Dx is almost identical to Dy.

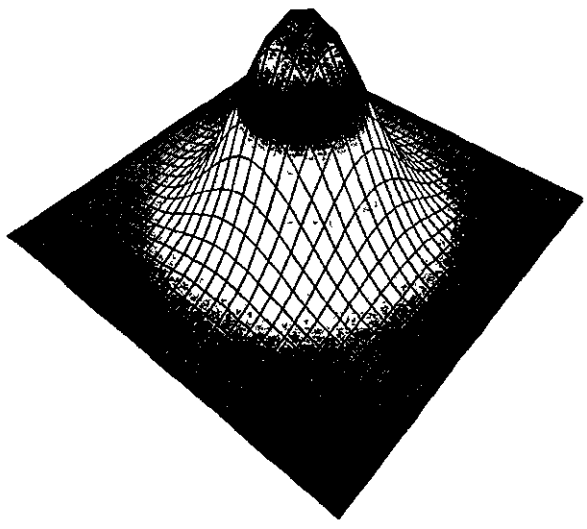

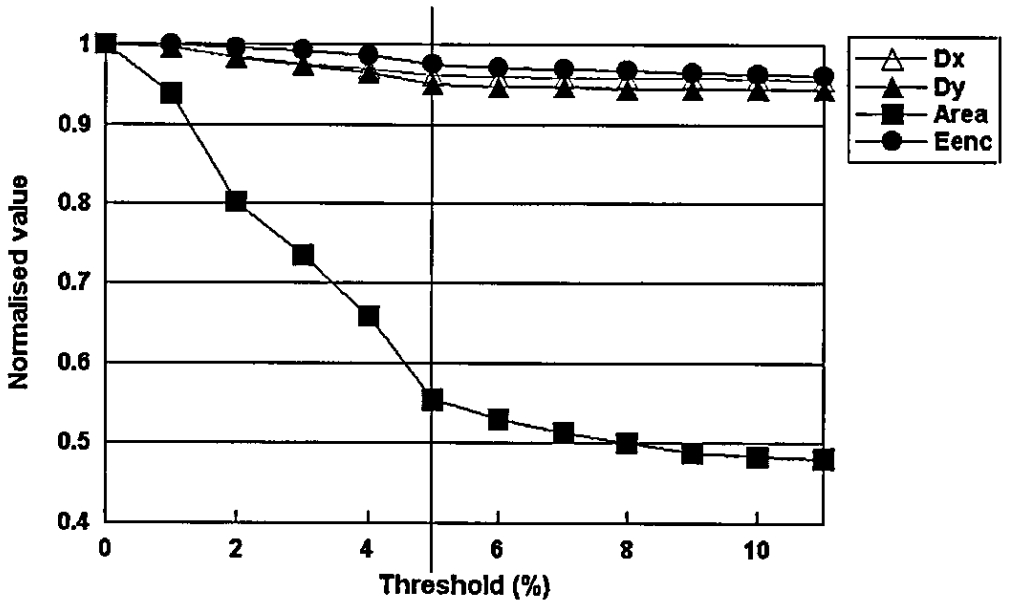

Fig 4.8 (b)
The variation of key beam parameters with threshold for a flatop profile Excimer beam. Note in contrast to the Gaussian case the small change in beam width with varying threshold

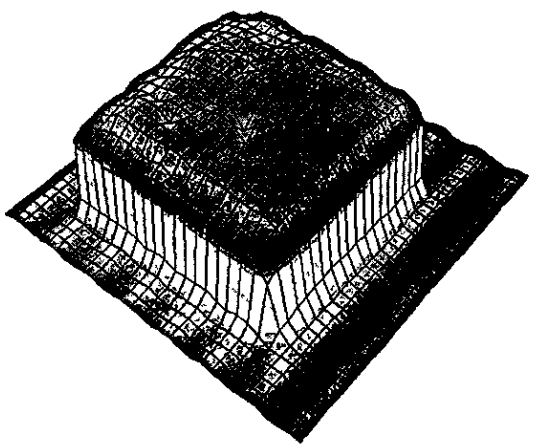

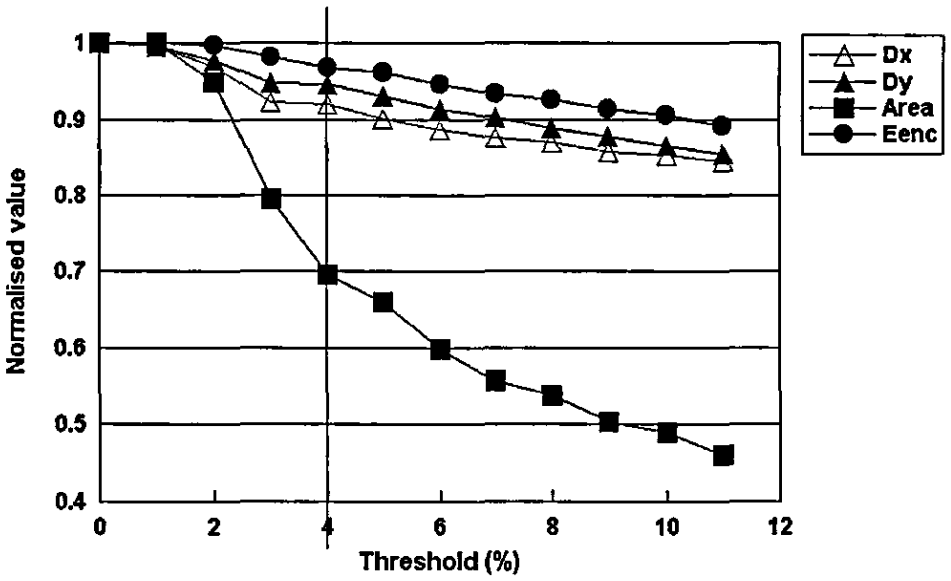

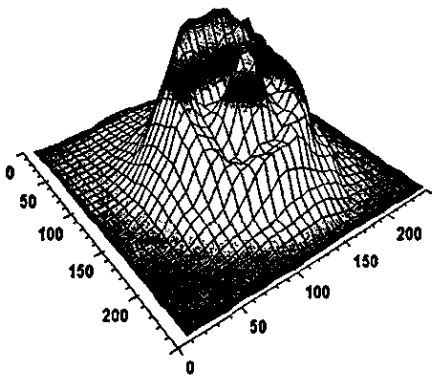

Fig 4.8 (c)
The variation of key parameters with threshold level for a multimode beam from an Nd:Yag laser.

Alternatively limits can be placed using a spatial aperture of integration. The ISO 11146 draft recommends integration apertures, which are 2 to 3 times the second moment beam width.

Other methods, which are not included in the current draft standards, combine the two techniques described above. These involve noise filtering techniques and the use of weighted Gaussian sampling windows [10]. They are still the topic of research.

4.3.8 Beam Shape Measurements.

There are several ways to fit an arbitrary theoretical distribution to a measured one. Typically least squares fit techniques can be used to fit Gaussian, super Gaussian and top hat distributions. However there is no one *correct* method of least squares fitting to non linear distributions, and each method will give differing results dependent upon the levels of background noise and the type of measured data to be fitted. Fits should be made to the least squares of the relative deviations, as opposed to the absolute deviation, which over weights the wings of the distribution against the centre.

A simpler fitting model is to use just three parameters, the measured centroid location, beam widths and total beam power to fit the theoretical distribution. This is relatively simple and fast to compute. Once calculated the quality of fit, and roughness of fit, of the measured distribution can be found.

The draft standard ISO 13694 also allows for the calculation of beam flatness, edge steepness and plateau uniformity. These are particularly useful for characterising flat top profiles such as those produced by an excimer beam homogeniser. Figure 4.9 shows the variation of these parameters calculated on a series of simulated excimer profiles. Further explanation of these parameters is given in chapter 5.

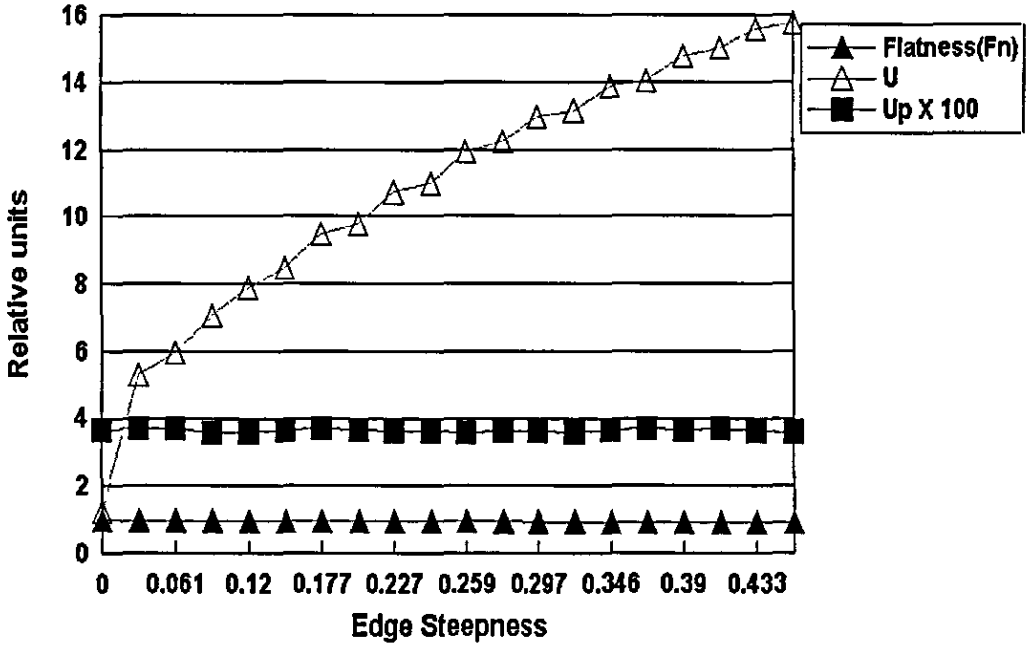

Figure 4.9

The variation in calculated beam uniformity, Flatness factor (F_n) and Plateau Uniformity (U_p) for a simulated flat top beam with varying edge steepness. Threshold (n) = 50%. Note how the U_p remains constant while the Uniformity varies with edge steepness.

4.3.9 Calibration.

Accurately calibrating the detector is not always an easy task, particularly if there are intermediate imaging optics involved. For direct one-to-one imaging applications it is possible to calculate the digitised pixel size of the detector system. In fluorescent imaging applications such as those used to characterise excimer laser beams it is possible to calibrate beam size by white light imaging a measurement graticule at the test plane. These two methods were used for calibration purposes in this experiment

For power and energy calibration, after careful background correction it is necessary to compute the whole beam integral and divide the power/energy reading from a meter at the workpiece by this sum. For an array detector this will yield the grey level per pixel responsivity.

4.3.10 Discussion

With careful data analysis it is possible to obtain consistent results despite the limitations of detection and beam sampling components.

Moment integrals can give stable results with high accuracy and sensitivity if proper measures are taken to correct for background offset and detector noise. The centroid location of a beam can be found to within better than 0.1 pixel accuracy and 0.05 % rms stability despite rms detector noise being several times this.

Improvements in algorithms and the falling price of computing hardware are now making sophisticated beam analysis possible for routine measurements.

Figures 4.10, 4.11, and 4.12 show example Laser Test reports on a HeNe laser, excimer laser and a Nd:Yag laser , presented at the end of this section. Each of the parameters in the draft ISO 13694 standard have been measured over time and values calculated for mean and standard deviation of these parameters. Values and parameters of particular interest to each type of laser have been highlighted.

Figure 4.10 Beam Analysis Test reports for a commercial HeNe laser

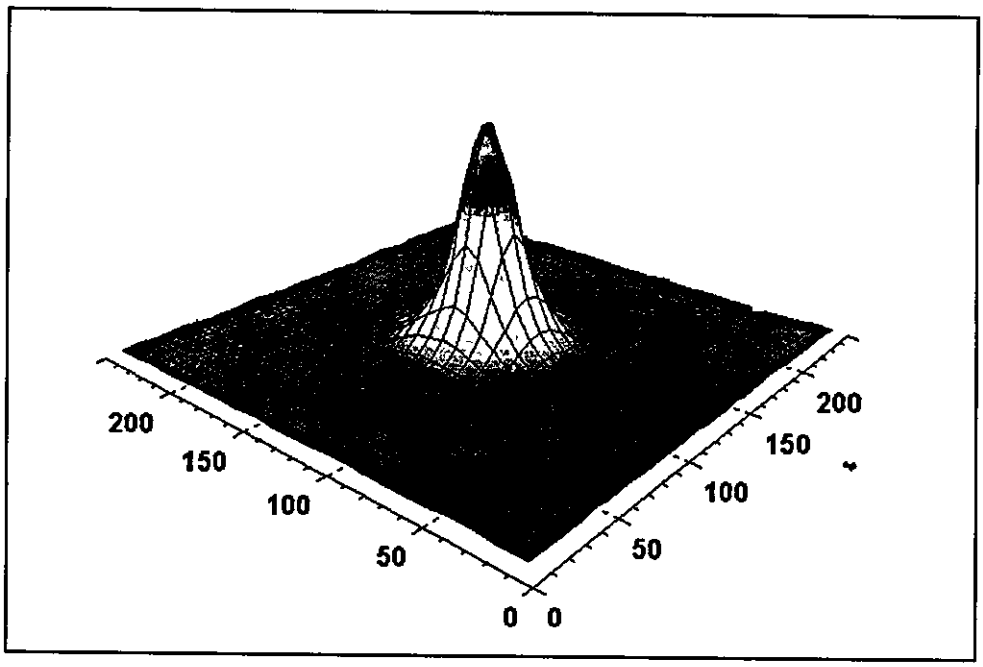

Laser type :	HeNe
Manufacturer :	Metrologic.
Wavelength	633 nm.
Polarisation :	Circular.
Average power:	2 mW CW.
Detection plane (z) :	200mm.
Laboratory system :	Theta = 0.
Detection system :	CCD camera
Type :	Pulnix TM6 ex
Properties :	{see Manufacturers specification }
Digitiser resolution :	512 x512 pixel ,
Dynamic range :	8 bit
Optical arrangement:	
Magnification :	1:1
Attenuation :	ND filters.

Beam shape (Footprint) :	**Mean**	**Std Dev**
Ellipticity(ξn)	0.986	0.6%
Flatness Factor (F_n)	0.18	0.78%
Uniformity (U_n)	-	-
Plateau Uniformity (Up)	0.848	14.9%
Fractional Power (f_n)	0.998	
Edge Steepness (s,0.1 - 0.9)	0.966	0.3%
Gaussian Fit		
Goodness of Fit C	0.879	1.0%
Roughness of Fit R	0.11	2.9%
Threshold (n)	**1%**	
Background	**3 counts**	**0**
Integration check	**1.001**	**0**

Beam Power :	**Mean**	**Std Dev**
Beam Power (P)	2.10 mW	0.23 %
Effective Power (P_n)	2.095 mW	0.23%
Average Power Density (H_n)	415 mW/cm^2	0
Beam Location :		
Maximum Location (X_{max},Y_{max})	96.9,143.7 pixels	0.3%,0.5%
Centroid Location (X_c,Y_c)	**97.6,143.9 pixels**	**0.05%,0.02%**
Effective Beam sizes :		
Azimuth angle (Φ)	0	0
Widths (d_{nx},d_{ny})	**520.7,516.7 uM**	**0.3%,0.45%**
Diameter(d_n)	518.7 uM	0.38%
Effective Area (A_n)	0.21 mm^2	0.73%
Effective Irradiation area (A_n')	0.50 mm^2	0.22%

Figure 4.11 Beam Analysis Test reports for a commercial Krf excimer laser

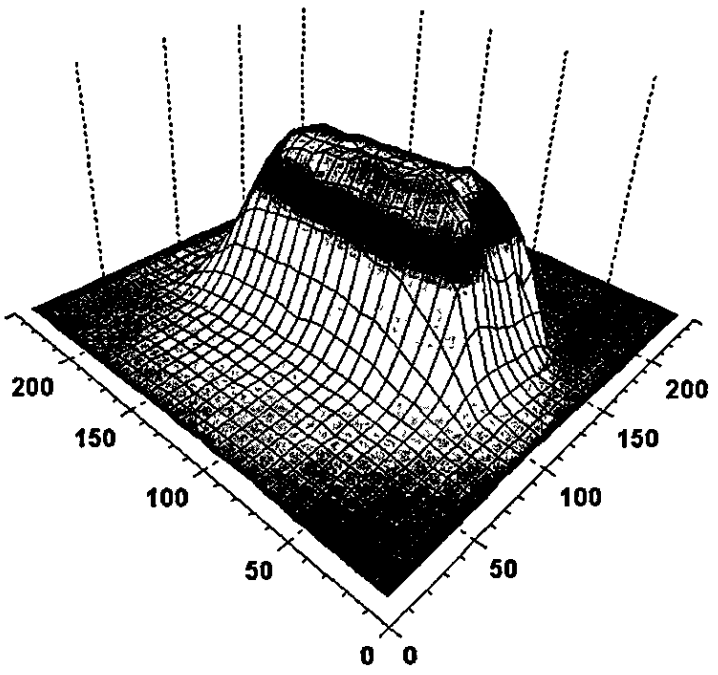

Laser type :	Excimer
Manufacturer :	Lambda Physik.
Wavelength	248 nm.
Polarisation :	Unpolarised.
Average Energy:	300 mJ PULSED.
Detection plane (z) :	Mask plane before beam homogenisation
Laboratory system :	Theta = 0.
Detection system :	CCD camera
Type :	Cohu 4712
Properties :	{see Manufacturers specification }
Digitiser resolution :	256 x 256 pixel ,
Dynamic range :	8 bit
Optical arrangement:	
Magnification :	1:10
Attenuation :	EXIU-F interface unit

Beam Energy :	**Mean**	**Std Dev**
Beam energy (P)	351 mJ	2.4%
Effective energy (P_n)	262 mJ	3.5%
Average Energy Density (H_n)	1050 mJ/cm^2	2.1%
Beam Location :		
Maximum Location (X_{max},Y_{max})	**90.4,125.2 pixels**	**18.5%,10.2%**
Centroid Location (Xc,Yc)	**122.5,131.1 pixels**	**0.2%,1.47%**
Effective Beam sizes :		
Azimuth angle (Φ)	-2.2 deg	18%
Widths (d_{nx},d_{ny})	7.460,3.967 mm	0.7%,2.8%
Diameter(dn)		
Effective Area (An)	-	-
Effective Irradiation area (A_n')	24.9 mm^2	3.6%

Beam shape (Footprint) :	**Mean**	**Std Dev**
Ellipticity(ξn)	0.53	2.3%
Flatness Factor (Fn)	0.736	1.9%
Uniformity (Un)	16 9%	1.6%
Plateau Uniformity (Up)	0.55	43.1%
Fractional Power (fn)	0.746	3.5%
Edge Steepness (s,0.1 - 0.9)	0.91	4.1%
Gaussian Fit		
Goodness of Fit C	-	-
Roughness of Fit R	-	-
Threshold (n)	**50%**	
Background	**6.7 counts**	**7%**
Integration check	**1.056**	**0.16%**

Figure 4.12 Beam Analysis Test reports for a commercial Nd:Yag laser

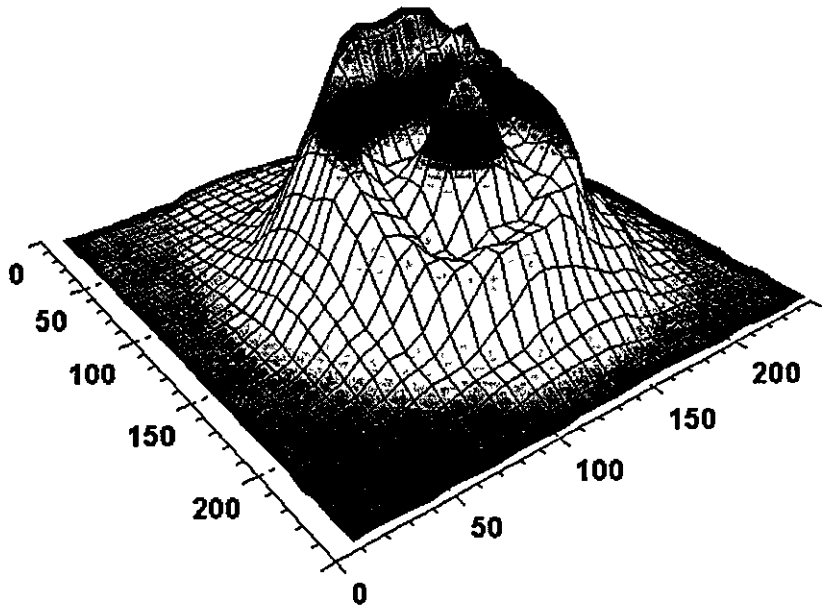

Laser type :	Nd:Yag
Manufacturer :	Spectron.
Wavelength	1064 nm.
Polarisation :	Circular
Average Energy:	7 mJ PULSED.
Detection plane (z) :	400mm from output coupler
Laboratory system :	Theta = 0.
Detection system :	CCD camera
Type :	Pulnix TM6
Properties :	{see Manufacturers specification }
Digitiser resolution :	256 x 256 pixel ,
Dynamic range :	8 bit
Optical arrangement:	
Magnification :	1:1
Attenuation :	EXIU-Mini interface unit

Beam shape (Footprint) :	**Mean**	**Std Dev**
Ellipticity(ξn)	0.95	2.9%
Flatness Factor (F*n*)	0.22	0.85%
Uniformity (U*n*)	-	-
Plateau Uniformity (Up)	0.547	15%
Fractional Power (f*n*)	0.998	-
Edge Steepness (s,0.1 - 0.9)	0.971	0.14%
Gaussian Fit		
Goodness of Fit C	0.12	33%
Roughness of Fit R	0.39	3.5%
Threshold (n)	**1%**	
Background	**4 counts**	**-**
Integration check	**1.17**	**-**

Beam Energy :	**Mean**	**Std Dev**
Beam energy (P)	6.93 mJ	3.7%
Effective energy (P*n*)	6.92 mJ	3.7%
Average Energy Density (H*n*)	50.1 mJ/cm^2	2.8%
Beam Location :		
Maximum Location (Xmax,Ymax)	123.8,108 pixels	14.9%,0.2%
Centroid Location (Xc,Yc)	133.4,128.9 pixels	0.25%,1.61%
Effective Beam sizes :		
Azimuth angle (Φ)	-	
Widths (d_{nx},d_{ny})	2.812,2.965 mm	0.27%,2.95%
Diameter(d*n*)	2.89 mm	
Effective Area (A*n*)	-	-
Effective Irradiation area (A_n')	13.8 mm^2	1.27%

4.4 General conclusions

The results of the experiments have in general confirmed the validity of the proposed beam characterisation algorithms for the ISO standard. However it is clear that careful analysis must be done of background and signal noise as this can have a dramatic effect on the accuracy of moment and beam width calculations. The concept of reduced moments (equation 4.7) is particularly useful as a method of noise reduction.

In practise only a small number of the beam parameters evaluated in this chapter will need to be used to characterise a beam, depending upon the type of laser and the application. The concept of threshold uniformity is a great value when characterising homogenised excimer laser beams but inappropriate when measuring a TEM_{00} HeNe beam. Similarly, using the second moment method for measuring the width of an excimer beam would be inappropriate, as it would not yield a physically meaningful result.

The results of this work have been published and presented at conferences (see references [8] & [9]) and have provided a contribution to the development of ISO standards on laser beam profile characterisation.

4.5 References

1). A E Siegman, "New developments in laser resonators", SPIE Vol 1224 "Optical Resonators",(1990)

2). B A Ward, "An experimentalist's approach to laser beam characterisation and the emerging Measurement standards", 2nd Workshop on laser beam characterisation, Berlin, June (1994)

3). B Eppich et al, "Reliability of beam parameter measurements with CCD cameras", 1st Workshop on laser beam characterisation , Madrid ,July (1993)

4).R Castenada, J Kross, "Evaluation of point spread functions of microscope objectives using moments by modified definitions", SPIE Vo.1781, "Specification and measurement of Optical systems" ,(1992)

5). ISO/TC/SC9/WG1/CD 11 146, "Optics and optical instruments, Test Methods for laser beam parameters: Beam widths, divergence angle and beam propagation factor "

6). ISO/TC/SC9/WG1/CD 11 146, "Optics and optical instruments, Test Methods for laser beam parameters: Beam widths, divergence angle and beam -propagation factor"

7). ISO/TC/SC9/WG1/WD 13694, "Optics and optical instruments, Test Methods for laser beam parameters: Power (Energy) Density distribution"

8). P Apte, M C Gower, "Experimental testing of integral truncation algorithms for the calculation of beam widths by proposed ISO standard methods", SPIE Vol 2375,pg349, (1995)

9). P Apte, M C Gower, "Computational methods for beam Amplitude characterisation", Proceedings of the 2nd Workshop on laser beam characterisation, H Weber et al eds, FestKorper Laser Institut ,Berlin (1994)

10). C Maier, M Scholl, "Test of Standardisation Draft of ISO/CD 11146 for Industrial laser systems". SPIE Vol 2375,pg375, (1995)

CHAPTER 5

THE CHARACTERISATION OF EXCIMER LASER BEAMS

5.1.Introduction

The characterisation of excimer laser intensity profiles is key to the successful implementation of several industrial processes that use excimer radiation. In this respect, it is one of the first lasers to be accurately quantified in terms of beam shape and uniformity. However because excimer wavelengths are short (typically 157 nm to 351 nm), there are special considerations when designing beam sampling optics and image acquisition systems. For this reason excimer laser beam diagnostics is still somewhat of a specialist topic worthy of special study and of particular importance to industrial applications [1].

The author has been responsible for the development of the world first commercially available excimer beam diagnostic system, the Exitech P256D, which was launched in 1988. At the time of writing, over 200 beam diagnostic systems are in use or have been integrated into excimer laser processing tools.

5.2 Beam sampling techniques for excimer lasers.

On-line beam profile monitoring is very important in excimer workstations. It is important to sample the beam accurately whilst introducing the least possible distortion and power loss to the beam. Moreover, considerations of cost and complexity are important in industrial machines. For beam sampling various methods have been tested including the use of very thin fused silica pellicle beam splitters, through mirror beam sampling using a high reflectivity mirror, and glass plate fluorescers placed directly on the workpiece.

5.2.1 Fluorescent converters.

The basic principle is to use a fluorescent material to convert incident coherent UV radiation to broad band incoherent visible radiation .In this form it is easily imaged using a CCD video camera with 'off the shelf' macro focusing optics.

The choice of fluorescer material is application dependent. Various doped glasses and crystals are available commercially, higher doping giving greater sensitivity at the expense of linearity. For excimer applications ordinary glass microscope slides (Borosilicate glass) are a convenient choice for non critical applications. All of these materials exhibit very good resolution and reasonable linearity over several orders of magnitude exposure. This greatly eases the problems of beam attenuation, low fluence beams ($< 1 Jcm^{-2}$) can be sampled directly and the camera image controlled using the lens iris. Some of these materials have already been investigated [2] for use in excimer laser applications.

5.2.2 Material tests.

Three different glass samples were tested for conversion efficiency, linearity and lifetime. Tests were made at 193 and 248 nm over a range of fluences. Conversion efficiency is not a problem because of the high level of laser energy available and the sensitivity of CCD cameras used to image the fluorescence .Of greater concern is the linearity of the conversion process and the optical stability of the material to prolonged laser exposure.

The glass samples were Corning glass, Borosilicate glass (microscope slide), and Mihara glass. The glass samples were exposed directly to a homogenised excimer beam via a variable optical attenuator. The resulting fluorescence was imaged onto a CCD camera using a macro-focusing lens and the profiles analysed using P256 beam analysis software. The experimental setup is shown if figure 5.1.

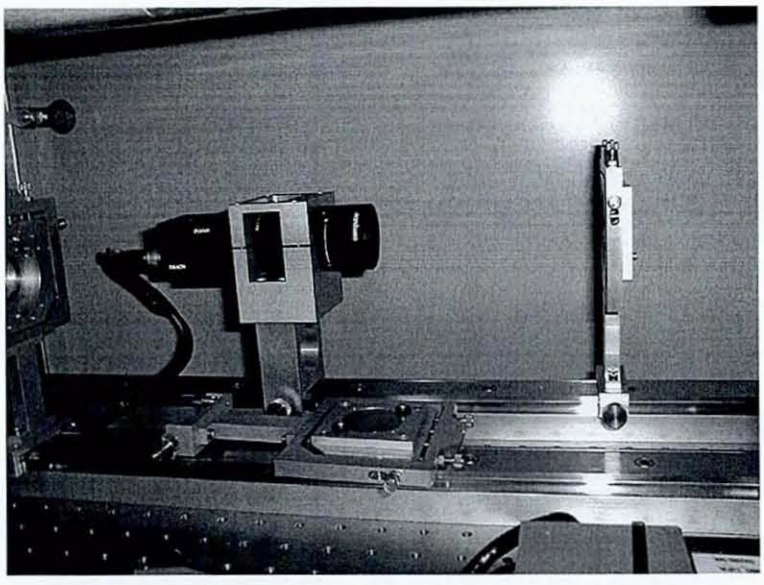

Fig 5.1

Setup using CCD camera with zoom lens and Fluorescent converter.

The linearity plots figures 5.2a,b,c show the variation of fluorescent output with incident energy for the different types of glass

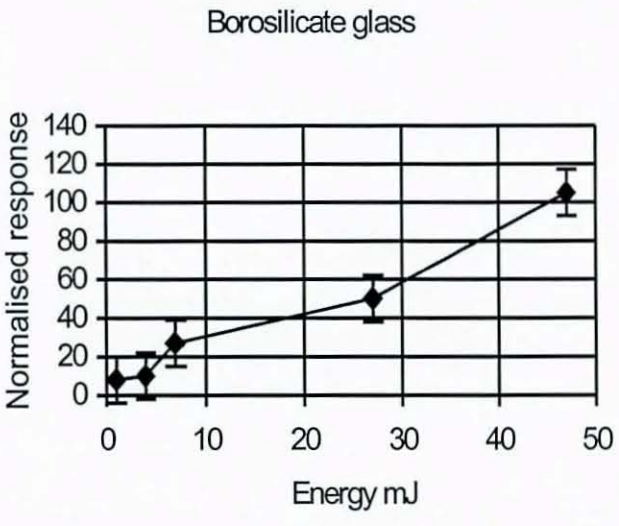

Figure 5.2a
Response curve for Borosilicate glass (Microscope slide).

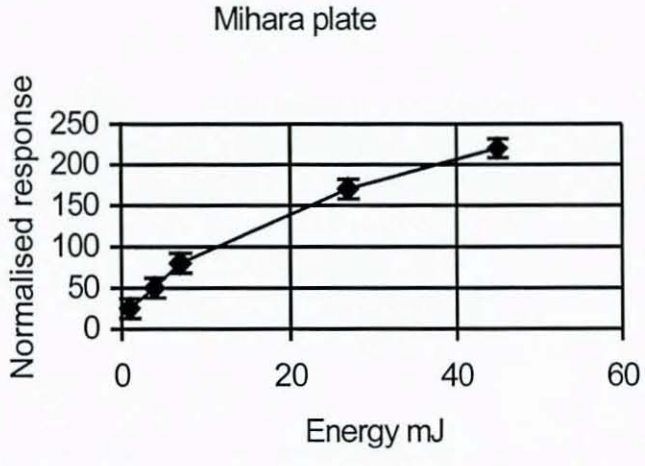

Figure 5.2b
Response curve for a Mihara glass plate.

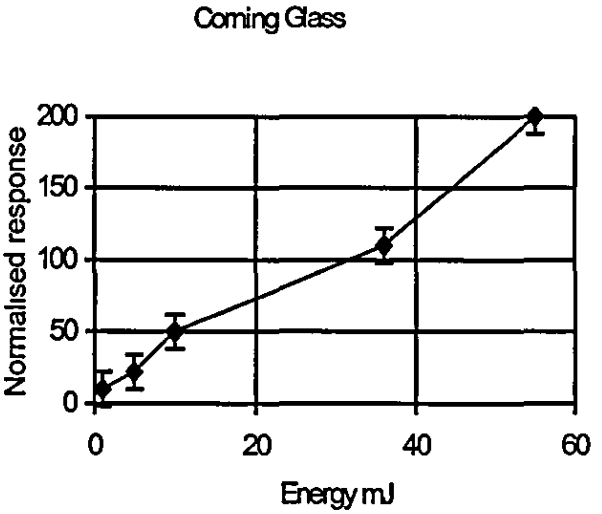

Figure 5.2c
Response curve for a Corning glass plate.

As can be seen from the graphs reasonable linearity is exhibited by all of the samples.

Lifetime testing was then performed by exposing the sample materials to 10,000 or 20,000 shots of 248 nm radiation at 330 mJ/cm^2 over a 7 x 7 mm square. The output uniformity of each sample was then measured and comparisons made. The results are shown in table 5.1.

Sample	**Shots**	**Fluence (J/cm^2)**	**Dose (kJ)**	**Sensitivity reduction**
Corning Glass	20,000	0.33	6.6	Not measurable, within experimental uncertainty
Borosilicate glass (microscope slide).	10,000	0.33	3.3	11 %
Mihara glass	20,000	0.33	6.6	Not measurable, within experimental uncertainty

Table 5.1. Summary of glass fluorescer tests

In these tests the Borosilicate glass performed poorly while the other two samples gave excellent results. Further long term exposure tests at higher fluences and different wavelengths will be performed in due course. For critical applications the Mihara plate gives the best cost /performance compromise. An example of an excimer beam profile taken using this technique is shown in fig 5.3

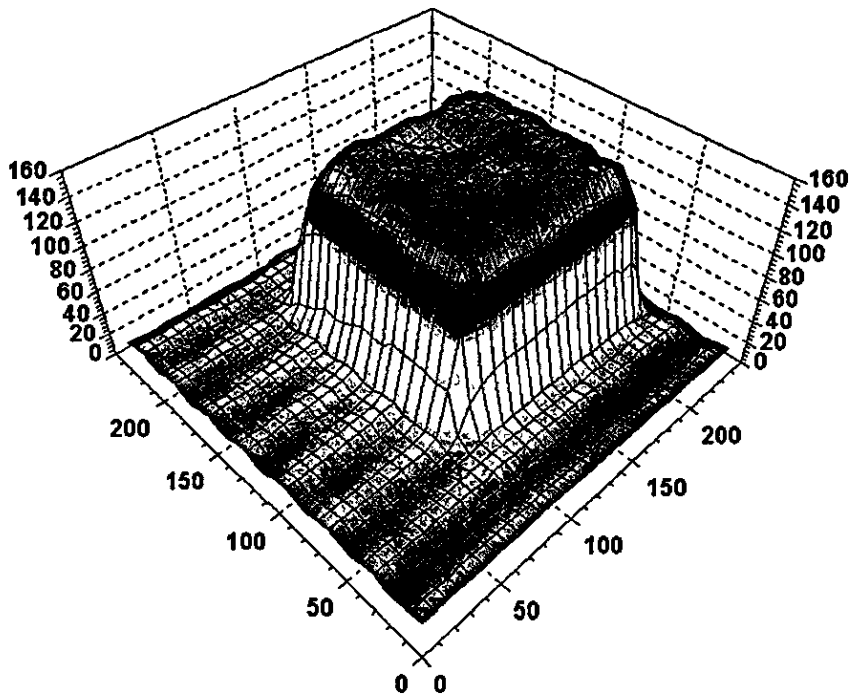

Figure 5.3. KrF Excimer profile taken using a Mihara glass fluorescer plate, from a system used for Silicon doping with beam size control.

5.2.3 Pellicle Beam splitters.

Exitech also uses thin (400 μm) fused silica AR coated pellicle beam splitters for in line beam sampling. The advantage of these is that they create minimal deviation of the beam as compared to using a traditional prism beam sampler. The back surface of the pellicle is anti reflection coated, leaving a 'ghost' image of about 5% of the front surface reflection overlaid onto the main image with approximately a 200 μm shift. In practical terms this is rarely a problem, but can give some difficulties when examining very small beams and fine detail on an imaging mask. The total sampled beam is about 4% of the main beam intensity.

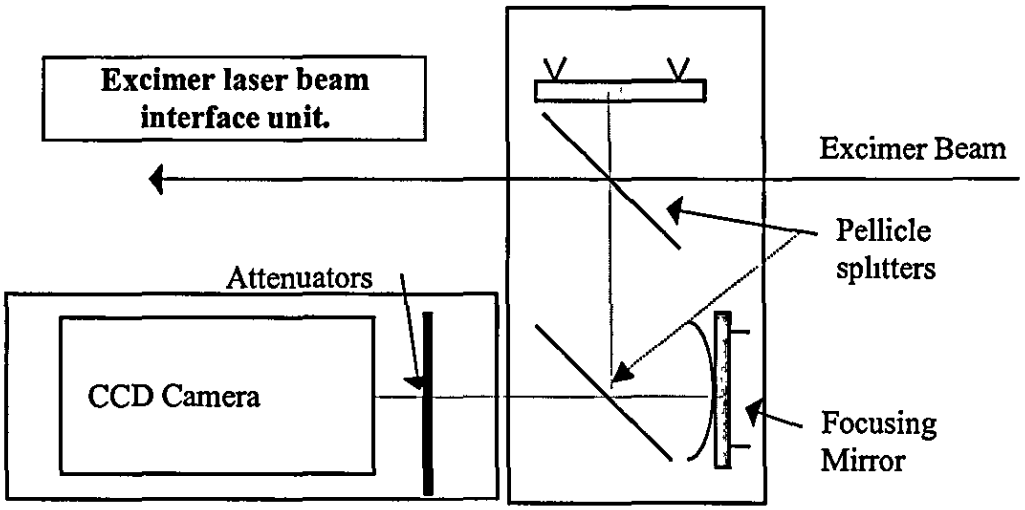

Figure 5.4. Excimer laser beam interface unit, with pellicle splitter.

The wafers used are Hoya 3W40 UP (Ultra parallel grade). These have proved more than adequate for most applications. They are 400 μm thick (+/- 1.5 μm), with a total thickness variation of less than 0.5 % over their entire surface, and are available in quantity at a reasonable price. These are then given a wideband colloidal silica AR coat on the rear surface.

5.2.4 Performance of pellicle splitters

The arrangement shown in Fig 5.4 is the basis of the Exitech EXIU UV excimer laser beam interface unit. It has proven very versatile giving reliable long-term operation at 193,248, and 308 nm. The image plane can be changed to focus the mask plane by sliding the camera towards or away from the focusing mirror and the whole assembly can sit in line during laser processing.

The only potential drawbacks are due to the shifted 'ghost' image created by the pellicles, but in most practical situations this is not usually a problem. An example of an excimer profile taken with this interface unit is shown in figure 5.5

This type of arrangement will only work satisfactorily with lasers of short coherence length, less than the thickness of the pellicle, otherwise interference fringes will be produced. Most excimers fall into this category, but this is certainly not so with third

and fourth harmonic Nd:Yag. For these types of laser a quartz prism beam splitter is more suitable.

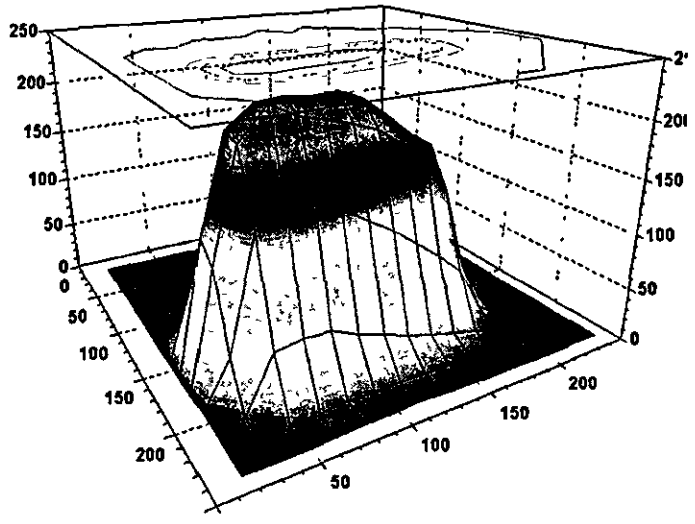

5.5. KrF excimer profile taken using an in line pellicle beam splitter, (EXIU interface unit).Raw beam output from LPX excimer laser used for cavity alignment ,variable beam size.

5.2.5 Through mirror Beam sampling

In principle this is a convenient way of sampling a beam in an excimer projection system. The final turning mirror is replaced with a partially reflective component. The transmitted beam is then imaged onto a UV CCD camera via suitable attenuation filters. This approach is used on Exitech S7000 Micro machining workstations, and allows the beam diagnostics to be fitted into a very compact space. Problems arise due to coating non-uniformities on the mirrors and the subsequent worsening of this effect as the coatings age. This is particularly severe with high reflection coatings. For example in the case of a nominally 99% reflecting mirror, a 1% change in reflected power (to 98 %) would result in a doubling (from 1% to 2%) of the transmitted power. Hence the effects of coating ageing are magnified by two orders of magnitude in the monitored (transmitted) beam.

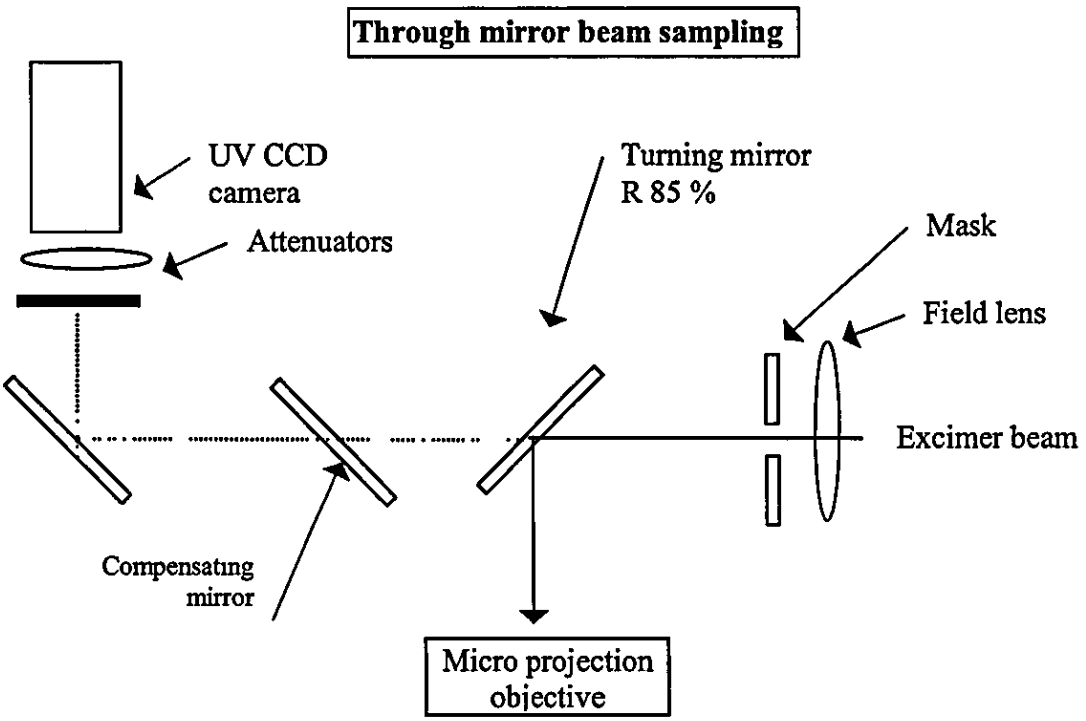

Figure 5.6. In line Beam sampling scheme for micro machining workstations.

In practice it is found best to employ 85% - 95% reflective mirrors to reduce the effects of coating non uniformity. The power loss due to this is usually not a problem in micro machining applications. Further improvements can be made by using an identical compensating mirror from the same production run.

5.2.6 Performance of through mirror sampling

An example of an excimer beam profile taken with this arrangement is shown in figure 5.7. Good results can be achieved if care is taken in the initial set up of the compensating mirror to give a uniform response. The arrangement shown in figure 5.6 is typical of that employed in an excimer micro projection system.

5.2.7 Comments

It was found that for very critical applications such as the annealing of semiconductors direct detection using a pellicle splitter will give the most reliable long term operation. Moreover the ability to sample at different image planes can be very important and is an advantage to the system designer.

In less critical applications the use of fluorescer plates is acceptable and much more flexible. This technique allows the beam to be monitored directly at the workpiece, or via a beam sampler for in-line monitoring. The main drawback is that degradation of the fluorescer material can give unreliable long-term results, though this can easily be remedied by regular replacement.

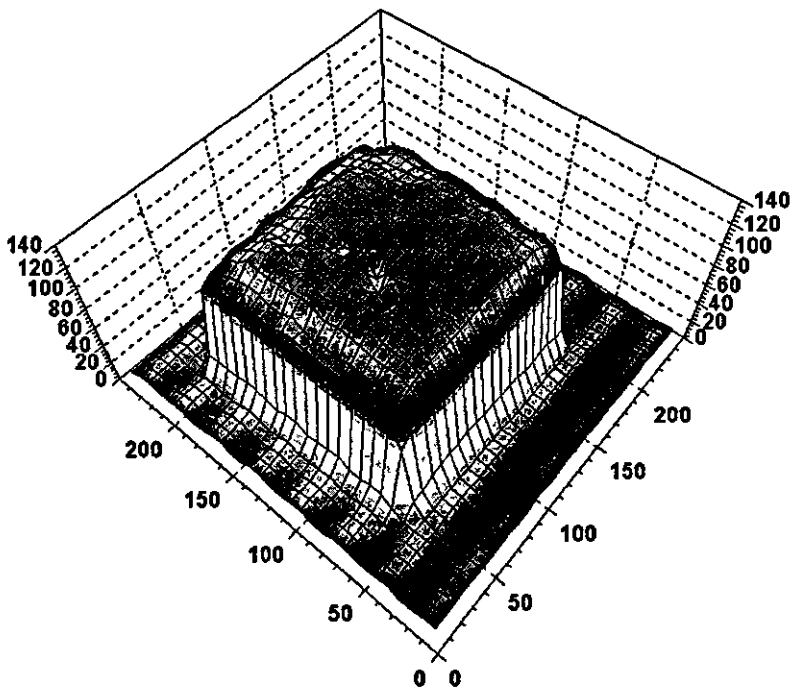

5.7. Excimer beam profile taken by through mirror sampling. (S7000 Micro projector mask plane monitoring), on an industrial micromachining system.

Through mirror beam sampling has been used in situations where the other methods are difficult due to lack of space, typically in micro machining workstations that have low beam energy and throughput. It is particularly sensitive to mirror coating degradation and damage and is not the recommended first choice, but if carefully set up can give reliable results.

5.3 Data acquisition and system integration.

5.3.1 Introduction

The video signals from multiple CCD cameras can be digitised using a standard video frame grabber. In Exitech systems, the Matrox Pulsar and Orion cards are used. These support up to 8 video inputs, allowing multiple beam monitors to be installed on Laser processing tools. These cards digitise with 8 bits grey scale resolution, which is quite sufficient for standard applications when using standard CCD cameras such as the Pulnix TM6.

5.3.2 Work station integration

Typically as shown a system would consist of an excimer laser, beam delivery system, beam control system, imaging optics, workpiece motion control and component handling.

A main control computer handles stage motion control, interlock monitoring and laser control. This pc communicates to other devices via multiple RS232 serial links. The beam diagnostics reside in another computer and feed information back to the control pc via an RS232 link. This decoupled approach is adopted because on line beam analysis is a very processor intensive operation. This would overload the control computer under certain circumstances, reducing its ability to respond quickly to other external events. Figure 5.8 shows an example of this software, as installed on an excimer laser Micromachining system.

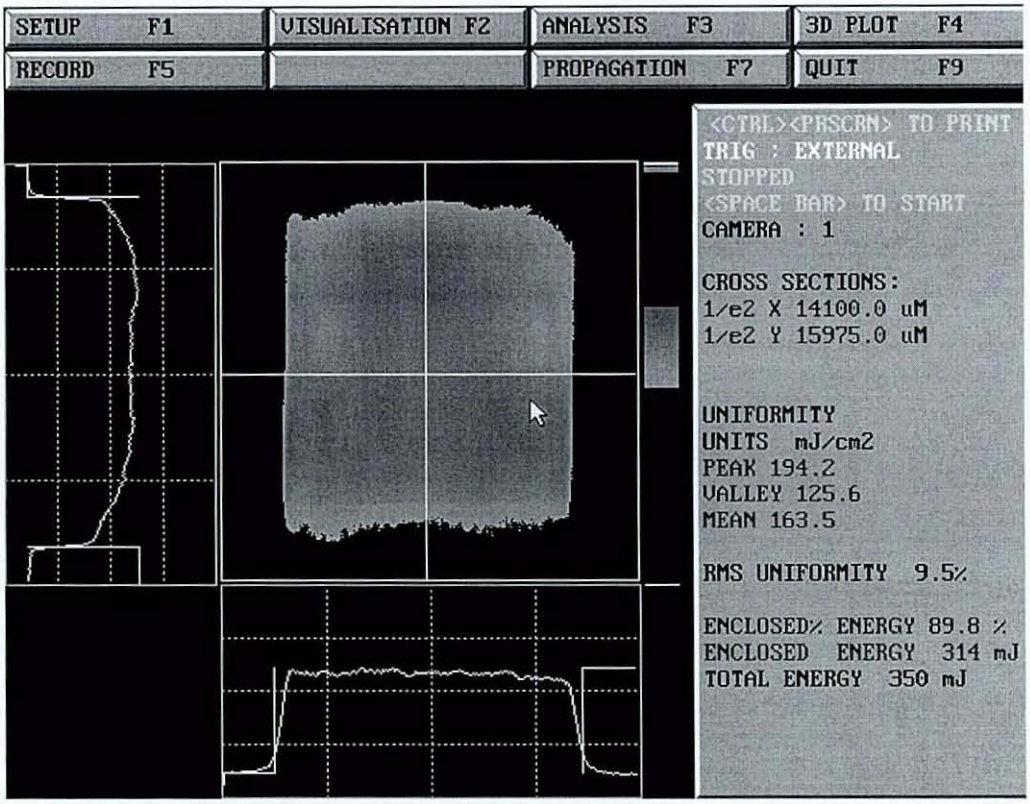

Fig 5.8 Beam Intensity "footprint" of an excimer laser beam.
Analysis software integrated into the machine control system.

5.4.The characterisation of excimer laser line beam profiles

This section describes techniques for the measurement of high aspect ratio line focus beam profiles. Such line beam profiles are required in a number of industrially important excimer laser applications, such as the annealing of α-Si for TFT displays or the patterning of thin film solar panels. Such line beams may be in excess of 250 mm in length whilst having a cross sectional width of less than 100 um. This presents special problems for the design of beam sampling optics because of the small field size (typically 6 x 4 mm) of CCD detectors.

To overcome some of these problems a UV sensitive CCD detector was mounted upon a high speed translation stage and scanned along the length of the line beam. Using position synchronised laser triggering it was possible to achieve high data acquisition

rates allowing a complete line scan to be acquired in approximately one second. This data was then analysed by a powerful image processing system using techniques for the characterisation of laser beam energy distribution as described in draft ISO standard ISO 11146. The measurement speed of such a system allows near real time visualisation of the line beam profile, greatly facilitating the setup and maintenance of the complex optics required to produce high aspect ratio line beams.

5.4.1 Background

The range of Industrial applications of excimer laser systems has widened considerably in recent years. In particular the application of line beam optics [3] has found new and novel uses in a number of areas such as flat panel TFT annealing and blind via hole drilling for MCMs. These types of beam present special difficulties in terms of characterisation because of their high aspect ratio. The requirements of the latest line beam processes demand accurate beam characterisation, a requirement notably for optical design and setup, but increasingly because there is a need for on-line monitoring and control on industrial machines during the production process.

Line beam characterisation data will be presented in this section that was taken from both laboratory experimental rigs and real industrial machines.

5.4.2. Applications

Flat panel TFT annealing is one of the main applications of line beam optics. A single pulse from an excimer laser is sufficient to transform amorphous Silicon to polycrystalline Silicon. It has been found that the best way to deliver the pulse to the Silicon surface is by a scanning line beam. This form of delivery produces a very uniform transformation of the Silicon surface in comparison to step and repeat exposure. This process will only give good results however if the line beam is very uniform over its length. In the computer industry the production of so-called "blind vias" involves using a copper conformal mask to define a via hole pattern on the surface of a mutlichip module (MCM). Processing by laser etches through material layers within the MCM to form vias. The efficiency of this process can be improved by the use of a scanning line beam.

Another new application area is the patterning of Si solar cells. The line beam is used to cut channels in the solar cell structure as part of one step in the production process. Using a line beam makes for efficient use of the laser energy and greatly increases production speed. Similarly in the production of ink jet printer nozzles the use of line optics can increase throughput whilst maintaining production quality.

All of the processes mentioned have a high economic potential and new applications are continually being found for line beam processing in advanced manufacturing.

5.4.3. Experimental setup

In order to develop and test characterisation methods an experimental rig was constructed around an LP3000 excimer laser with simple line beam optics, a configuration normally used for PCB processing at 308 nm. In addition, data was also taken from production industrial machines equipped with line beam optics and Exitech beam diagnostic systems.

The primary experimental set-up as shown in figure 5.9 consists of a high-speed translation stage (Aerotech) onto which a UV sensitive CCD camera (COHU 4712) is mounted. The system is controlled by a PC and fitted with frame grabber, energy monitor and motion control boards. A 2mm thick beam splitter mounted just below the final cylindrical doublet projection lens deviates a fraction of the beam to an equivalent focal plane where the CCD camera is situated. Inconel coated silica UV attenuation filters are mounted on the front of the camera to reduce the incident beam energy by several orders of magnitude. The active detector area of the CCD chip is 6.4 mm by 4.8 mm, corresponding to a digitised pixel size of 16.8 μm over an array of 384 x 288 pixels (CCIR standard video). The actual pixel resolution of the detector is twice this figure, but the effects of video interlace reduce the resolution by half (a single field) for pulsed laser imaging.

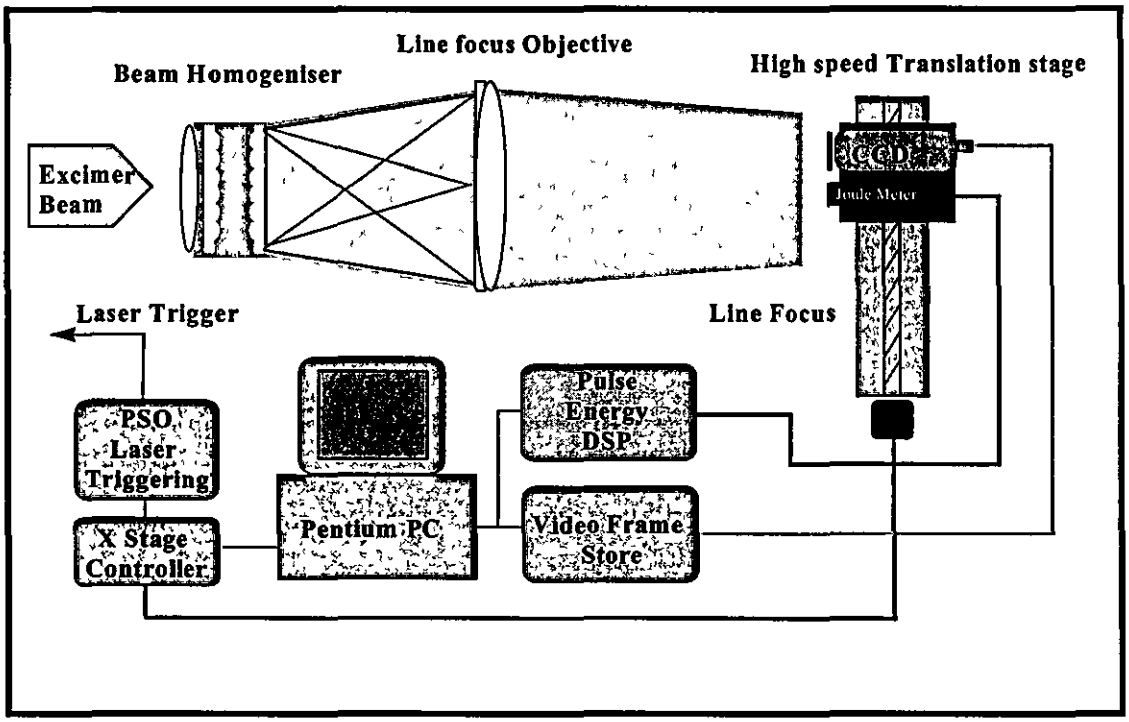

Figure 5.9. Architecture of the line beam scanning system.

Typical line beam lengths handled by the system range from 50 mm to greater than 300 mm, requiring from 8 to more than 40 CCD fields to be captured. The acquisition speed of the system is not limited by the frame grabbing hardware but by the stage speed. The maximum acquisition frame rate of the system is 50 Hz, hence a stage translation speed in excess of 300 mm per second is required to realise maximum frame rate.

5.4.4 Energy monitoring

Figure 5.10 shows the energy monitoring system. It consists of a wedged silica beam splitter sampling a portion of the line beam onto a fast responding Pyroelectric head. The signal from this detector head is digitised using an A/D card with on board Digital Signal Processing (DSP). The peak of the detector signal varies linearly with the amount of energy falling upon the detector. The on board DSP is used to extract the peak value of the input waveform and store the value in a data buffer. Due to the fast response of the electronics the system can in theory handle laser repetition rates in excess of 1kHz, though in this system the maximum rate that it was tested to was 200 Hz. The fast processing of the DSP also allows the calculation of laser energy statistics, such as mean, minimum, maximum and standard deviation in near real time. The computation

of Fourier transforms is also possible in order to extract time varying data from the laser energy statistics.

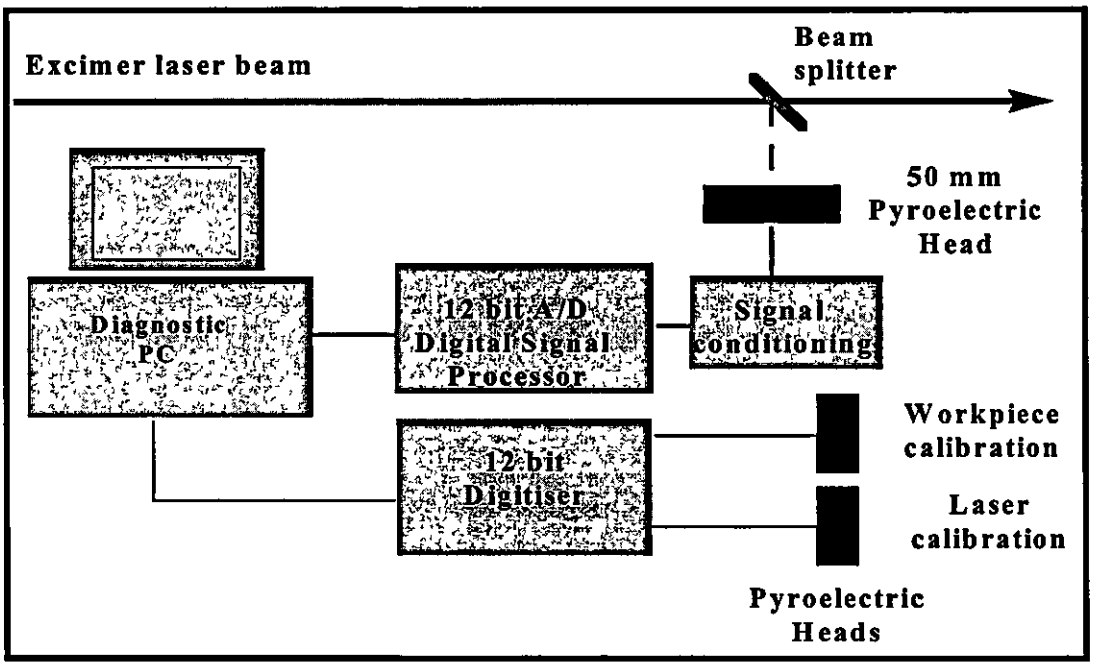

Fig 5.10 On-line energy monitoring system

5.4.5 Synchronisation and image processing

The choice of image capture and processing hardware is flexible. For these experiments a National Instruments IMAQ PCI -1408 frame grabber board was used, installed into an industrial Pentium PC. This card is capable of capturing a full resolution video sequence into computer memory at 50 fields per second. The laser trigger pulses are generated by an Aerotech PCPSO card, which works by generating a trigger pulse on sub multiples of the translation stage encoder counts. This technique of position synchronised firing allows the entire line beam profile to be scanned 'on the fly' without stopping the stage at incremental positions in order to capture the beam profile data. This allows profile data to be acquired very quickly; typically a 100 mm long line beam can be scanned in under one second.

In practise it is desirable to average several pulses per translation stage position along the length of the line beam for which the stage must be stopped; however the 'on the fly' scanning technique is potentially very useful during the set-up and alignment of the line beam optics because it allows rapid visualisation of the entire beam.

5.4.6 Workpiece embedded beam diagnostics.

An alternative approach, particularly useful for industrial applications is to embed the beam diagnostic camera and energy monitor into the workpiece chuck. This has the advantage of being able to measure the real beam profile "in situ". The setup is shown in figure 5.11. A thin fluorescent glass plate embedded below an aperture in the chuck is imaged by a microscope objective mounted from below, and a high attenuation neutral density filter placed above the objective attenuates the fluorescence to a suitable level for the CCD camera.

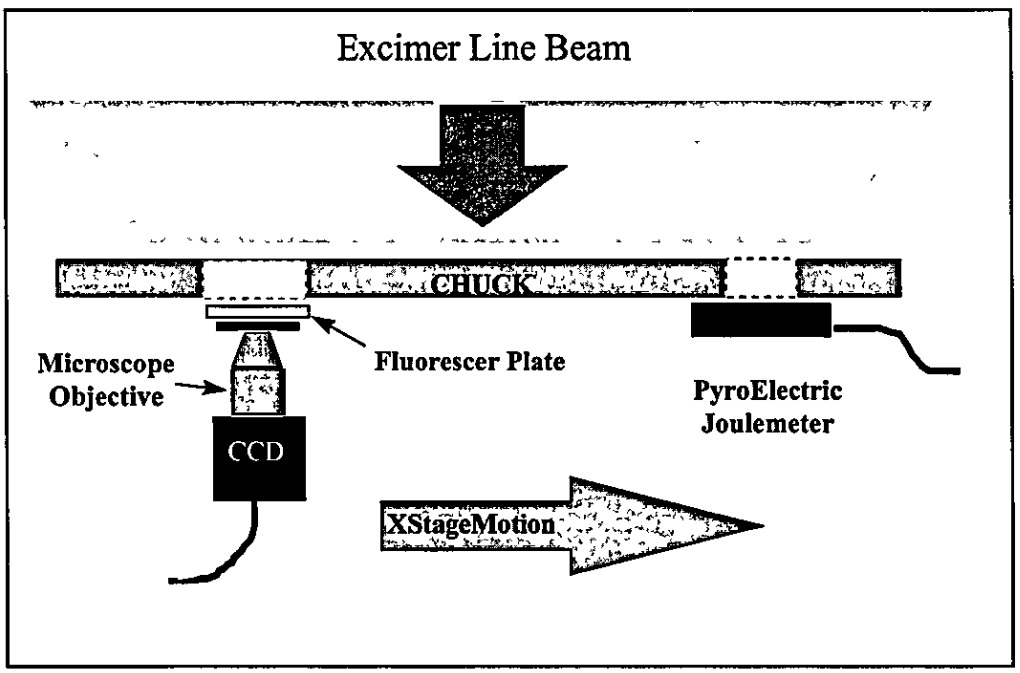

Fig 5.11. Layout of a workpiece line beam diagnostic system

A Pyroelectric joulemeter is also mounted on the chuck, slightly offset from the fluorescer plate. The line beam measurement is performed by scanning the stage in the X direction along the length of the beam and capturing a sequence of profile segments. The line beam width can be set by the user by adjusting the Z height of the workpiece, once this operation has been performed the joulemeter is moved into position over the line beam and the laser pulse energy measured. From knowledge of the beam width and the size of the joulemeter aperture the beam fluence at the workpiece can be calculated. The laser system is fitted with a computer controlled attenuator unit that allows the operator to adjust the line beam fluence over a 10: 1 range dependent upon process

requirements. The attenuator is also used when measuring the line beam profile to reduce the workpiece fluence by an order of magnitude to below 50 mJ/cm^2, when measuring the profile. This prevents damage to the fluorescer plate, which would eventually suffer from bleaching if exposed continually to the full process fluence.

5.4.7 Data processing and visualisation.

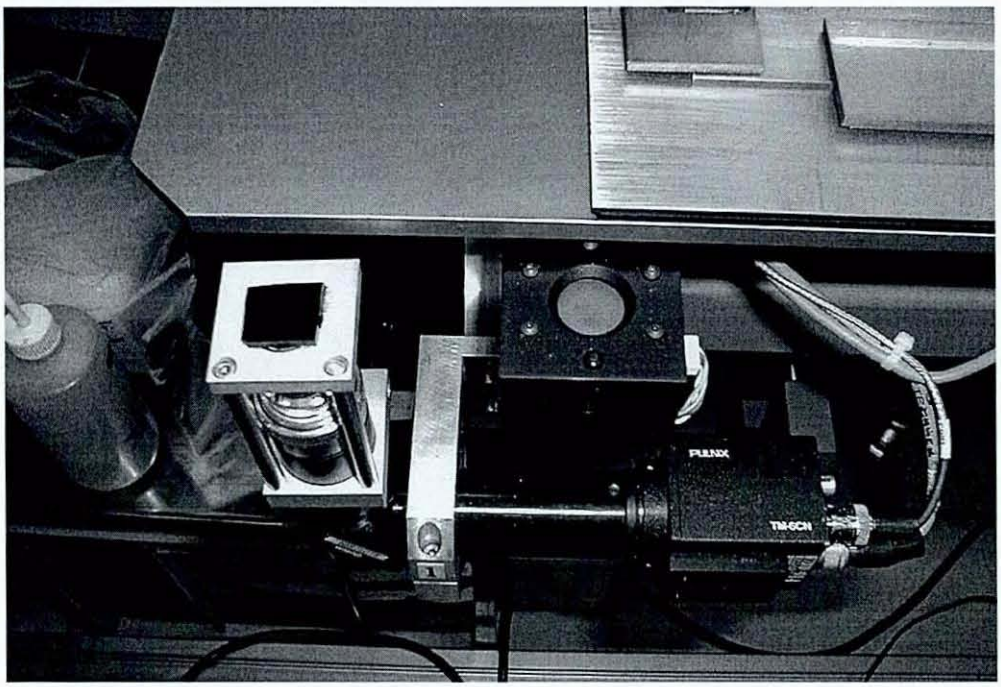

Fig 5.12 : Example of In-Chuck beam profiling camera with energy monitor

The size of data set acquired is dependent upon the line beam width and is typically from 10 to 40 frames of data. Each frame of data is a 6.8 mm segment of the line beam and is digitised at 384 x 288 pixels 8 bit resolution which corresponds to 110 kbytes per frame. Hence a complete line scan on a 300 mm beam would take over 4 Mbytes of data. However recent advances in microprocessor speeds and 32 bit operating systems mean that data files of this size can be analysed fairly easily on a personal computer or Industrial PC

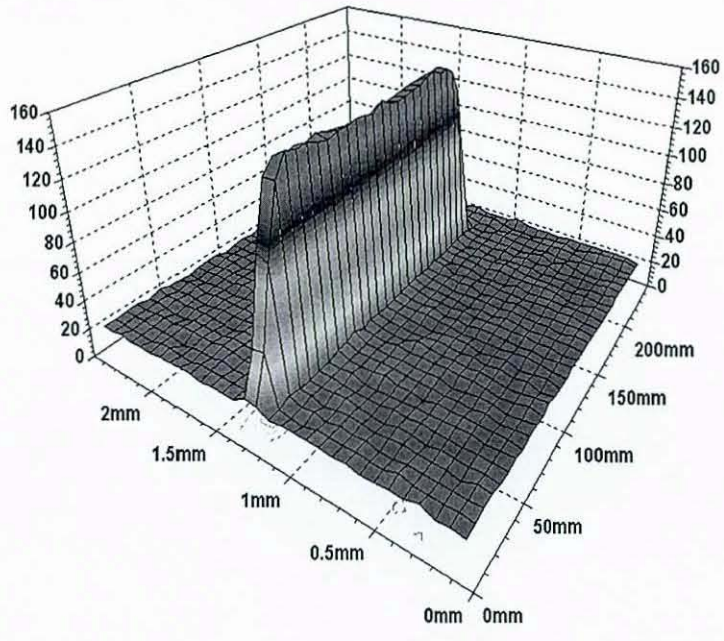

Fig 5.13 (b) Composite of several line beam segments

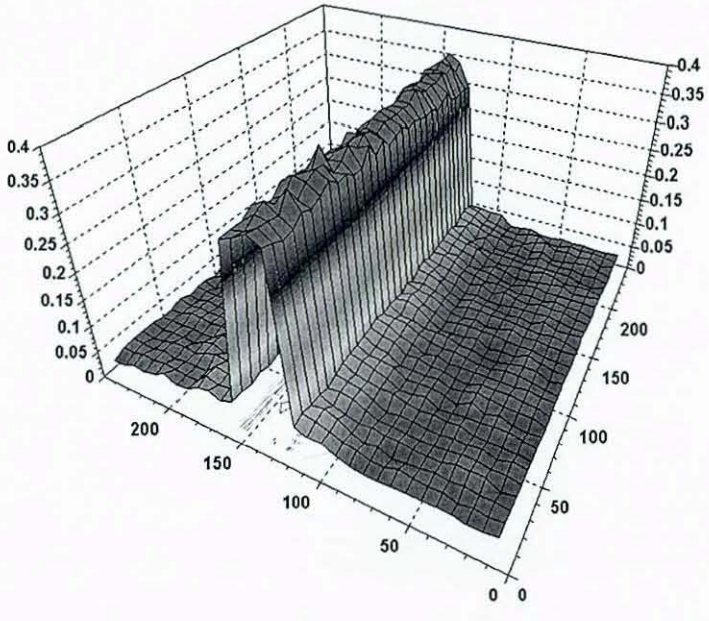

Fig 5.13 (a). Line beam segment

The function of the visualisation software is to 'stitch' together the array of individual line segment beam profiles to reconstruct the entire line focus. This can then be displayed as a false colour 2D map or as a 3D Isometric plot. To aid on screen viewing the data can be scrolled like a chart along the length of the beam viewing only a small segment at a time. Fig 5.13a shows an individual line beam segment; fig 5.13 b shows

the result of 'stitching' together a series of these segments to reconstruct the full line beam.

5.4.8 Beam analysis algorithms

In order to provide quantitative data about the line beam profile suitable for process optimisation it is important that the correct beam analysis algorithms are used. In this instance algorithms defined in the draft standard ISO/CD 13694 were used [4]. These are defined as follows:

5.4.8.1 Threshold uniformity

The calculation of this parameter is very important in the assessment of excimer laser beam quality. The threshold beam uniformity U is calculated [5] as the standard deviation of the power density histogram distribution, see figure 5.14.

$$U_n = \frac{1}{A_{ave}} \sqrt{\frac{1}{Area_n} \sum\sum (A_n(x,y) - A_{ave})^2} \; . \qquad \text{Equ (5.1a)}$$

Where

$$A_{ave} = \frac{1}{Area_n} \sum\sum A_n(x,y) \qquad \text{Equ (5.1b)}$$

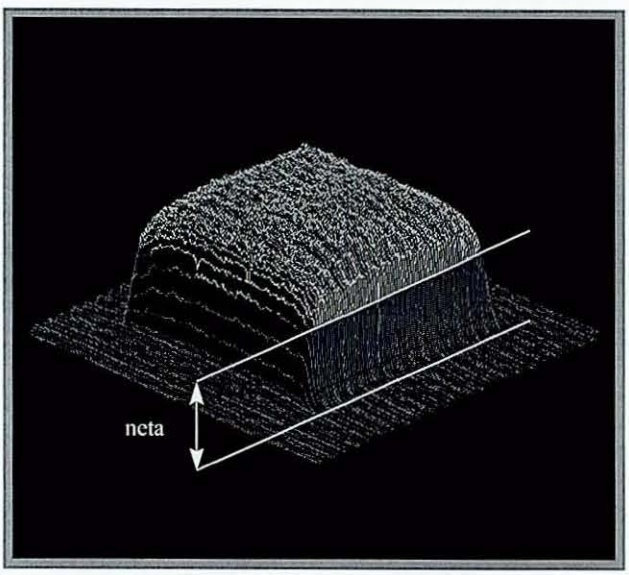

Integrations made only upon pixels with an intensity value greater than neta % of peak.

The beam Uniformity is the rms deviation of this distribution.

Fig 5.14. Illustration of the concept of threshold beam uniformity.

These integration's are usually performed only for pixels above the threshold power density ηE_p, The value of η is chosen empirically to simulate the desired beam interaction footprint, and is usually above 0.5 for distributions with $U \leq 0.1$

5.5.2 Calculation of plateau uniformity and edge steepness

The following algorithms have been shown [6] to be useful in the characterisation of steep edged, flat top beam profiles.

The plateau uniformity Up can be defined as

$$U_p = \frac{\Delta N(H_{\max})}{H_{\max}} \qquad \text{Equ 5.2}$$

where $\Delta N(H_{max})$ is the FWHM of the beam intensity histogram distribution $N(H_n)$ about the peak H_{max}.

The edge steepness S(z) is defined as

$$S(z) = \frac{A'_{01}(z) - A'_{09}(z)}{A'_{01}(z)} \qquad \text{Equ 5.3}$$

Where A'_n is the enclosed beam area above threshold intensity n.

Care has to be taken in the evaluation of these algorithms particularly with respect to the subtraction of background offsets and noise. For many edge steepness measurements it is desirable to apply equation 5.3 only to a cross sectional profile of the beam instead of the whole beam. This is particularly true of line beam profiles. This type of "stitching noise" can be clearly seen in the beam profile plot shown later in this chapter, in figure 5.18.

5.4.9 Experimental results

Line beam scans taken from both the experimental rig and an industrial laser workstation is now presented. The data shown here represent the start of initial trials of the experiment. The scans in figs 5.15 a,b were taken from a 200 mm line beam optical system working at 308 nm, the workpiece fluence being approximately 200 mJ/cm^2 and the average beam width 280 μm. Multiple line scans were averaged to get the results.

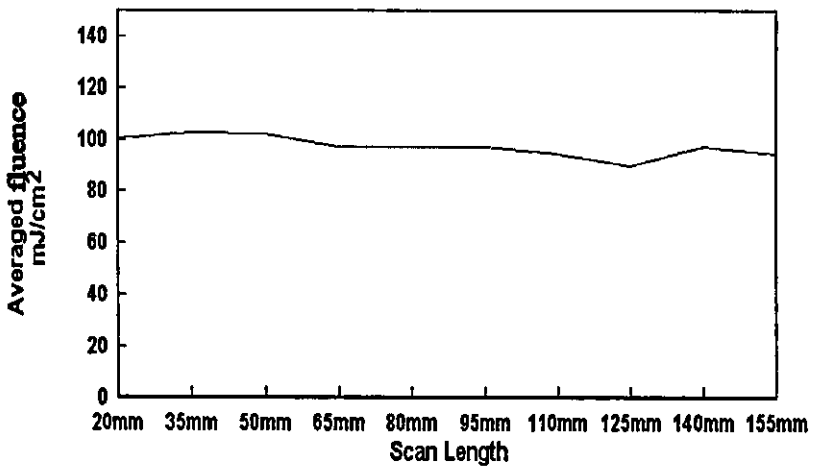

Fig 5.15 (a)

Averaged Plot of beam fluence

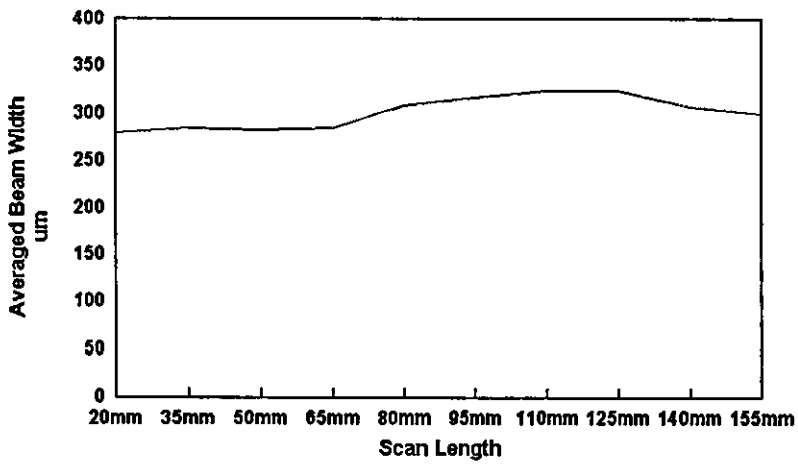

Fig 5.15 (b)

Averaged Plot of FWHM (50% cut) width.

The line beam displays 3.5% rms uniformity over 150 mm and the beam width varies by 5.5% over the same length.

5.4.10 Pulse to pulse variations

Figures 5.16 a,b show pulse-to-pulse changes in line beam shape 15 mm beyond focus. In this mode the quasi near field is being imaged and the variations are due to worn electrodes on the laser. The laser was running on a system that produced fibre gratings at 248 nm, 400mJ pulse energy, with a 50mm by 0.8 mm line beam. When looking at the focus the profile shape is relatively constant. This example serves to illustrate the usefulness of beam diagnostics for monitoring system performance.

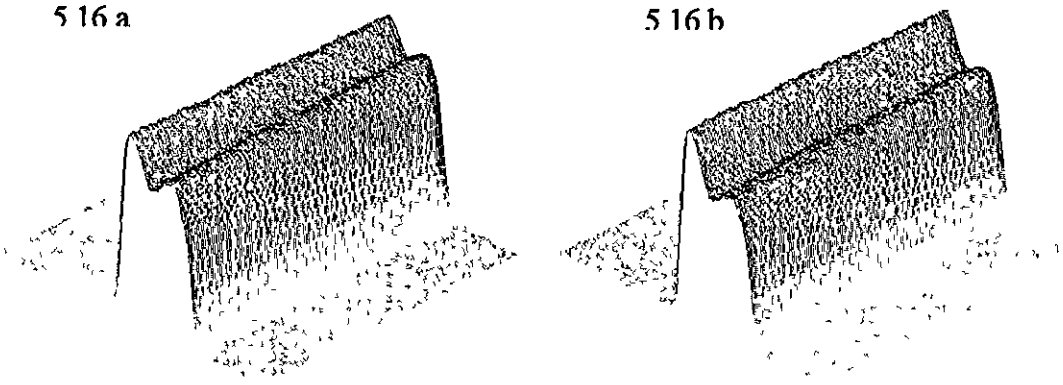

Fig 5.16 a and b. Two profiles showing pulse to pulse variations of a segment of the line beam beyond focus. The variation in beam symmetry is due to electrode wear in the laser.

5.4.11 Results from a Silicon annealing tool

The line beam data in figures 5.17 and 5.18 was taken from an industrial system equipped with embedded line beam diagnostics of the type shown in figure 5.9. The graphs show reconstructed beam profile scans using the embedded workpiece diagnostic system described in section 5.4.3. In this case although the line beam system had not quite been optimised, an overall uniformity figure of 3.6% over 150mm of the beam was achieved, which was well within the application specification. When properly optimised overall uniformity figures of better than 2% can be achieved.

The graphs in figures 5.17 show several reconstructed profile scans of the beam superimposed on one another. They show the variation of line beam widths and line beam average intensity over the length of the beam. The differences between scans are due to pulse to pulse variations of the laser.

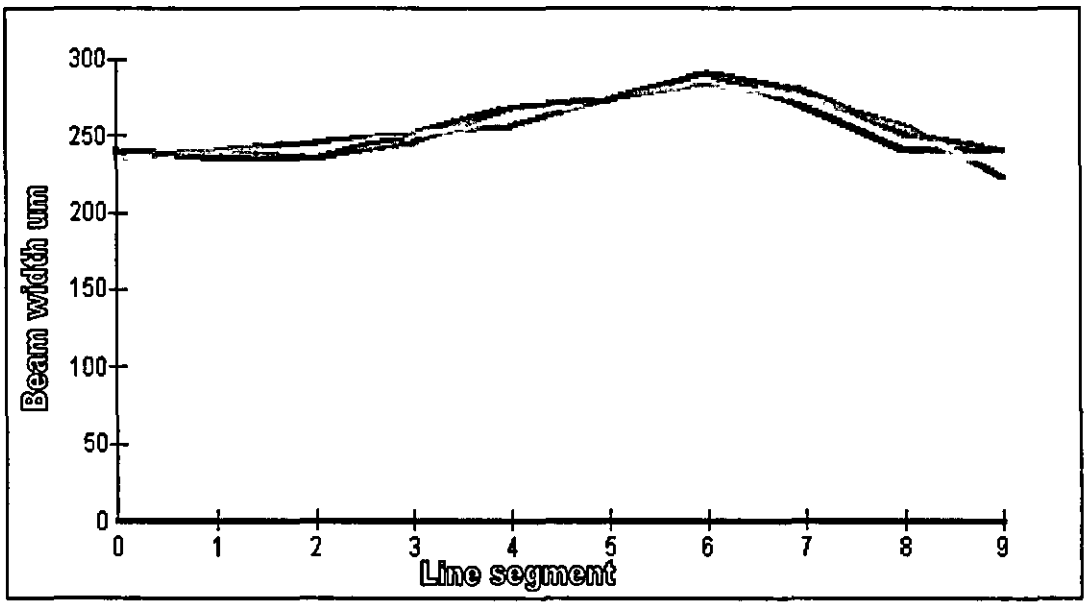

Fig 5.17(a) Variation of Line Beam width over the scan length

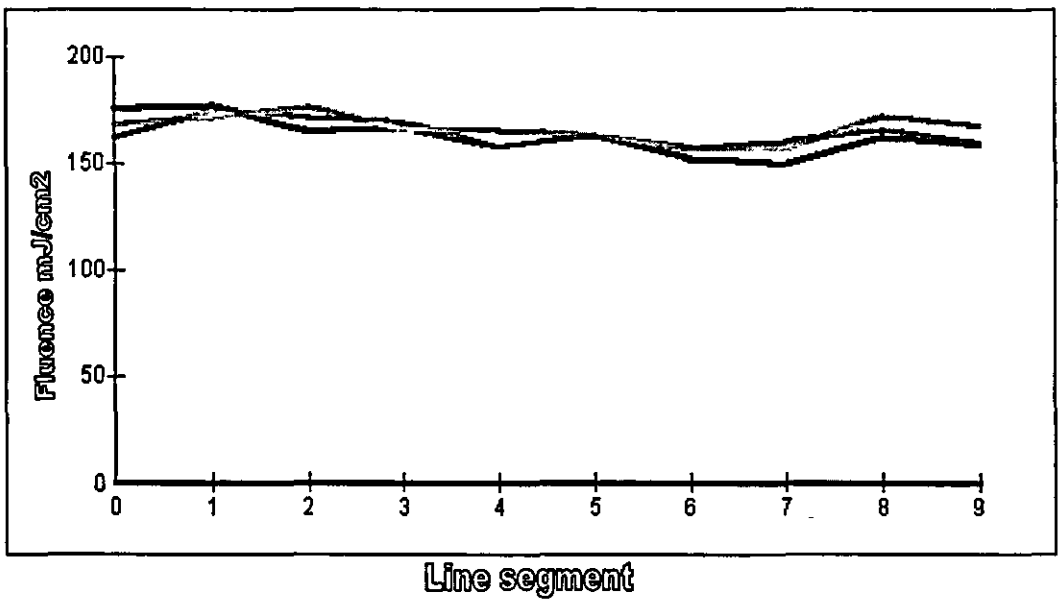

Fig 5.17 (b) Variation of Line Beam intensity over the scan length

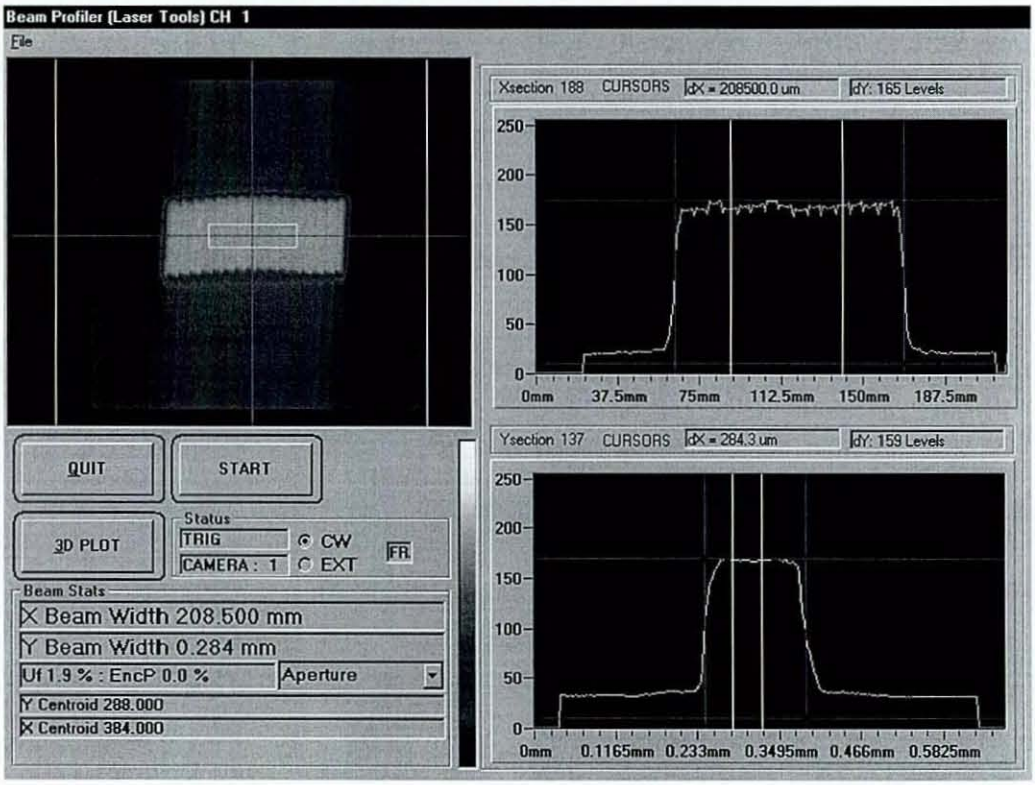

Fig 5.18. Screen shot from the beam analyser system, showing a complete line beam. This system is integrated into an excimer laser Silicon annealing tool.

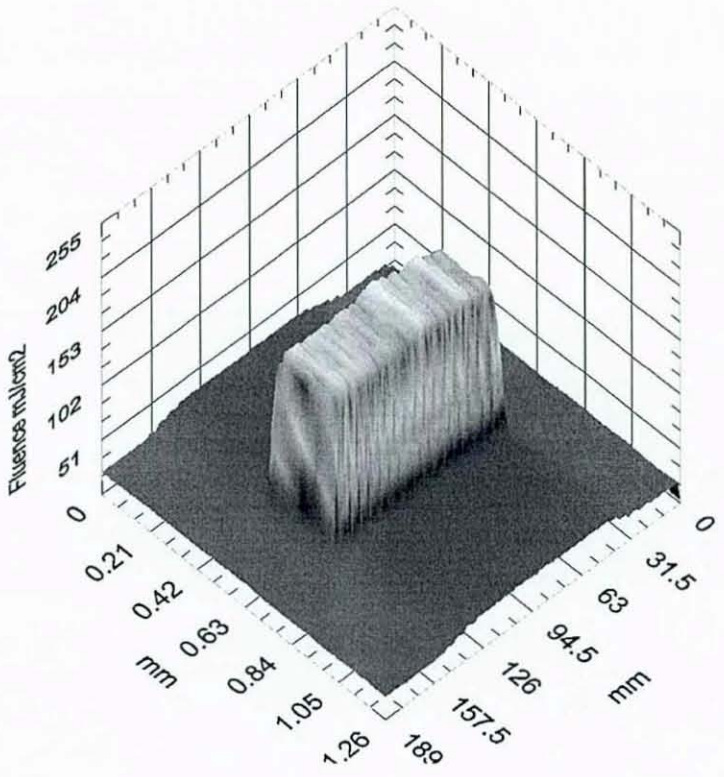

Fig 5.19. 3D plot of the line beam profile

5.4.12 Discussion

Improvements in algorithms and the falling price of computing hardware are now making sophisticated beam analysis possible for routine measurements. The latest generation of industrial computers now make possible sophisticated real time image analysis for laser process control and monitoring. It has been shown that line beam analysis measurements can be made off line in an industrial laser workstation. For the next generation of workstations it is proposed to implement real time line beam analysis during materials processing, further enhancing process quality and repeatability.

5.5 Industrial Beam Diagnostics

The techniques described in this chapter are readily applied to industrial systems. The author has been involved in numerous systems and applications, some of which are described in the following chapters. Typical workstation applications are in the semiconductor, electronics and biomedical fields. Figure 5.20 shows a prototype workstation for cleaning Silicon wafers. It features fully integrated beam diagnostics.

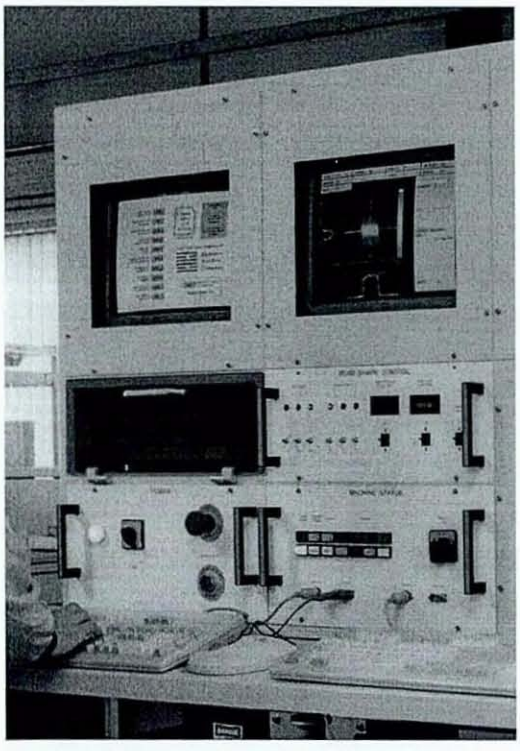

Fig 5.20. Wafer cleaning workstation, featuring fully integrated excimer beam diagnostics and beam shape control

The operator has full control over the beam shape, size and fluence by means of a system of motorised optics and attenuator plates [7]. These are used in conjunction with the integrated beam profiler, which gives a real time display of beam size, shape and fluence.

This allows the operator to quickly setup new process parameters without having to manually adjust any beam line component. Not only does this provide a great degree of experimental flexibility, but enhances system safety by removing the need for the operator to change optics in the beam line manually whilst the laser is running. In the previous lab prototype of this machine all optical changes and beam monitoring had to be performed manually.

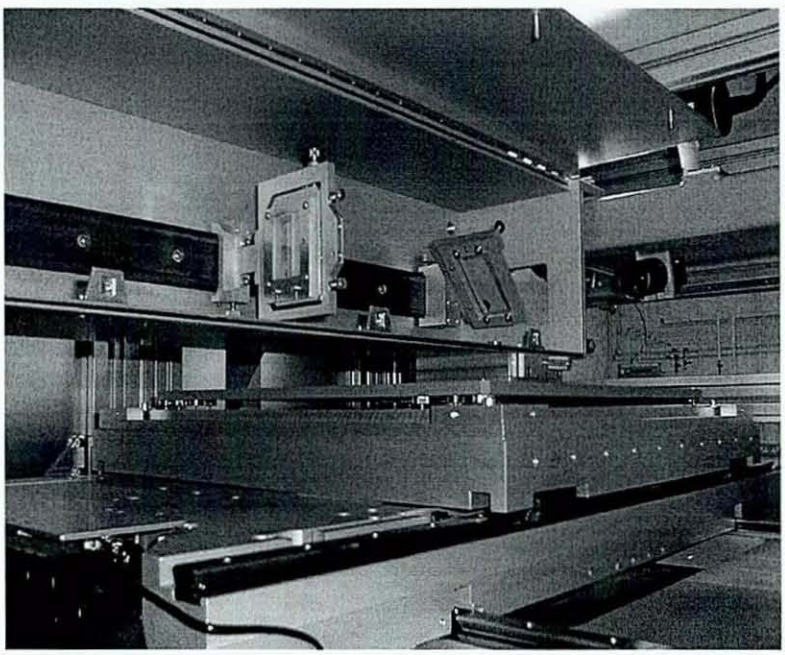

Fig 5.21: CCD camera, with zoom lens and fluorescer plate mounted in beam line, to monitor the mask plane beam profile.

The beam profiler interfaces to the control computer via an RS232 serial interface. The control application periodically polls the beam monitor for information about the beam energy, fluence, uniformity and alignment. If any of these parameters fall outside of user set limits the processing is stopped by the control computer. The beam monitor application itself can also display visual and audible alarms and flag an external I/O line to operate a laser safety shutter. This provides much faster response than via the control PC. Figure 5.21 shows the optical arrangement for such as system integrated into an

Exitech M8000 excimer laser workstation. Note the use of a fluorescer plate and CCD camera equipped with a zoom lens to image the beam profile. This type of arrangement provides a great deal of flexibility as the beam diagnostic camera can be placed some distance from the imaging optics, and space is always an issue when designing beam delivery systems.

An alternative version of this configuration is shown in figure 5.22. This system is implemented on an Exitech M2000 Micromachining system and combines through mirror beam sampling (as described in section 5.2.5) with a fluorescent converter plate.

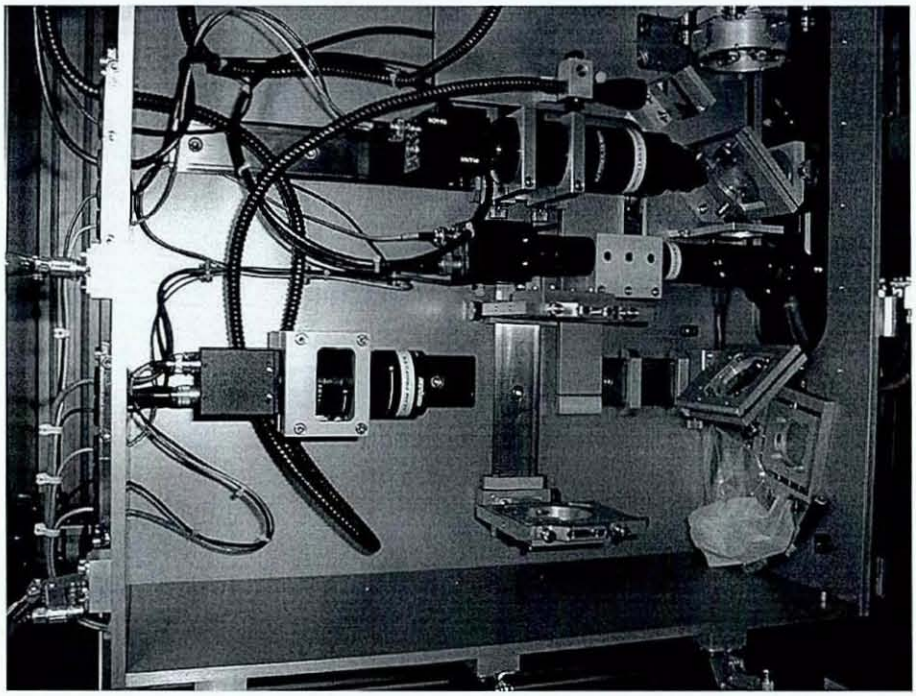

Fig 5.22: Integrated on line diagnostics, using through mirror beam sampling

With this arrangement a through the lens viewing microscope can be used in the system, whilst simultaneously allowing the mask plane beam profile to be monitored. Through the lens viewing can be used for target location, alignment and focussing of process samples and is a special feature of the M2000 system.

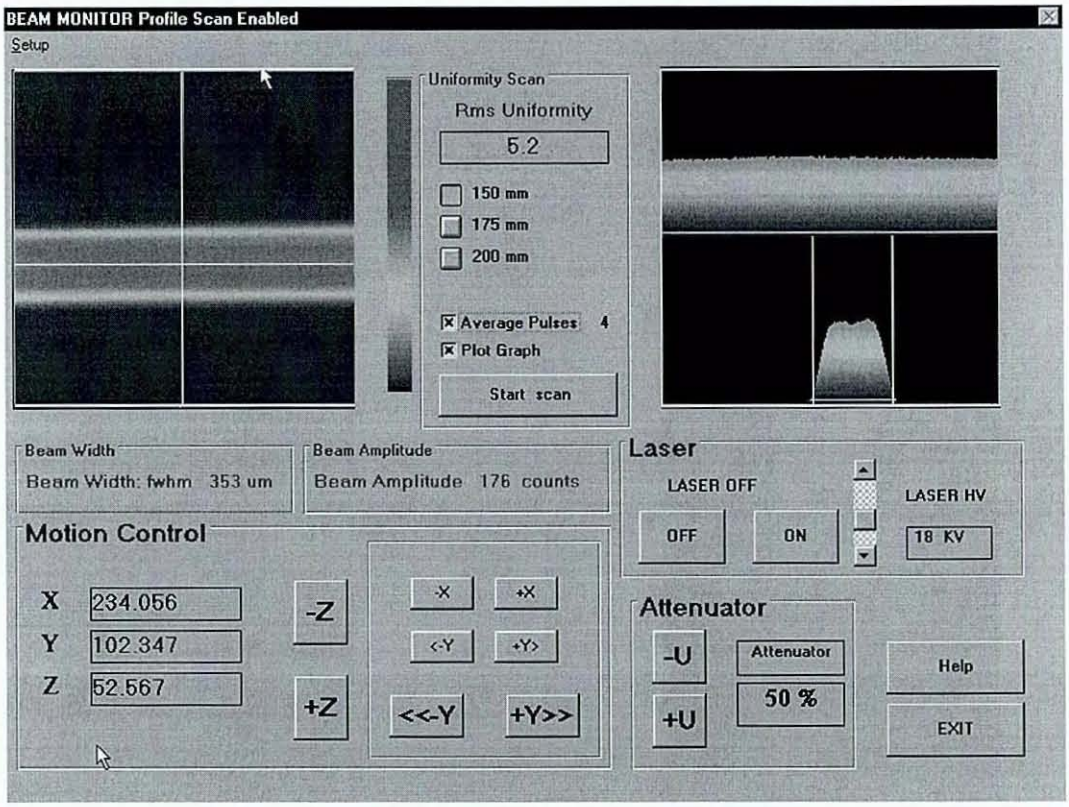

Fig 5.23: Example of excimer beam diagnostics fully integrated into machine control software.

Figure 5.23 shows the screen display from an integrated beam profiler installed on an excimer laser tool used for processing multi chip modules. The system uses the same configuration as described in section 5.4.6. The software also integrates control functions for moving XY stages and controlling a laser attenuator to adjust process fluence.

There are safety benefits in integrating beam diagnostics into laser processing systems, which are closely related to the process, and quality benefits that such equipment brings. Even small improvements to reliability and yield will quickly justify the cost of integrated beam monitoring. This has the additional benefit of greatly simplifying laser and optics alignment procedures hence reducing the risk of a laser accident, as engineers will need to spend less time working on an open beam line and adjustments can be made remotely.

5.6 Conclusions

Of all laser types commonly used in industrial systems, excimer lasers require good laser beam diagnostics in order to operate reliably and effectively. In this chapter a number of topics have been discussed, including beam sampling techniques, analysis algorithms and systems integration. One of the first uses of in-chuck beam profiling has been described; this equipment is now integrated into many Exitech laser tools.

Methods for the measurement and analysis of high aspect ratio line beams have also been described, techniques that require special hardware in addition to special analysis algorithms. These techniques are now in use and have been successful in aligning and characterising systems for Silicon annealing.

Over a period of almost 10 years, the author has been involved in the design and integration of many beam diagnostic systems for use in a diverse range of industrial excimer laser tools. In all of these applications, effective beam monitoring has been of great importance to the operation of the laser tool. Some applications of these tools are discussed in the next chapters.

5.7 References

1). K Mann, A Hopfmuller, "Characterisation and shaping of excimer laser radiation" Proceedings of the 2nd Workshop on laser beam characterisation, H Weber et al eds, FestKorper Laser Institut , Berlin ,(1994)

2). D C Emmony and B Omar, Journal of Applied Optics, September,(1988)

3). Lambda Physik Industrial report No 10, p6, May, (1996)

4). ISO/TC/SC9/WG1/WD 13694, "Optics and optical instruments, Test Methods for laser beam parameters: Power (Energy) Density distribution"

5). P Apte, M C Gower, "Computational methods for beam Amplitude characterisation", Proceedings of the 2nd Workshop on laser beam characterisation, H Weber et al eds, FestKorper Laser Institut, Berlin , (1994)

6). K Mann et al, "Characterisation of excimer Laser beam parameters", Proceedings of the third international workshop on Laser beam and optics characterisation, SPIE Vol 2870 (1996)

7). Report on UV detector evaluation for 2D beam monitoring, EU643 task 21103, Exitech, (1993)

CHAPTER 6

EXCIMER LASER SYSTEMS AND APPLICATIONS

6.1 Introduction

Laser based micromachining using excimer laser has been well established in many industrial processes, covering a broad range of applications from drilling ink jet printer nozzles to annealing amorphous silicon flat panel displays [1]. Several novel machine architectures have been developed to bring excimer micromachining into mass production environments.

This chapter describes some excimer laser micromachining applications and systems designed for production. The first system is the Exitech M8000, which is a general-purpose mask scanning system that is used for research as well as production. The second system, the GWS200 is a mask writer that uses contact phase masks and an excimer laser to write fibre Bragg gratings.

All of these systems use advanced beam monitoring and diagnostic systems to assist in calibration and alignment, using systems developed by the author.

6.2 Excimer laser micromachining

Since the early 1980's UV excimer radiation has been used for micro ablation and micro machining [2]. During the past decade tremendous growth has been seen in both the applications of excimers and the types of laser system available. The standard excimer party trick is to etch micron scale patterns in human hair without damage to the surrounding material, as shown in fig 6.1.

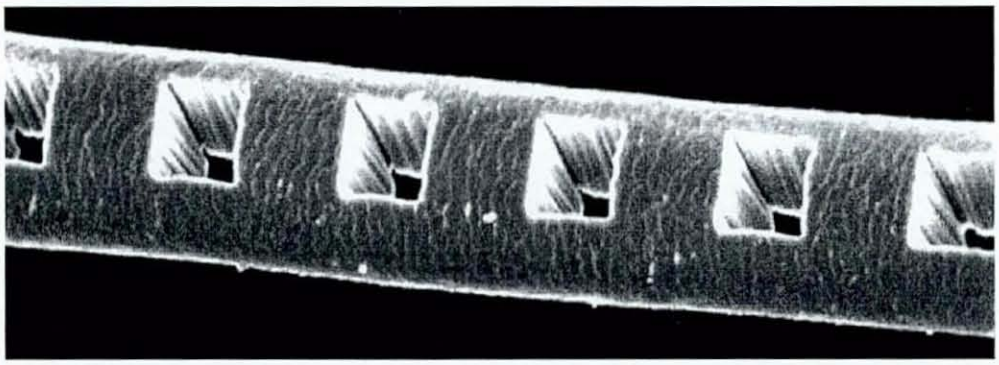

Figure 6.1. ArF laser-micro machined 50um square holes though a human hair (Provided by the author).

As early as 1983 excimer laser Micromachining was being used to fabricate specialist targets in laser-fusion implosion experiments [3]. Figure 6.2 shows ArF laser machined polystyrene microshell targets used for studying Rayleigh-Taylor plasma instabilities. The fabrication of micro machined components using excimer lasers was one of the first practical applications for this technology. The special properties of short pulse high power UV radiation have been quickly applied to a wide variety of micro fabrication operations. The potential range of applications is great, covering surface modification, micro actuator fabrication, micro channel fabrications and circuit interconnect patterns.

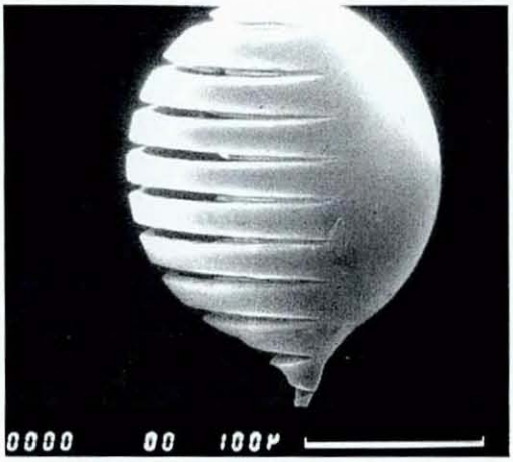

Figure 6.2. ArF laser machined features in 150um diameter polystyrene laser targets, from ref [3].

6.2.1 Applications

Examples of the types of surfaces that can be structured by excimer laser ablation are shown in Figures 6.3 a & b. Blazed grating and pyramid-like structures can be readily fabricated on surfaces by mask-dragging techniques [4]. Such methods can be used for making micro-optical surfaces like those shown below. The micro lens array shown in Figure 6.4 is used for shaping beams from laser diodes. Each lenslet in this array has a focal length of 1mm. Excimer laser ablation is being used to manufacture '*biofactory-on-a-chip*' (BFC) cell-sorters and sensors that consist of laminated layers of channels, chambers and electrode conveyor tracks. Figure 6.5 shows examples of micro fluidic channels and ramps being used in this device as well as in medical sensors [5] such as pregnancy testers.

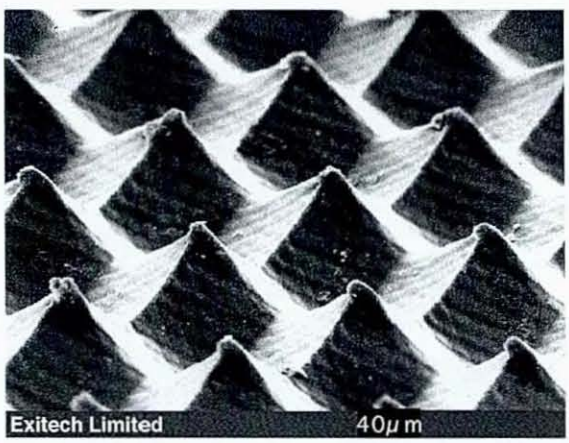

Fig 6.3a. Pyramids KrF laser produced surfaces in polycarbonate produced using mask-dragging techniques

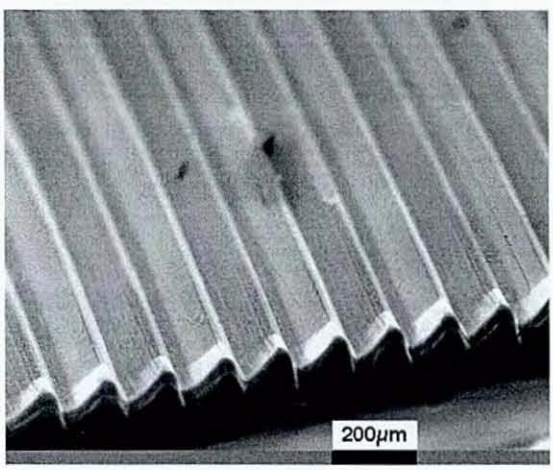

Fig 6.3b. Blazed grating structure in polycarbonate, produced using mask dragging

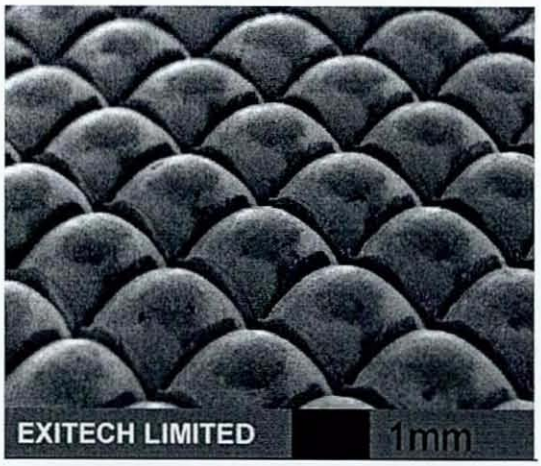

Figure 6.4. Micro-lens surfaces in polycarbonate, fabricated by KrF laser micromachining and orthogonal mask-dragging

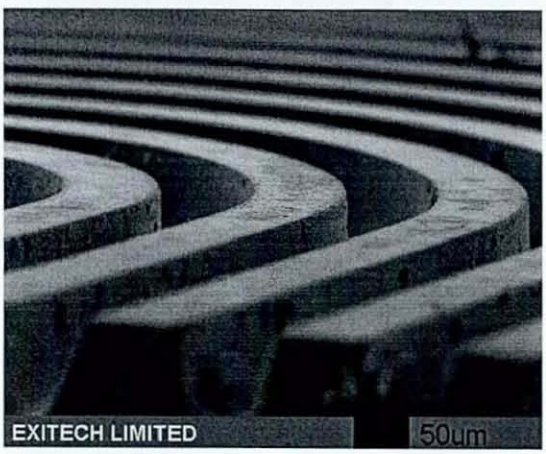

Figure 6.5. KrF laser micro machined micro fluidic channels in polyester

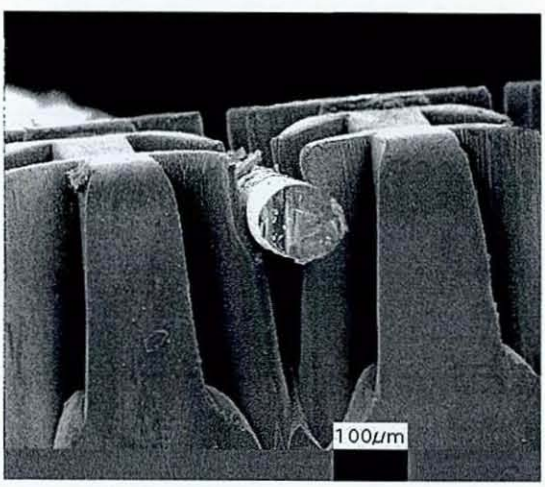

Fig 6.6. KrF laser machined 100um fibre clamp in polycarbonate.

The structures shown in figures 6.6 and 6.7 (a) & (b) show an experimental application to fabricate polymer fibre holders for telecom applications [6]. Figures 6.8 (a) & (b) show KrF laser-machined 3D-structures in polycarbonate using an Exitech Series 7000 CNC-controlled micromachining system.

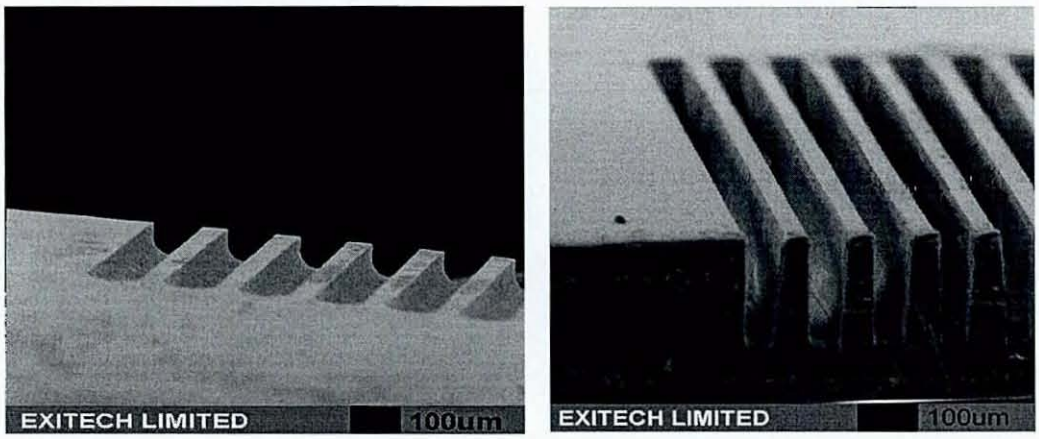

Figure 6.7 a & b. KrF laser micro machined fibre holders in polyester

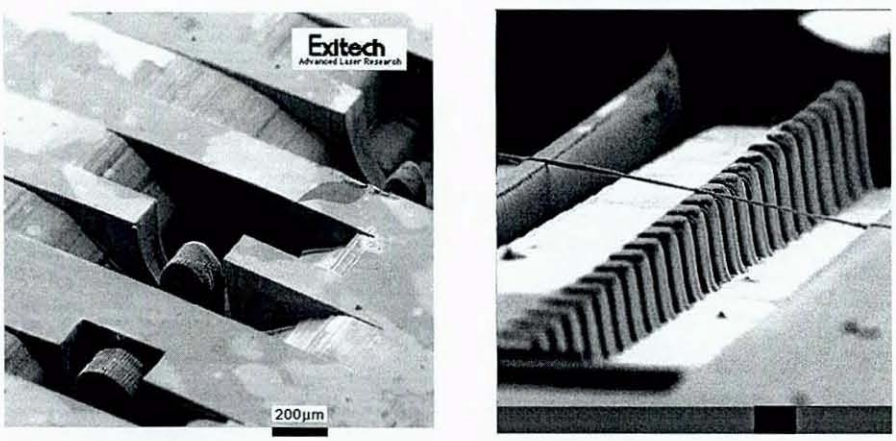

Figure 6.8 a & b. KrF laser machined
ramps, channels and bars in polycarbonate

6.2.2 Micro via fabrication

The continuing demand for finer interconnects and more compact designs for a number of electronic applications has driven the adoption of laser technology. The drilling of micro vias using pulsed Nd:Yag laser and CO_2 laser was pioneered in the 1980's.

Excimer lasers have proved very effective at ablating polyimide dielectric layers used in the fabrication of multi chip modules for super computers. This process was developed on an industrial scale by Siemens Nixdorf in Germany, where 80 um diameter vias were KrF laser drilled in MCM modules using a conformal mask [7]. This was one of the first ever examples of the use of excimer lasers on an industrial scale, with more than 15 lasers in use at the plant during the early 1990's. A laser beam diagnostic system developed by the author was used in the setup and maintenance of these laser systems. This technique is now widely adopted for micro via fabrication.

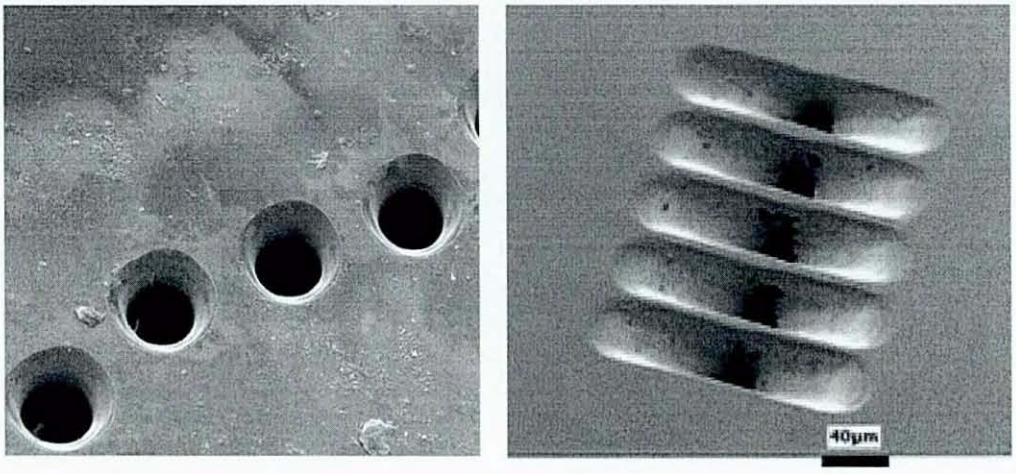

Figure 6.9 a, b. KrF micro machined nozzle structures in polyimide

6.2.3 Inkjet printer nozzle drilling

This is now a major application of excimer lasers on an industrial scale. The author has contributed to the development of a number of these systems with particular regard to the design of beam diagnostics and laser process control.

Inkjet printers comprise a row of small tapered holes through which ink droplets are squirted onto paper. Adjacent to each nozzle, a miniature resistor rapidly heats and boils ink forcing it through the nozzle orifice. Increased printer quality can be achieved by reducing the nozzle diameter, decreasing the hole pitch and lengthening the head. Modern printers like HP's Desk Jet 800C and 1600C have 300x 28µm input diameter nozzles giving a resolution of 600 dots-per-inch (dpi). Earlier 300dpi printers consisted of a 100 nozzle row of 50µm diameter holes made by electroforming thin nickel foil.

Trying to fabricate more holes with smaller diameters reduced even further the already low 70-85% production yield. The laser-drilling of nozzle arrays has allowed manufacturers to produce higher performance printer heads with greater yields. At average yields of >99%, excimer laser mask projection is now routinely used for drilling arrays of nozzles having consistent size and wall angle [8]. A large proportion of the ink jet printer heads currently sold (e.g. by HP and Canon) are excimer laser drilled on production lines in the US and Asia. Figure 6.9(a) shows an excimer laser drilled nozzle array in a modern printhead.

Figure 6.9(b) shows nozzles with nonlinear tapers that aid the laminar flow of the droplet through the nozzle. Some advanced printers use piezo-actuators. Rather than being constrained to produce nozzle profiles characteristic of the process, excimer laser Micromachining tools with appropriate CNC programming can readily engineer custom-designed reverse-tapered, $2^{1/2}$ D and 3D structures. Figure 6.10(a) shows an array with ink reservoirs machined behind each nozzle while Figure 6.10(b) shows an example of a rifled tapered hole, which spins the droplet like a bullet to improve its accuracy of trajectory.

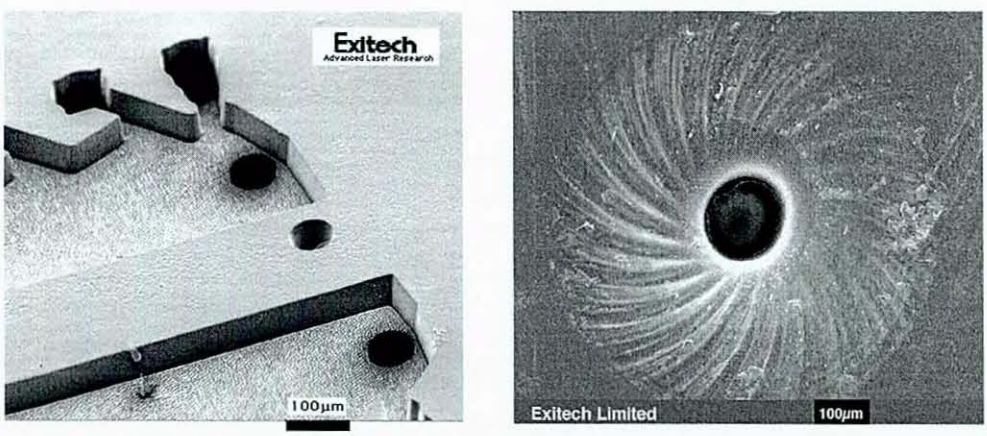

Fig 6.10 (a) Nozzle array with ink reservoirs. 6.10 (b) Tapered nozzle with rifling. KrF laser-micro machined nozzle structures in polyimide

6.2.4 Biomedical devices

The drive to increase miniaturization with extra functionality has aided the rapid

progress being made in the biomedical industry. Precision micro drilling with excimer lasers is now routine for the manufacture of the delicate probes used for analysing arterial blood gases (ABGs) [9]. ABG sensors measure the partial pressures of oxygen (PaO_2), carbon dioxide ($PaCO_2$) and hydrogen-ion concentration (pH) used for monitoring the acid-base concentration essential for sustaining life. In intensive care units, ABG results are used to make decisions on patient's ventilator conditions and the administration of different drugs. An example of an excimer machined sensor is shown in figure 6.11. These sensors have been in routine production using excimer lasers at Exitech for more than 10 years.

Figure 6.12 shows an example a ABG catheter for monitoring blood in premature babies. The hole at the side of the PVC bilumen sleeving tube through which blood is drawn is machined using a KrF laser. In this case the clean cutting capability of the laser provides the necessary rigidity that prevents kinking and blockage of the tube when inserted into the artery

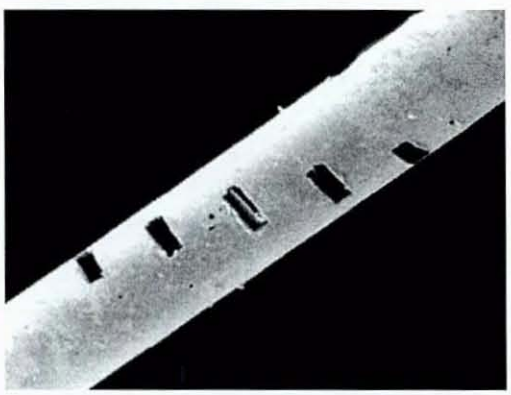

Fig 6.11. ArF laser-drilled holes in PaO_2 and $PaCO_2$ acrylic fibres, for an arterial blood gas sensor.

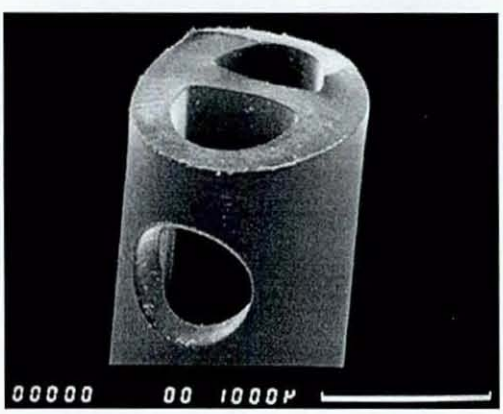

Fig 6.12. KrF laser-drilled hole in side of PVC bilumen catheter, for blood monitoring in new born babies.

6.3 The M8000 micro machining system

Laser systems are being employed increasingly in many diverse micro-systems technology (MST) sectors such as biomedicine, automotive manufacture, telecommunications, display devices, printing technologies and semiconductors [10]. These applications areas are using lasers in different ways ranging from basic research and development stages to full production environments. The requirements of the high-specification products, which are now being considered, are often quite stringent and this has led to many refinements and developments in the lasers systems and laser techniques, which are used. These advances, in turn, have promoted the uptake of laser-based technologies by providing technical, manufacturing and economic benefits.

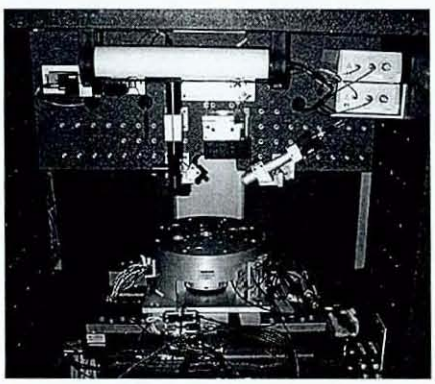

Fig 6.13. The Exitech M8000 micromachining system

6.3.1 System Architecture.

The M8000 is a general purpose excimer laser micromachining tool (Figure 6.13) that can be used for both research and production applications. The basic configuration couples a set of high resolution XY translation mask stages with XY translation workpiece stages. The use of a sophisticated motion controller allows the two sets of

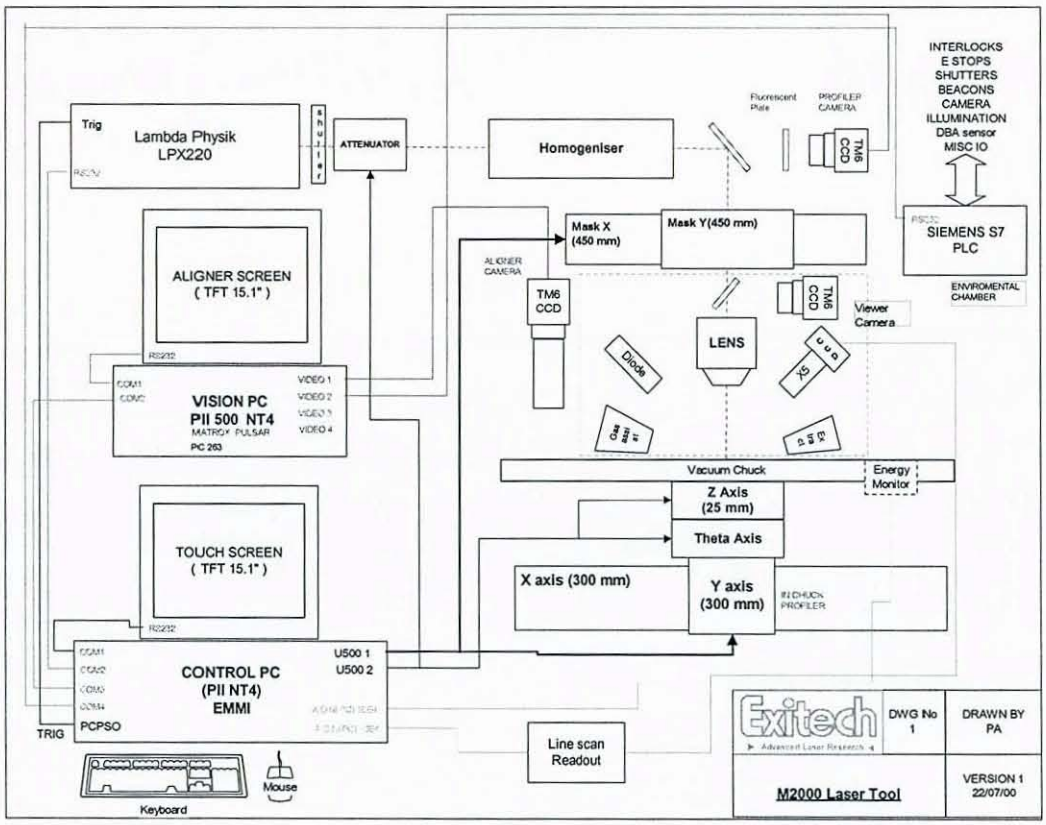

Fig 6.14. M8000 control system

stages to be electronically geared together, enabling the mask scanning techniques described in this chapter. A diagram of the control systems is shown in figure 6.14. Additional stages for focus (Z) and rotary alignment together with precision height sensing and alignment systems, allow the M8000 to position with sub micron accuracy.

6.3.2 MEMS fabrication

Most of the excimer laser systems used in manufacturing applications today use the technique of mask projection [11][12]. The optical properties of excimer lasers mean that direct beam focusing is not an effective use of laser energy. Projection methods are more efficient for the production of various microstructures. Mask projection methods used with excimer lasers can provide many desirable features [13] but the most important ones of interest to MST are high feature resolution, fine depth control, excellent reproducibility and the ability to cover large sample areas efficiently. For example such features, which are depicted in figures 6.15 for the machining of polyimide, have led to excimer laser systems being used in the mass production of ink-

jet printer nozzles.

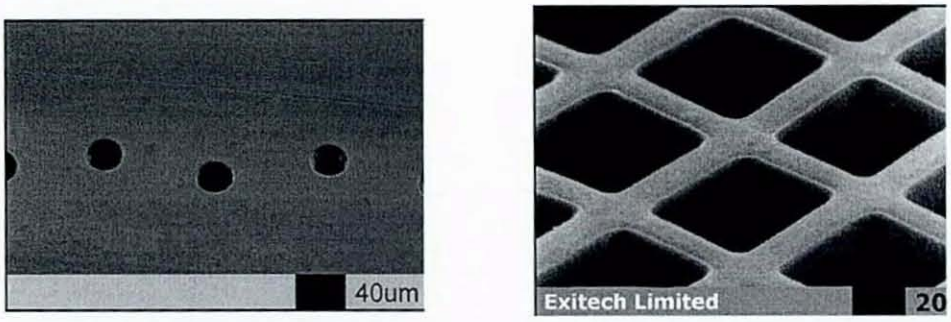

Figure 6.15 (a) Micro-machining of polyimide and 6.15 (b) ink-jet printer nozzles, both produced using excimer laser mask projection

In standard mask projection systems, the depth of the microstructures is controlled by the numbers of laser shots which are fired and the resolution of the features are determined by the mask and the optical projection system. This is demonstrated in figure 6.16 where micro channels of 18μm depth have been produced in a polymer. The entire sample area (which can be many tens or hundreds of cm^2) is machined under the same laser conditions and so all the microstructures are produced to the same depth. This is, in fact, highly desirable in most applications since uniformity of depth is of particular importance.

In some emerging areas, however, there is a need to tailor the depth profile of the micro-machined structures across the sample area. These applications include micro-fluidic systems, printing devices, bio-medical analytical chips and rapid prototyping technologies – all sectors where multi-functional units are being developed which utilise micro-optical-electro-mechanical systems (MOEMS). The integration of these sub-units having a variety of functions has led to the need for increasingly elaborate designs for these devices and instigated the development of new micro-machining techniques.

6.3.3 Overlay Mask scanning

Standard mask projection techniques are very versatile and depth information can be imparted into micro-machined samples by an appropriate synchronisation of the sample

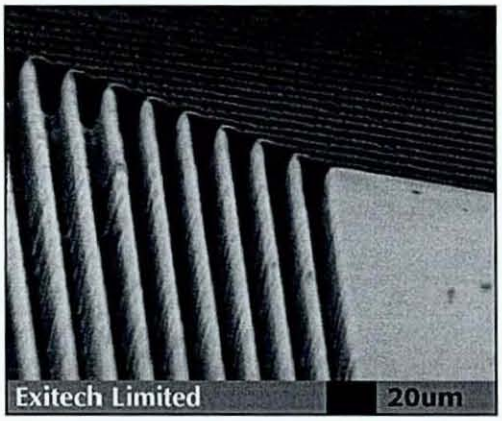

Figure 6.16. Micro-channels produced by mask projection in polymer showing depth control.

position and the laser firing sequence. The level of control of the depth profile required in the above-mentioned applications, however, means that these standard methods do not extend far enough. To overcome this limitation, a new technique – *synchronised overlay scanning* (SOS) – has been developed.

The basics of standard synchronised mask scanning systems have been described in detail previously [14]. To extend this technique and add depth information, the SOS method additionally shapes the laser beam which is used, and it is this choice of beam shape which determines the depth profile which is imparted to the microstructures. The concept of synchronised overlay scanning is discussed in more detail in ref [15].

The SOS technique uses standard synchronised scanning where the mask and the workpiece are moved in unison but in addition to this, an aperture is also placed above the mask to tailor the shape of the beam. The shape of the aperture (i.e. the shape of the beam) determines the depth profile in the sample – hence a triangular beam shape will give rise to a triangular depth variation in the material as seen in cross-section. Another feature of the SOS method is that the choice of mask (which determines the features to be made) is independent of the choice of beam shape aperture (which controls the depth profiling). This means that there is great scope for selecting appropriate combinations of masks and apertures depending on the specific requirements of the application.

An example of synchronised overlay scanning are shown in figures 6.17 (a) & (b) where different combinations of beam shapes and mask have been used. For the example in figure 6.17(a), an open rectangle mask was used with a double-triangle aperture as shown. This combination produced the double ramp structure as shown. For the example in figure 6.17 (b), the mask was made of open slots, which produced channels on the double ramped slope.

Synchronised overlay scanning techniques are now being applied in many different developmental areas where the combinations of high resolution micro-structures and changes in feature height can be of benefit in the micro-product designs.

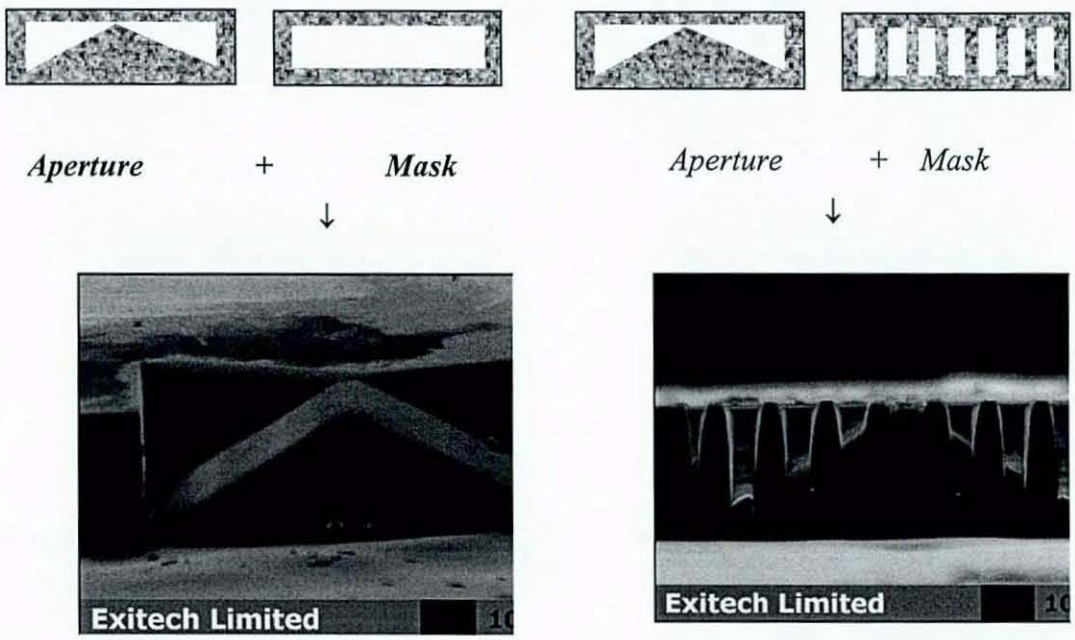

Figure 6.17 (a). Double ramp produced in PET using Synchronised mask scanning. Figure 6.17(b) ramp with channels fabricated using the same technique.

These applications include:

- Micro-fluidic transport systems and mixing devices where fluids (including inks for printing applications) need to be channelled mixed and/or transferred through nozzles.
- Innovative designs include those for lubrication equipment where the lubricant

needs to be inserted, propelled and extracted from arbitrarily shaped mechanical parts.

- Components for micro-parts for MST devices, whether produced directly or as a master for further replication.
- Optical devices used for on-chip sensing or for display panel enhancements.

Figure 6.18 shows other examples of the results of synchronised overlay scanning where channels and holes have been combined onto variable depth substrates.

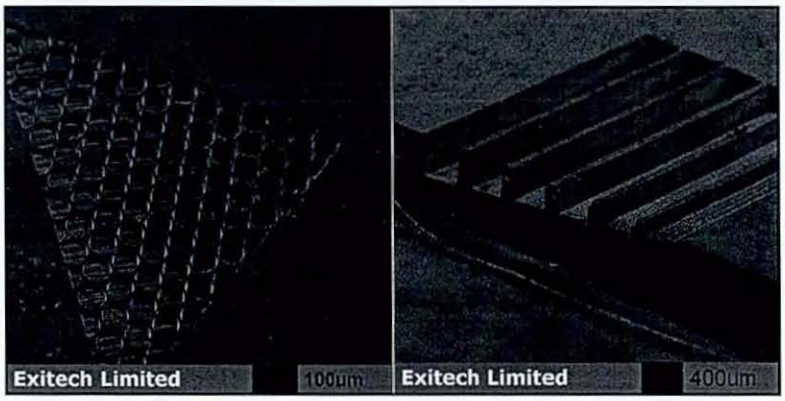

Figure 6.18. Demonstration of multi-level micro-structuring using synchronised overlay scanning.

The laser microprocessing techniques described here are part of a number of on going developments in advanced manufacturing that are bringing new technologies to the mass market. All these techniques require precise control and characterisation of laser energy in order to be successful.

6.4 The GWS 200 Fibre Bragg Grating writing system

6.4.1. Introduction

The GWS200 is production system for the writing of Fibre Bragg grating structures in Optical Fibres using a 248nm excimer laser and a contact phase mask [16]. These gratings have a variety of applications from spectral filtering in Dense Wavelength

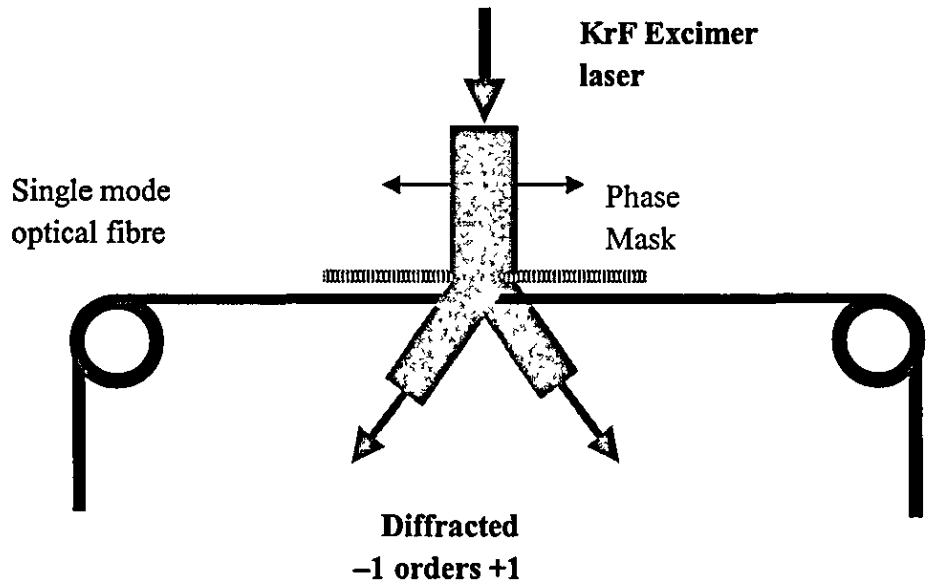

Figure 6.19. Writing fibre Bragg gratings

Division Multiplexing (DWDM) systems to temperature and strain sensing [17]. The system uses a KrF excimer laser, spatially filtered and beam shaped. The measurement of beam uniformity, the fibre to mask alignment and control of the total exposed dose are critical to reliable grating production.

The author has developed a fully integrated control system that automated the fibre exposure process with accurate laser dose control and beam profiling. There now follows a description of the system.

6.4.2 System description

The system is fully integrated and comprises of a number of subsystems. These are beam delivery shaping, safety systems, energy control, beam profiling, fibre viewing and alignment, fibre handling, fibre tensioning and mask & fibre stage motion control. A highly integrated control system consisting of a single control computer is used for all functions. It is shown in figure 6.20.

In the current configuration functions are provided to view the fibre for alignment, measure the laser pulse energy at the exposure plane and control of the laser dose onto

the fibre. Full motion control of the mask stage and fibre jig stage is provided for multi step exposure cycles, together with computer control of the fibre tension.

The software is written in Visual Basic and provides a simple intuitive user interface that guides the operator through system functions using a sequence of screens. The graphical layout has been designed to allow easy touch screen operation. Process data can be logged to a remote hard drive. The use of a modular architecture based upon ActiveX components allows easy modification and extension of the system functionality.

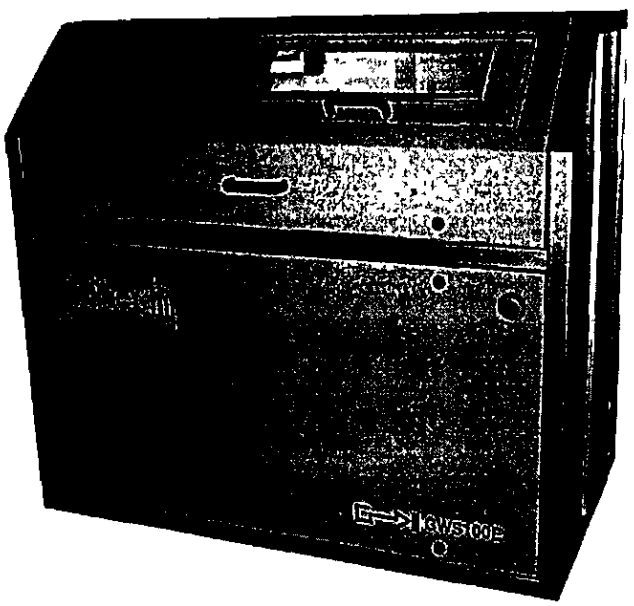

Fig 6.20 The GWS 200 FBG Writing system

6.4.3. Control software

The main menu is displayed on system boot up, as shown in figure 6.21. It provides access to all the system functions and displays system status in a Task bar at the top of the screen together with system log information. The operator is first invited to log on (indicated by a flashing red border around the appropriate button). Having logged on the system it must be initialised by pressing the Initialise button before the system can be used. This will home all stages to their initial positions and test the initialisation of all ancillary hardware. After Initialisation the system is ready for use. However on

initial power-up before a fibre processing shift commences it is advisable to check the detector Fluence calibrations, the laser beam profile and set the process Fluence.

The control system uses an industrial PC for system control interfaced via an RS232 link to a Siemens S7 PLC (equipped with ASI bus) that handles I/O and interlock functions. Motion control is implemented using an Aerotech U500 card, that controls the mask axis, fibre jig axis and laser attenuator. A Coherent Ealing PCM100 card is used to control a motorized micrometer for setting of fibre tension.

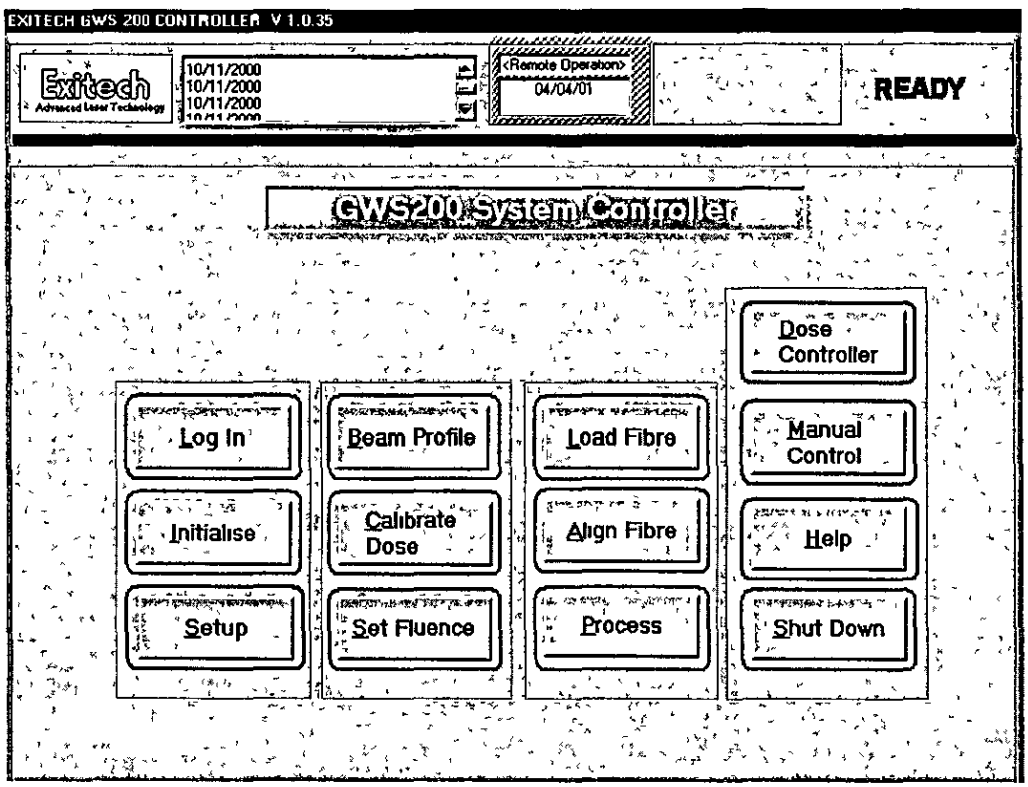

Fig 6.21 : Main control screen

The fibre viewing and beam profiler functions are implemented using a Matrox Orion vision card. The energy monitoring and dose control use a National Instruments A/D card. A multi port RS232 Communications card and an Ethernet card are installed for system communications. Stage motion control is handled by an Aerotech Unidex 500 card. This controls the mask stage, fibre jig translation stage and a motorized laser power attenuator. The stage parameters are stored in U500 parameter and project files

separate from the main application INI files, and are configured using the Aerotech U500 MMI software. These are loaded on system initialisation. Stage control is fully integrated into the process control and calibration software. However direct manual control using jog keys and command line G codes is available from the system manual control screen. The process flow for a grating exposure is shown in figure 6.22.

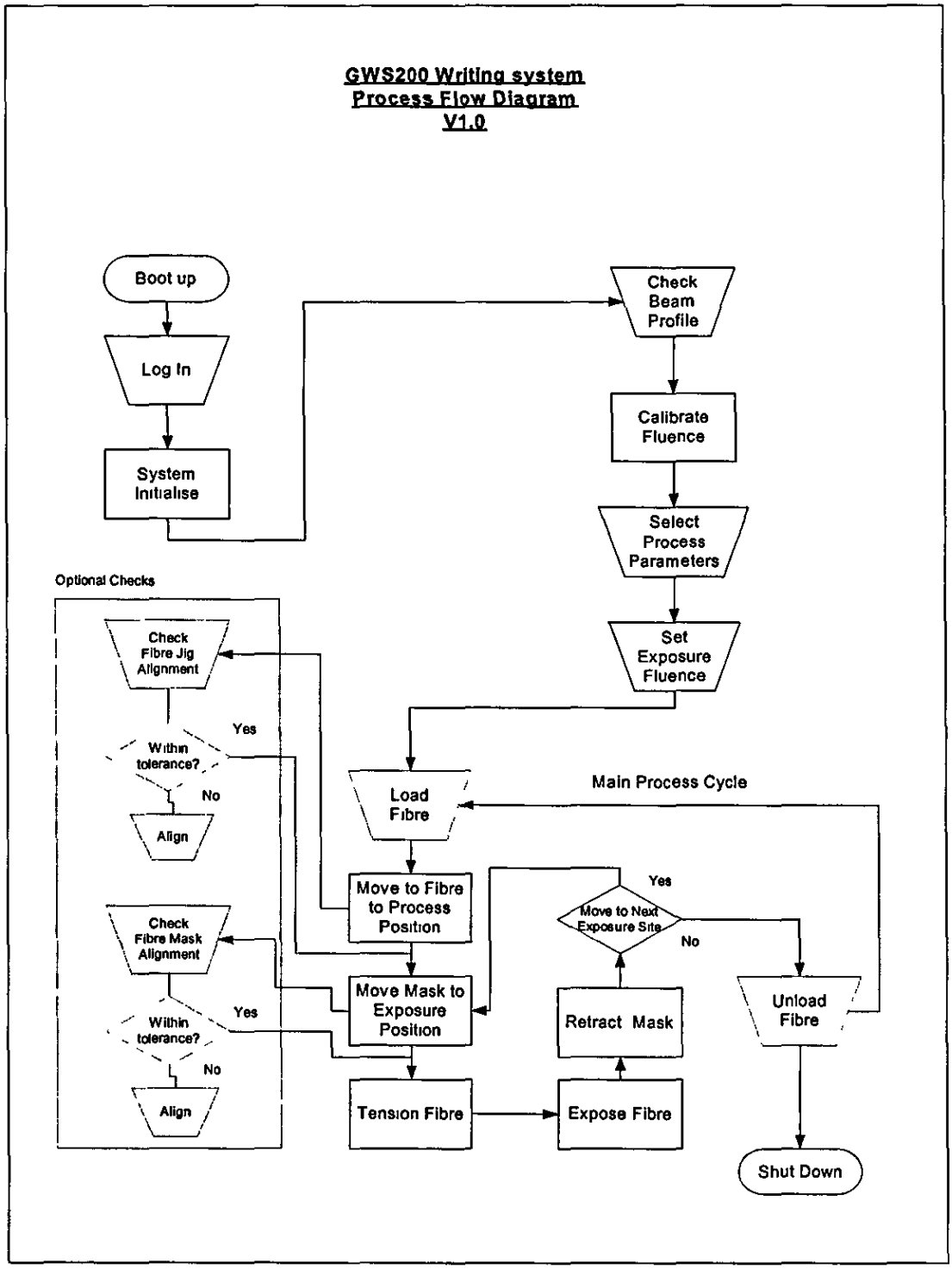

Fig 6.22: Process flow diagram.

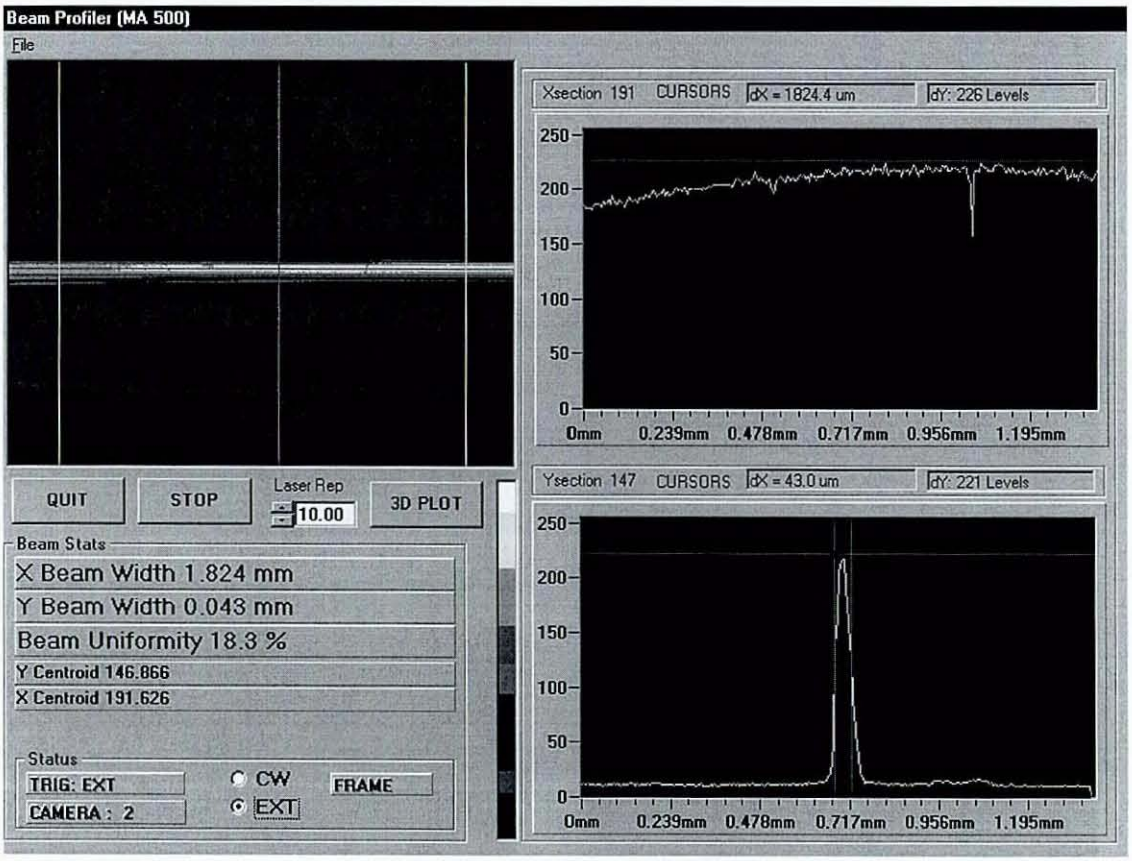

Fig 6.23 The beam profiler display, showing an intensity profile of the excimer beam after shaping and homogenisation.

6.4.4 Integrated beam profiler

A real time false colour map of the beam profile is displayed together with X and Y profile cross sections taken through the beam centroid, as shown in figure 6.23. When the profile acquisition is stopped these cursors can be placed under mouse control anywhere on the false colour map to provide measurements of the cross section. A real time 3D plot window can also be displayed by clicking the 3D plot button, an example of this being shown in figure 6.24. In low resolution mode the profile image is digitised within a rectangular window of square pixels at 384 x 288 pixels and displayed in false colour window on screen. Cross sectional displays of X & Y cuts through the beam centroid are displayed, together with automatic calculation of beam widths, uniformity and fluence using ISO compliant algorithms as described in previous chapters.

With profile acquisition stopped measuring cursors may be moved over the cross

sectional profiles in order to make more detailed measurements of beam size. The cursor separation is displayed in microns.

Automatic measurements are made of beam width (FWHM), beam centroid (X&Y position) and peak intensity (specified in digitiser counts). The beam width and centroid locations are displayed by cursors overlaid on the real time false colour image.

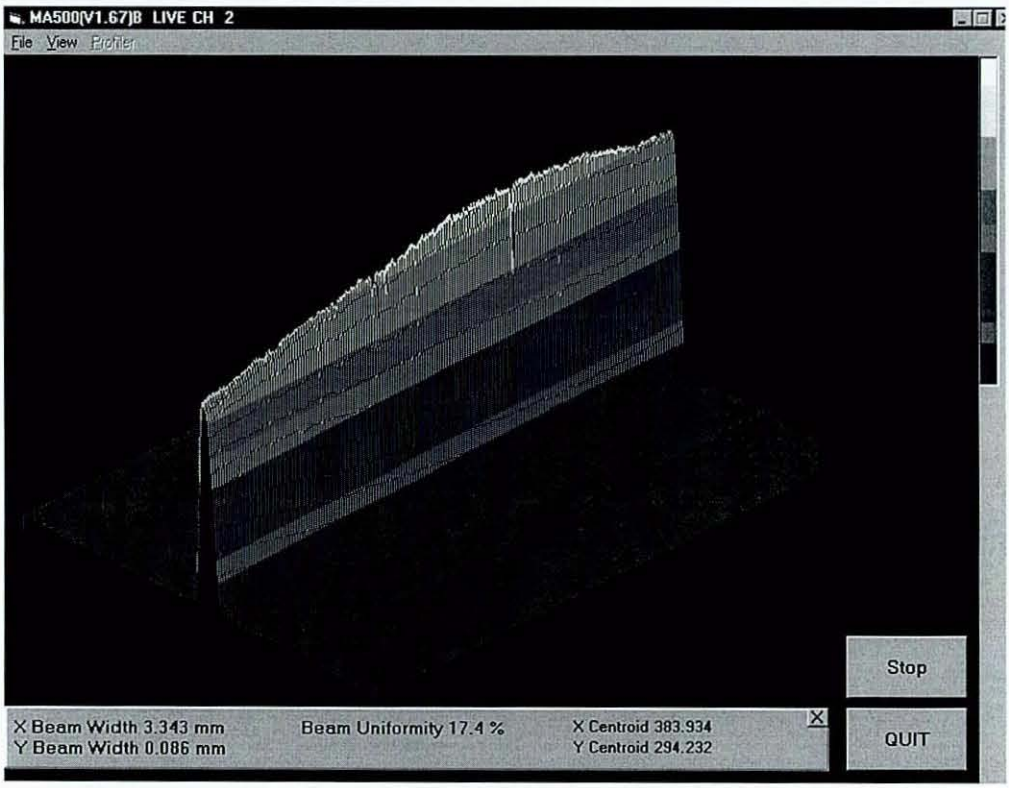

Fig 6.24 Beam profiler 3D plot, showing the intensity profile at the mask plane.

6.4.5 Exposure Dose controller

The function of the exposure dose controller is to deliver an exactly controlled dose of laser energy to the fibre. It does this by triggering the laser, measuring the energy of the pulse, summing this with a running total of previous pulses and then firing the laser. When the running total exceeds a preset level the laser trigger is stopped.

The application uses a National Instruments PCI data acquisition card to capture the signal from a Molectron energy probe in response to each laser trigger. The signal processing algorithms are then implemented in Visual Basic. This system does not use an embedded real time processor but instead relies upon the speed of the NT operating system and a asynchronous triggering scheme as described below. The acquisition and triggering is run in a tight Do Loop in order to maximise reliable triggering speed.

The operation sequence is as follows:

1). A TTL trigger pulse is generated with a delay equal to the laser repetition rate period and a duration of 200 μs.

2). The digitiser captures the output pulse waveform of the joule meter probe (about 100 samples at 50kHz)

3). The peak value of the waveform is measured and this is used as the pulse energy reading

4). The pulse energy is summed as a running total (dose Sum).

5). If the dose Sum is less than the target dose then the loop repeats and another trigger pulse generated.

Note :

1). Using this asynchronous sequence ensures that a laser trigger is issued only after a pulse has been successfully digitised and summed. This avoids the problem of pulse "dropouts" that might occur if synchronous triggering is used due to the non "real time" nature of Windows NT, which currently runs up to 100 Hz on a PII, 400 MHz CPU.

2).It is important however to minimize the number of background tasks when the dose control loop is running as this may result in apparent unstable operation of the laser trigger. For this reason all RS232 Communications polling is suspended during dose control operation.

3). In fibre Bragg processing the term "dose" actually refers to "Integrated fluence" i.e the measured figure is not the total integrated energy on fibre but the integrated fluence. This is in fact exactly equivalent to integrated energy in this case because the mask area (and hence beam size) does not change during exposure.

The application provides a friendly user interface with a graphical display of the laser pulse energy history, energy statistics and text boxes to enter various system parameters including laser repetition rate and dose threshold.

6.4.6 Calibration

This function should be performed at the start of each production shift and certainly after making any changes to the mask or optical system.

The in line (dose control) detector is calibrated using the in-chuck detector (this has already been calibrated by the supplier Molectron to NIST standards, a sensitivity figure in Volts per Joule V/J is marked on the detector). With the in-chuck detector in place an averaged reading is taken at 25Hz for one second and this is then repeated for the in-line detector. The energy calibration factor is then calculated from the ratio of the two numbers and the effective area of the mask in mm^2 (pre set, not measured) is then used to calculate the fluence (fluence = energy/area).

Fluence setting should be done on a regular basis, certainly before processing a batch of fibres or after making any changes to the optical system. Fluence setting is accomplished by reading the in-chuck energy monitor using the second channel of the NI A/D card. The laser is triggered at 10 Hz and the fluence value is displayed on screen, the operator being then prompted to manually adjust the attenuator until the target fluence has been achieved, see figure 6.25.

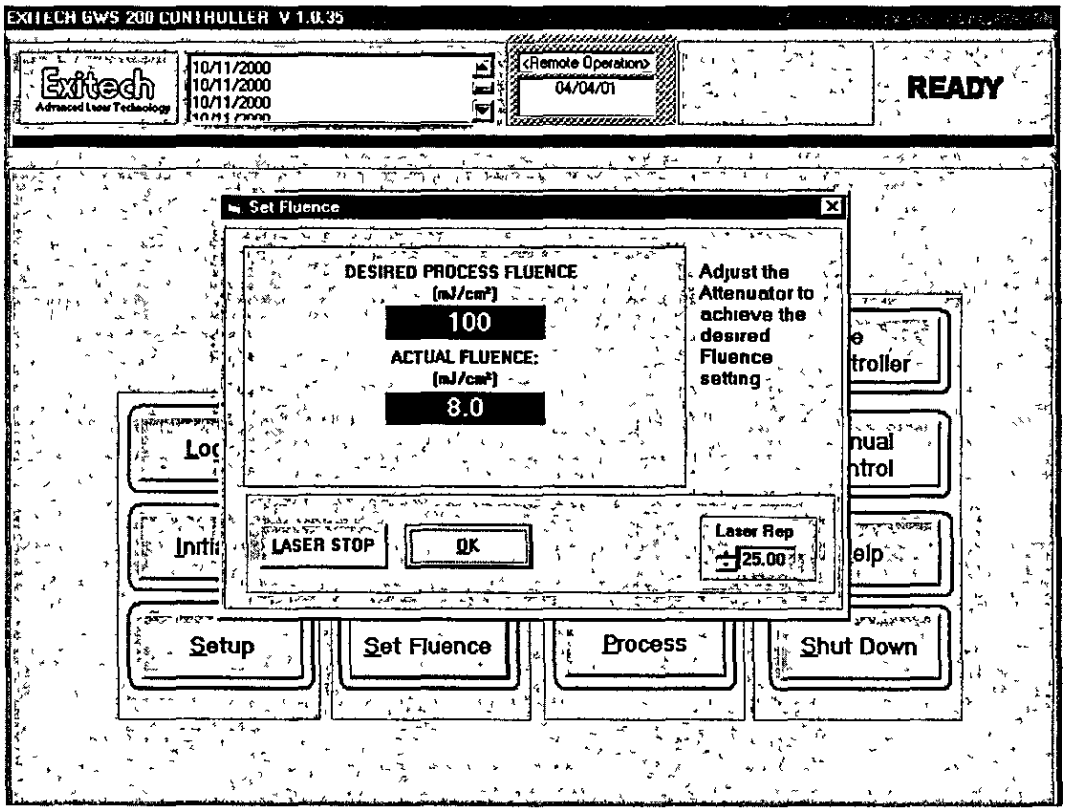

Fig 6.25 Process fluence setup screen

A DC Servo motor under U500 control drives the attenuator. Automatic checking and setting of the fluence is possible assuming that the laser pulse-to-pulse stability is good enough to allow reliable locking of the control loop, otherwise manual setting can be used as default. These options can be set in the system parameter setup.

The main parameters for the process can be saved or recalled to file. These process parameters include total dose, fibre positions, mask positions and fibre tension. The last set of parameters used is loaded as the default set on system boot up.

Spatial calibrations for the fibre viewing system and beam profiler can be set, as can energy probe calibrations. The system supports multiple INI files that can be saved and recalled from the root directory. This allows process recipes for different fibres to be saved and recalled. The setup tab also allows parameter settings for the system cameras (black level offsets and gain) and the beam profiler analysis options.

All setup information is saved in readable ASCII text format to an INI file stored in the application root directory.

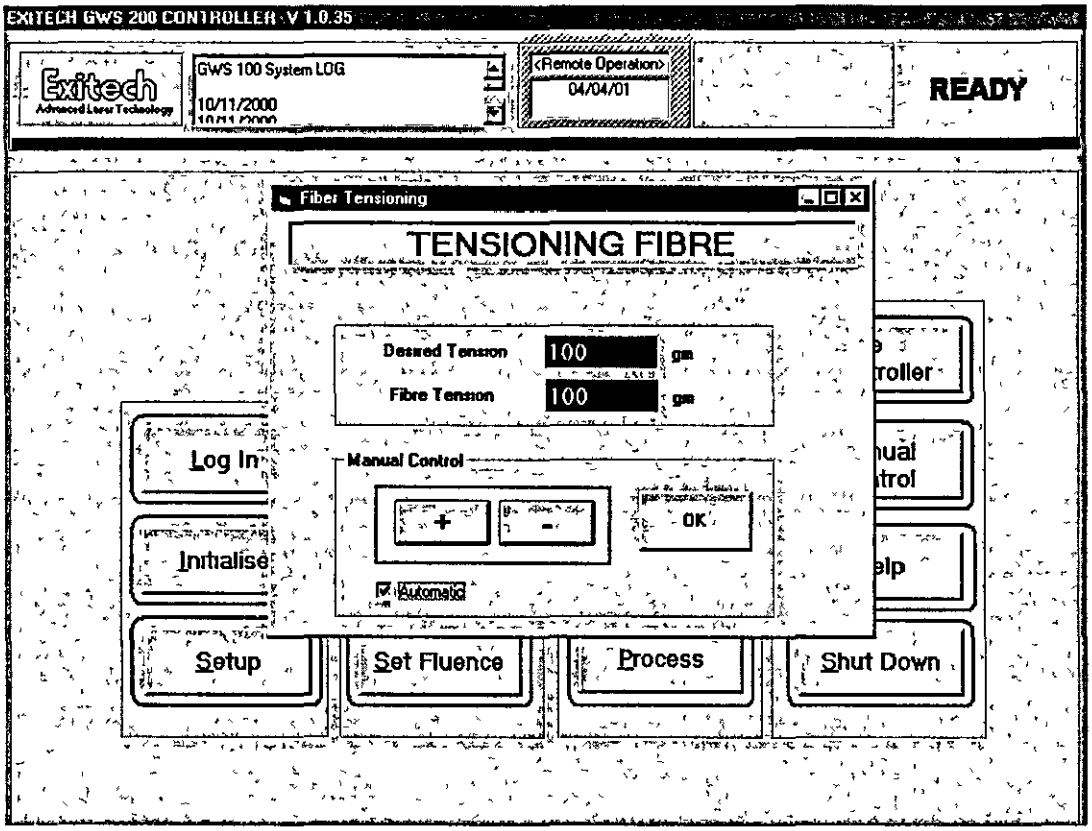

Fig 6.26 Fibre tensioning setup screen

6.4.7 Fibre load and tensioning

The fibre tension is set using a motorized micrometer and measured by a strain gauge load cell that returns a calibrated analogue output that is proportional to the fibre tension. The micrometer control is handled by a Coherent Ealing PCM1000 DC servo control card, which provides simple closed loop positional control of the micrometer position, which in turn is used to directly tension the fibre by stretching it between two clamps on the chuck. The setup screen is shown in figure 6.26.

During the process cycle a separate display window is used to display the fibre tension parameters during operation. The tensioning can either be manually controlled using jog buttons or automatically set from the parameter setup. Automatic setting occurs as part of the fibre load cycle before the exposure sequence is allowed to start.

Pressing on the Load Fibre button on the main menu starts the process cycle. This causes the stages to move to load positions, overrides the door interlocks and prompts the user to load the fibre jig on to mounting pins on the stage.

Once loaded the user presses OK and the fibre tensioning display is shown. The door interlocks are then re activated and the fibre clamped. A tensioning cycle is started. The user has the option to manually or automatically set the tension. The fibre tension is set using a motorized micrometer and measured by a strain gauge load cell that returns a calibrated analog output that is proportional to the fibre tension. When the fibre is correctly tensioned (as required by the process setup) the user is returned to the main menu.

6.4.8 Process screen

The process screen displays all relevant data for the Exposure of the grating on one screen. This is shown in figure 6.27 and this includes the following:

a). An exposure dose control display showing target dose, current dose and dose per pulse. The laser repetition rate and current laser shot count are also displayed. A real time plot window showing the laser pulse shot history is displayed, together with a "fuel tank " indicator showing accumulated dose.
b). Mask stage positions and fibre jig stage positions are shown, including the site number for multiple exposure operations.
c). The fibre tension in grams is displayed.

When an exposure cycle is complete the user is prompted to press the unload button. This moves the stages to the unload position and overrides the load door interlocks. When the fibre is unloaded the user is returned to the main menu.

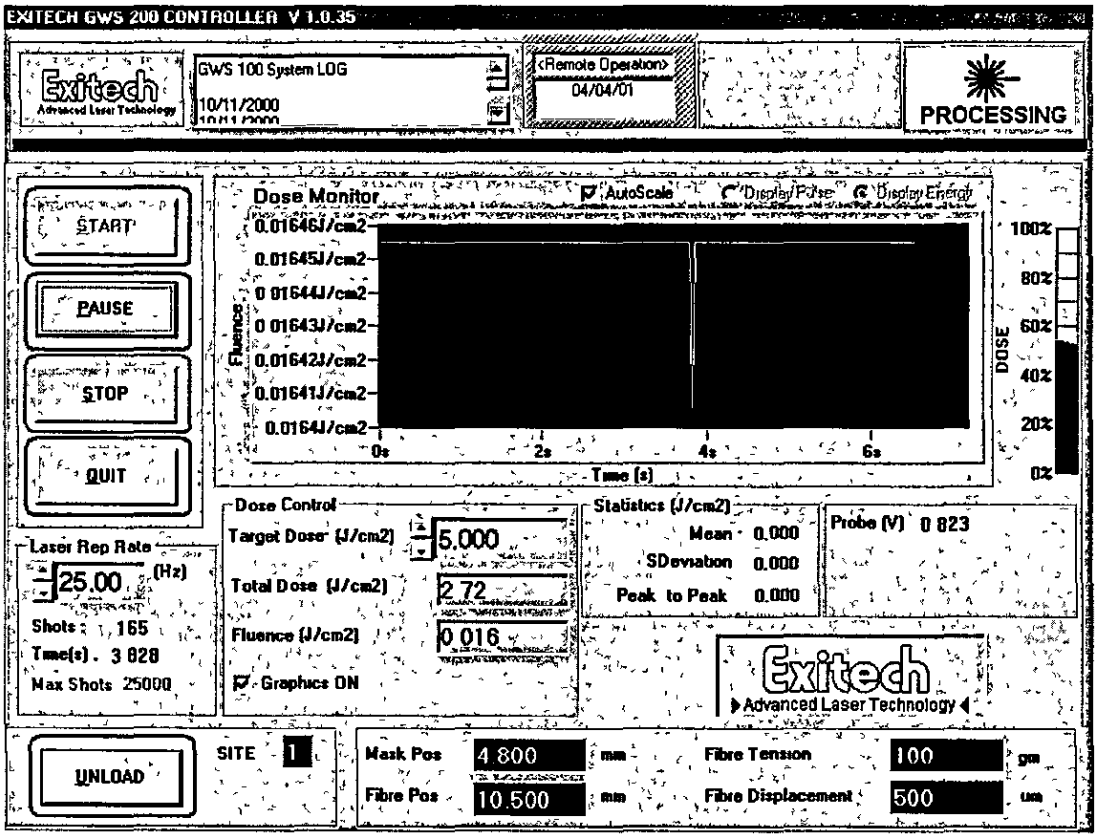

Fig 6.27 Process screen, showing the fibre exposure dose controller.

6.4.9 Summary

For commercial reasons results showing gratings produced by this system have not been described; however the performance of the GWS system in production has been excellent, and it is one of the most advanced tools of its kind commercially available. Its excellent performance is due in no small part to the advanced integrated beam profiling and energy measurement systems described in this section.

6.5 Conclusions

A range of excimer laser applications has been described. Micro machining is now a mainstream technology used in several advanced manufacturing applications. A wide variety of mass produced devices utilise laser tools in their production processes. The effective control and measurement of the laser beam intensity profile is important to maintaining the reliable operation of production tools.

In this chapter two very different laser tools have been described. Both tools serve practical micro fabrication applications on an industrial scale and both tools feature integrated beam diagnostics as an integral part of their design. They serve as good examples of state of the art laser processing tools and show how beam diagnostics are important to advanced manufacturing applications.

6.6 References

1). M C Gower, "Industrial Applications of Pulsed Lasers to Materials Microprocessing", SPIE Conference on High-Power Laser Ablation, Santa Fe, New Mexico, SPIE Vol. 3343, April (1998)

2). Y Kawamura, K Toyoda and S Namba , "Effective deep ultraviolet photoetching of polymethyl methacrylate by an excimer laser", Appl Phys Letts 40, (1982)

3). P T Rumsby et al, "Target production and development", Central Laser Facility Annual Report, SERC Rutherford Appleton Laboratory (1983)

4). E C Harvey & P T Rumsby, "Fabrication techniques and their application to produce novel micromachined structures and devices using excimer laser mask projection", Micromachining and microfabrication process technology III, SPIE 3223, (1997)

5). M C Gower, E C Harvey, N H Rizvi, P T Rumsby, J P H Burt, M S Talary, J A Tame and R Pethig, "Manufacture of miniature bioparticle electromanipulators by excimer laser ablation", Laser applications in microelectronic and optoelectronic manufacturing III, SPIE **3274**, (1998)

6). W Bacher, W Menz and J Mohr, "The LIGA technique and its potential for microsystems – A Survey", IEEE Trans. on Industrial Electronics, 42, No5, (1995)

7). F Bachman, "Excimer lasers in a fabrication line for a highly integrated printed circuit board", Chemtronics 4, (1989)

8). C Rowan, "Excimer lasers drill precise holes with higher yields", Laser Focus World, Aug (1995)

9). R S Gifford and D J Bartnik, "Using optical sensors to measure arterial blood gases", Optics & Photonics News, 9, 27, Mar (1998)

10). R C Crafer and P J Oakley, (eds) "Laser Processing in Manufacturing", Chapman & Hall, (1993)

11). E C Harvey, P T Rumsby, M C Gower and J L Remnant, SPIE Conference on micromachining and microfabrication Process Technology, vol. 2639, (1995)

12). G M Dubreucq and D Zahorsky, "KrF excimer laser as a future deep UV source for projection printing", Proceedings of International Conference on Microcircuits Engineering, (1982)

13). N H Rizvi , "Production of novel 3D microstructures using excimer laser mask projection techniques" SPIE Conference on Design, Test and microfabrication of MEMS and MOEMS, Vol. 3680, (1999)

14). E C Harvey and P T Rumsby, "Fabrication techniques and their application to produce novel micromachined structures and devices using excimer laser projection",

SPIE Conference on Micromachining and Microfabrication Process Technology III, vol. 3223, (1997)

15). N H Rizvi and P Apte, "Developments in Laser Micromachining Techniques" Proceedings of the ICOPE conference, Singapore, (2000)

16). R Kashyap, "Fiber Bragg Gratings", Academic Press, (1999)

17). K T V Grattan and B Meggit, "Optical fibre sensor technology: Advanced Applications- Bragg Gratings and Distributed sensors", Kluwer Academic Publishers, (2000)

CHAPTER 7

INDUSTRIAL MICROMACHINING SYSTEMS

7.1 Introduction

Laser based micromachining using frequency converted solid state lasers is now possible on an industrial scale thanks to improvements in laser design and materials [1], [2]. Several novel machine architectures have been developed to bring micromachining into mass production environments. This chapter describes two micro machining systems that use solid state lasers. The first system combines high speed galvanometer scanning mirrors with linear motor translation tables. The second system utilises fast stages and sophisticated multi beam optics. All of these systems use advanced beam monitoring and diagnostic systems to assist in calibration and alignment and are designed to meet the exacting requirements of industrial users.

7.2 The M5000 Flat Panel Display processing system

It is now possible to use frequency converted Nd:Yag and Nd:Vanadate lasers in a number of new and traditional applications [3],[4]. These solid state lasers promise much lower capital and running costs than excimers, and moreover they also allow new machine architectures to be implemented that offer greater speed and flexibility over their excimer laser based counter parts.

In conventional excimer systems material is processed using a combination of linear translation tables for both imaging mask and workpiece [5]. Using a 3rd harmonic Nd:Yag laser a combination of galvanometer scanners and linear stages can be used. In this architecture the Nd:Yag laser operates on the workpiece in a direct write mode as opposed to mask imaging as used in an excimer based system.

This machine architecture was developed for a European program for the manufacture of LCD (Liquid Crystal Display) panels. LCD components are made up of multiple

layers, e.g. an orientation layer for the alignment of the liquid crystals, and an Indium-Tin-Oxide (ITO) layer a transparent semiconductor, to apply an electrical field to the liquid crystals. The display is fabricated by sandwiching two glass panels together. In order for electrical contact to be made between the front and rear panels, a polyimide overcoat must be locally removed without damaging the ITO layer underneath. The current production method uses large printing screens and a special abrasive conductive glue, which abrades the polyimide off the ITO-surface during the printing and overlaying process. This process has the disadvantage of requiring a new printing screen to be fabricated for each new layout of LCD panel. The alternative of a direct write approach using a laser is more flexible as CAD data can be down loaded directly onto the machine controller negating the need to fabricate new masks

Importantly an in-chuck beam profiling system was used to characterise the laser beam intensity distribution at the laser process plane. This provided significant benefits in realizing accurate fluence control and alignment at the workpiece.

7.2.1 System Architecture

For a viable production process the prototype machine had to laser pattern over 2000 contact pads distributed over a 300 x 400 mm panel within 30 seconds. The only way to achieve this through put speed was to adopt a novel system architecture that combined galvanometer scanners with high speed translation tables. A diagram of the basic concept is shown in figure 7.1.

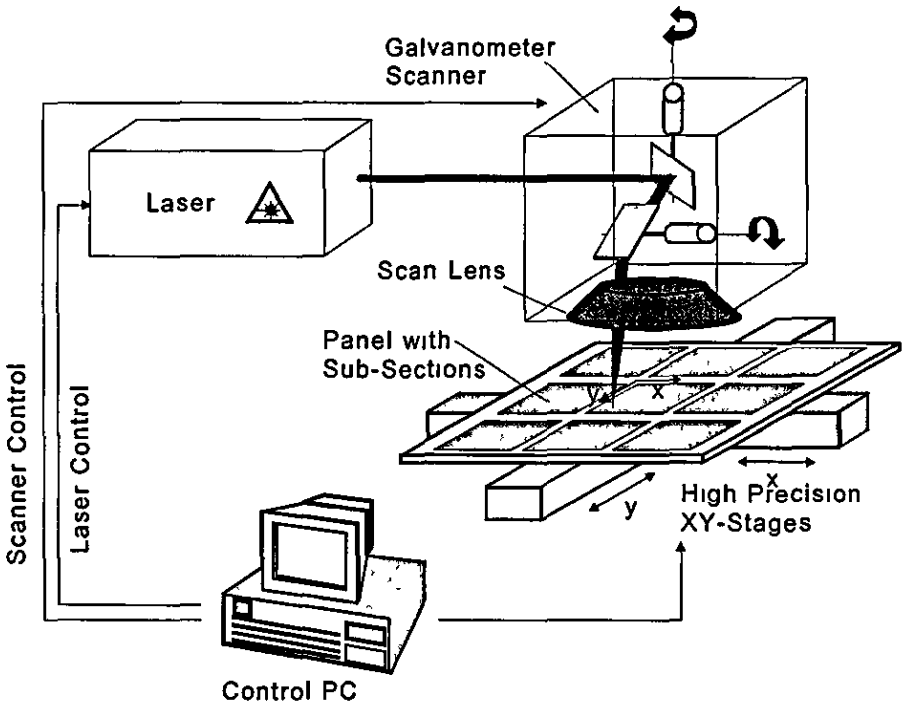

Figure 7.1: The machine control concept.

Wavelength	**355 nm**
Scan Area	**120 x 120 mm²**
Entrance Pupil of the Laser Beam	**6 mm**
Working Distance (between scan head and material surface)	**210 mm**
Maximum Positioning Speed	**7 m/s**
Accuracy	**< 2 µm**
Step Response Time (for a 1 mm jump)	**1.1 ms**
Minimum Spot Size	**12 µm**

Table 7.1: Technical Specification of the Scanner Set-Up [6]

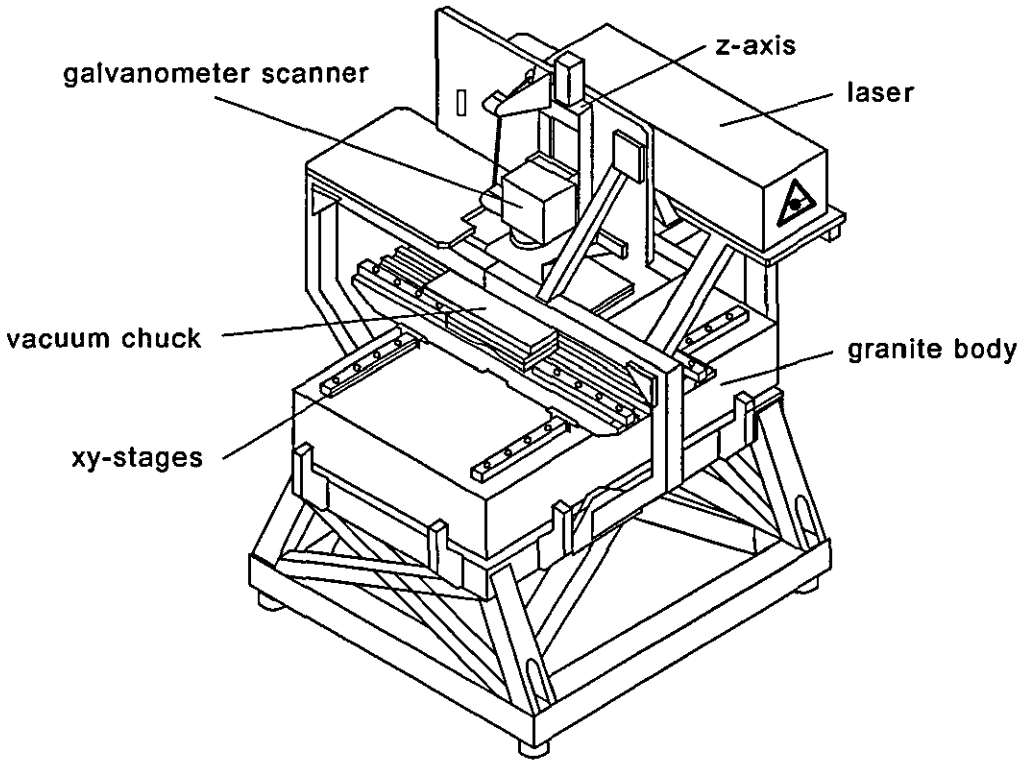

Figure 7.2: Internal mechanical layout.

The machine described here, built by Exitech Ltd, was reported at ICALEO 2000 (October,2000 in Dearborn, MI).It uses a combination of galvanometer scanners with high precision X,Y linear stages.

The galvanometer scanners consist of a pair of orthogonal mirrors driven by permanent magnet rotors. This provides for a very low mass arrangement with high acceleration. A flat field F-Theta lens [7] is used to focus the laser beam onto the workpiece surface. The pointing accuracy of the scanners is proportional to the scan lens focal length, hence increasing the scanner field decreases the accuracy, whereas a larger scanner field increases the processing speed. With a 50 x 50 mm field a typical positional accuracy of +/- 10μm can be achieved, with process rates of 1000 points per sec. The effective workpiece translation speed (analogous to linear stage speed) is in excess of 7 meters per second with an acceleration of several G. By comparison linear stages are an order of magnitude slower. The technical specification for the scanners is listed in table 7.1.

In order to overcome the limitations of a small scanner field size when processing large panels a "step and scan" approach was adopted that divides the workpiece area into an array of square tiles the size of a scanner field. The machine then processes each tile in sequence with the scanners and then steps between tiles using the linear stages.

The galvanometer scanner was mounted on a Z axis linear slide to allow automatic focus adjustment. The linear stages were mounted on a granite slab for stability and to reduce sensitivity to vibrations. The mechanical layout of the system is shown in figure 7.2. A specially designed multi zone vacuum chuck held the panels in place during processing. The stages were built in house by Exitech using Aerotech (Pittsburgh, USA) linear motors and controllers. They have a travel of 600 x 450 mm, and a maximum feed rate of greater than 500 mm/s with acceleration in excess of 0.5G. The stage accuracy and repeatability is better than +/- 2 μm, in part because an integrated machine vision based automatic calibration system is used to map the absolute accuracy of the stages in two dimensions.

7.2.2 Beam diagnostics and control

The Machine control system (see fig 7.3) is based upon a standard Exitech design. It utilizes an industrial PC running MS windows NT4 and custom software. An Aerotech U500 motion controller is used for stage control together with a Scan Lab (Munich, Germany) RTC2 scanner control card. Additional control interfaces link to a custom machine vision system and a programmable logic controller that manages peripheral tasks such as interlock control and safety beacons.

The control system also integrates auto calibration and diagnostic systems designed to be useful in production environments. These features allow relatively unskilled operators to run the machine. These systems include automatic process fluence setting using an in-chuck power meter feeding back to the laser attenuator and a non contact height sensor for measuring wafer thickness and automatically adjusting focus height.

Another innovation is automatic scanner calibration using an in-chuck CCD camera. Scanner field calibration is required to compensate for distortions in the scan lens. This can be mapped using the camera and the linear stages and then a calibration table

calculated. This feature also takes out misalignments in the optics and thermal drifts in the scanner.

For automatic workpiece alignment a CCD camera and alignment microscope are included. Reference marks on the panel are located using a machine vision system and alignment offsets automatically calculated. Finally an on line laser beam profiler is also included using another CCD camera.

7.2.3 Applications

The Exitech machine was originally developed for a European Union funded research project that involved the laser patterning of LCD display panels. These displays are fabricated as multi layer structures, including an orientation layer for the alignment of the liquid crystals and an indium-tin-oxide (ITO) layer that acts as a transparent semiconductor to apply an electrical field to the liquid crystals. Two panels are sandwiched together to make a full LCD display.

In order to produce an electrical contact between the top and bottom panels, a thin (20 to 40 nm) layer of polyimide must be removed from contact pads located at various positions over the LCD panel, without damaging the ITO layer beneath. The conventional way to remove polyimide is structure printing, which can be costly and time consuming as new printing screens must be made every time the display layout changes.

However using a 3rd Harmonic YAG laser the polyimide can be removed with a single 0.3 mJ laser pulse of 50 ns duration, the effective fluence at the workpiece being 0.8 J/cm^2 which is sufficient to remove the polyimide without damaging the underlying ITO layer. New panel designs are easily accommodated by downloading a new CAD file without the need to fabricate new masks. In trials the Exitech machine processed more than 2000 contact points in less than 30 s on a panel 350 x 400 mm^2 in size, which satisfied the throughput requirements of the production line.

Another promising application for this machine tool is the direct scribing of metal interconnect structures for the electronics industry. Conventionally these structures are

produced using the same resist etch techniques as for printed circuit boards (PCBs). There can, however, be questions related to reliability of etch processes when fabricating very-high-density structures. Laser-based processing allowed direct-writing of circuits with just 10-µm wide tracks by ablating a 5-µm copper layer on an epoxy substrate. Using a telecentric scan lens with a 56-mm focal length, the machine was able to focus the laser beam to roughly 4 µm using a laser source with an average output power of 1.5 W at 355 nm with a pulse repetition rate of 10 kHz.

The main control of the machine is implemented on an industrial PC running MS Windows NT4. As seen in the detailed diagram in figure 7.3, the computer hosts several control interfaces to various sub-components. For the stage control an Aerotech U500 motion controller PC-board is used. The U500 drives the xy-stages as well as the z-axis. The Galvanometer scanners are controlled by Scanlab RTC2 hardware, which also provides the laser trigger. Interfaces have also been implemented to a Vision system, the laser source, and a programmable logic controller (PLC), which manages peripheral tasks like interlocks, shutter, and illumination. Besides these sub systems, several novel features have been added to the machine tool, which automate calibration and setup allowing easy use in factory environments by semi skilled personnel. These features are described as follows:

Power calibration: The laser power can be measured automatically by a power meter. This can be used to adjust the beam attenuator automatically using the U500 axes controller (the attenuator is defined as an axes in the system), enabling a process specific beam energy to be set at the work piece.

Automatic scanner calibration: The relationship between distance moved at the workpiece and the angle of mirror displacement is non linear, being dependent on a number of factors including the lens design. By positioning a CCD-camera under the scan head and moving a defined number of scanner steps the ratio between scanner positioning units and actual displacement on the workpiece can be calculated and fed back into a calibration file.

Automatic work piece alignment: A high resolution CCD camera and microscope viewing optics are used for automatic work piece alignment. Pattern matching software

is used to identify alignment marks on the panel substrates, calculate alignment offsets and then align the panel.

Automatic beam profile analysis: For diagnostic purposes, the beam profile can be analysed by a CCD-camera. This is essential for quality control and diagnostic purposes.

Powerful User interface (GUI). The software is designed to be used even by inexperienced users. The interface is mainly based on graphics, supported by a touch screen panel.

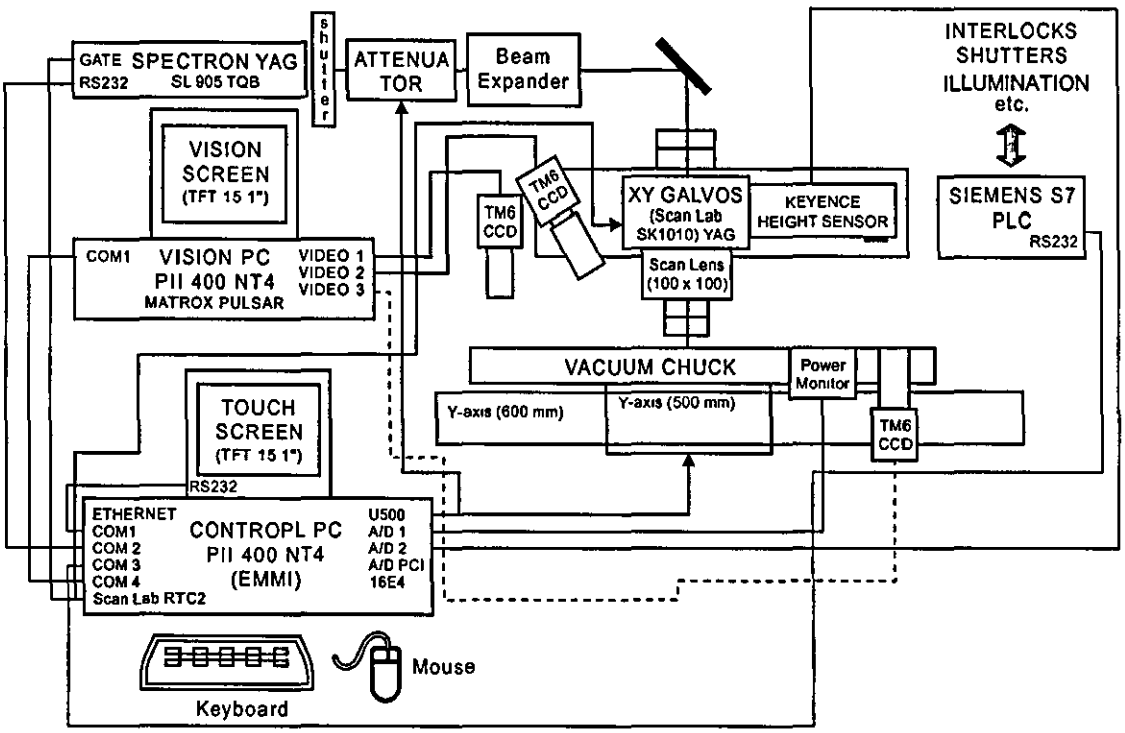

Figure 7.3: Control system diagram of the prototype machine, showing integrated beam diagnostics.

The prototype machine is shown in figure 7.4. For laser safety reasons the entire machine frame is enclosed and the process can only be observed from a laser safety window or by means of a viewing camera. This machine formed the prototype of a new machine series, the Exitech M5000, which is now widely marketed.

Figure 7.4: The industrial prototype

For CAD data exchange a common drill file format used by the printed circuit board industry has been used. These formats contain the coordinates of the transfer points and information of the ablation geometry. A typical drill file has the following format:

T01
X320.15Y94.26
X320.15Y92.36
X320.15Y90.46
.....
T02
X220.05Y94.26
X220.05Y50.26
X220.05Y92.36

The T0n defines the ablation geometry and size and can be programmed to meet the users requirements. The numbers represent the x and y coordinates of the transfer points, belonging to the drill determined by T0n. After the drill file has been loaded into the controller, the main program divides the panel into sub-sections according to

the available scan area, then calculates the scanner commands and the axes coordinates for each of the sub-sections. Rotational misalignments of the panel are dealt with by rotating the scan field data in software as opposed to physically rotating the panel. This has the significant advantage of removing the need to incorporate a rotational stage in the system.

7.2.4 Ablating Polyimide for LCD production

As shown in the cross section of an LCD cell in figure 7.5 a & b, the polyimide (Probimide 32, Ciba Geigy) layer has to be removed at contact points spread over the panel in order to form electrical contacts between the upper and lower ITO electrodes. The number of contact points can be up to 2000 on a panel of 350 x 400 mm², which can carry up to 16 single displays. The overcoat layer varies from 20 to 40 nm in thickness and must be removed from each 200 μm diameter contact pad without damaging the ITO layer beneath. In order to do this accurate control of the laser pulse energy and focal beam profile is required.

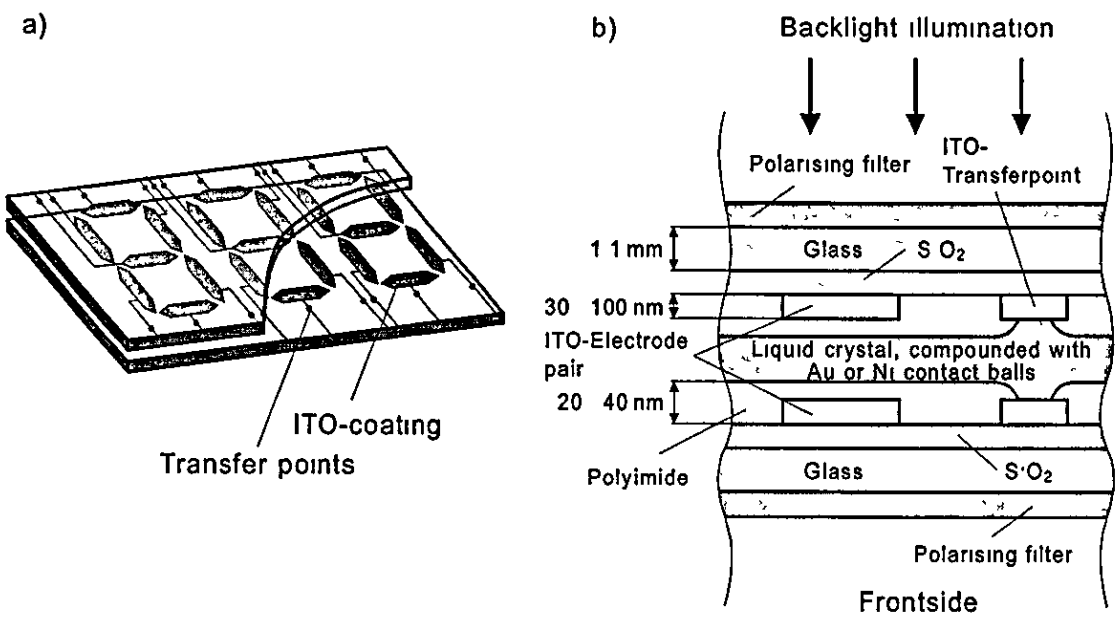

Figure 7.5: Structure of a typical Liquid Crystal Display

In figure 7.6, the absorption for both materials, ITO and polyimide is given for the wavelength range between 200 and 400 nm. These have been measured on 40 nm thick

layers, each coated on a 1 mm fused silica substrate, which is nearly transparent at these wavelengths.

Below 300 nm, the ITO layer shows nearly 100% absorption, which decreases down to 25% at 400 nm. The polyimide layer has an absorption of 60% at 200 nm, decreasing fairly linearly to 17% at 400 nm. At the wavelength of the processing laser (355nm) the absorption of the two materials is quite similar, resulting in a narrow fluence window for the process to be successful and hence the need for careful laser fluence control.

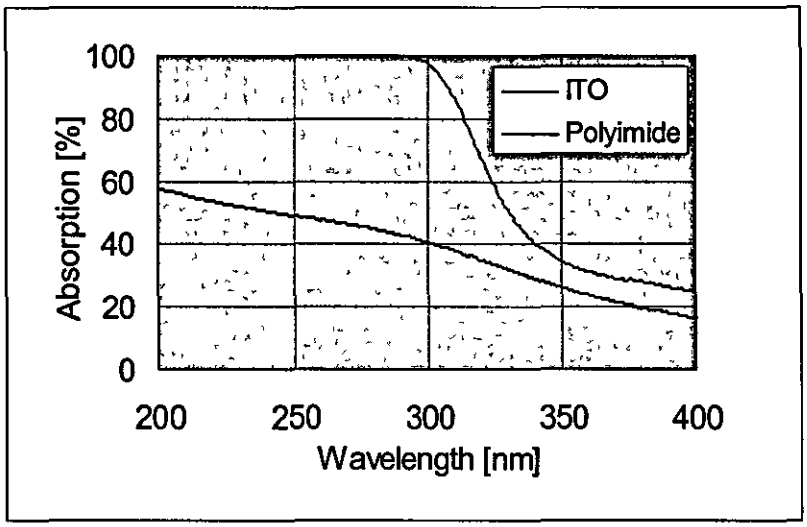

Figure 7.6: Absorption of 40 nm layers of Polyimide (Probimide 32) and of ITO as a function of laser wavelength

Laser		Process		Material	
laser: wavelength:	KrF excimer l =248 nm	energy density. number of pulses: image ratio	H = variable n = 1 5 1	material	polyimide Probimide 32

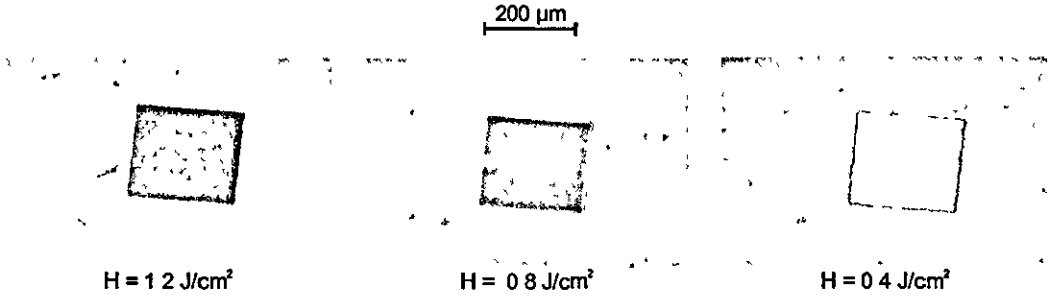

Figure 7.7: Ablation of Polyimide (Probimide 32) with KrF-Excimer laser

Figures 7.7 and 7.8 show comparative ablation trials using an excimer laser and the third harmonic Nd:Yag system. Although the excimer results are superior, the quality of the Nd:Yag system is adequate for the application.

When using a 3ω or 4ω Nd:Yag system, the required 200 μm spot size can be achieved by partial defocus of the laser spot. This enlarges the approximately Gaussian profile ablation spot and reduces the fluence. The result is a near circular ablation geometry with diffuse boundaries. For both wavelengths shown in figure 7.8, 266 nm and 355 nm, the polyimide has been removed without damaging the ITO. A pulse energy of 0.25 mJ gives to an average energy density of 0.8 J/cm² in the case of 266 nm, in case of 355 nm, 0.3 mJ pulse energy gives 1 J/cm² average energy density.

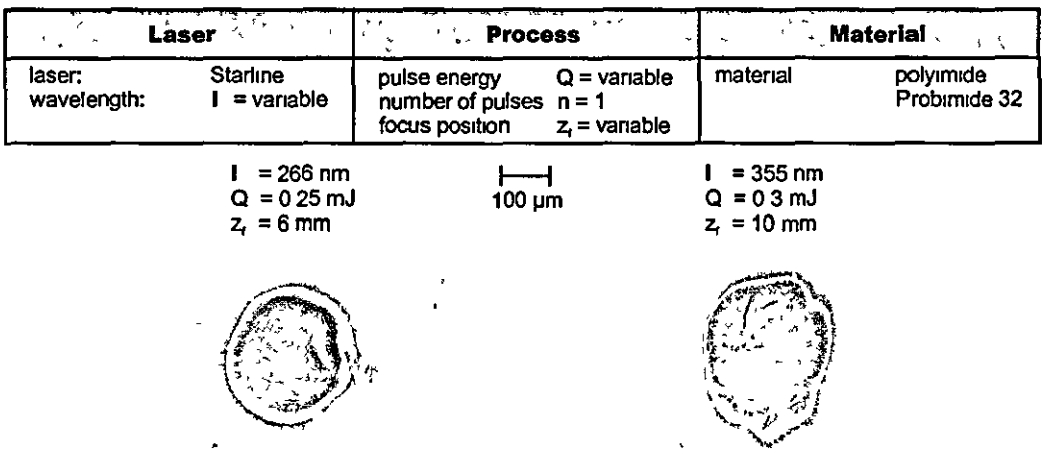

Figure 7.8: Ablation of Polyimide (Probimide 32) with 3ω (355 nm) and 4ω (266 nm) Solid State lasers

7.2.5 Industrial trials

After completing material process studies and evaluation of the machine architecture the final assessment of the tool has been carried out on LCD display panels, forming the layout of a dashboard display for the automotive industry. The size of these test panels was 400 x 500 mm, yielding 12 displays after separation and assembly. The layout of the transfer points and a separated display cell are shown in figure 7.9. The

main goal was to process the 2000 transfer pads each of 200 μm diameter in less than 30 seconds per panel, which is the operating throughput of the production line.

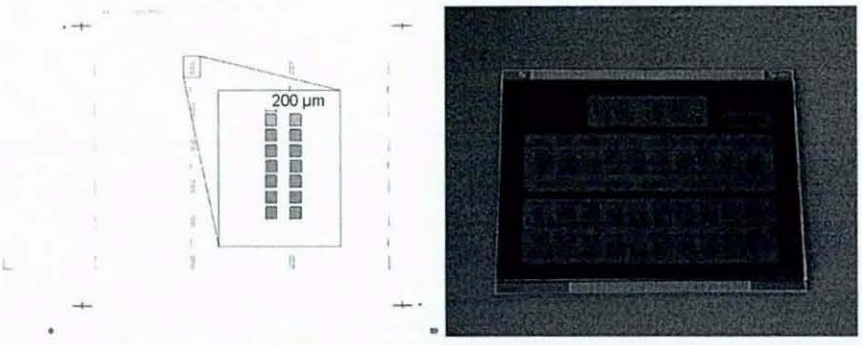

Figure 7.9: The transfer pad layout and an assembled display

For the tests three processing techniques were investigated:

1). Trepan the 200 µm pad using a tightly focused 12 µm spot with low pulse energy.
2). Defocusing the laser beam to 200 µm and ablating the sample with higher pulse energy
3). Expanding the laser beam and using mask imaging to project a 200 µm disk onto the work piece.

The trepanning method exhibited at very low energy densities traces of damage to the ITO layer. Due to the small focal spot size and the high peak intensity it was not possible to accurately control the depth of the ablation process.

The large spot defocus method exhibited non-uniform results. Only in the centre of the scan field were the results satisfactory. This is because at the limits of the scan field the laser spot geometry is distorted due to aberrations in the f-theta scan lens, which exhibits significant coma and spherical aberration.

The mask imaging technique yielded the best results, giving constant ablation profiles over the whole scan field. By expanding the laser beam so that only the centre of the beam with an approximately constant intensity profile can pass through the imaging

mask, a nearly top-hat intensity profile is imaged onto the work piece. In order to keep within the limits of the depth of field of the lens, the scan field has been reduced to 50 x 50 mm, thus reducing aberrations. Although this increases the number of scan tiles and therefore stage moves, the throughput was still within 30 seconds per panel.

The laser processed sample panels were put back into the production line, where they were processed and assembled into finished displays. A microscopic view of a laser processed contact pad after assembly is shown in figure 7.10. Within the ablated pad Gold contact balls can be seen. Remarkable is the fuzzy contour of the ablated area compared to the original circular ablation geometry. While the geometry of the contact pad directly after the laser process is circular with defined edges, after assembly of the cell, the polyimide has separated from the edges and has diffused into the contact area, causing a visible fringing effect. One reason for this separation may be due to heat induction in the surrounding material, changing the bond forces between the ITO and polyimide layer. This might cause the diffusion of the polyimide and create the visible fringes when the cell is filled with the liquid crystal. However, as can be seen in the photograph, there is still enough uncovered ITO surface for electrical contact between the layers.

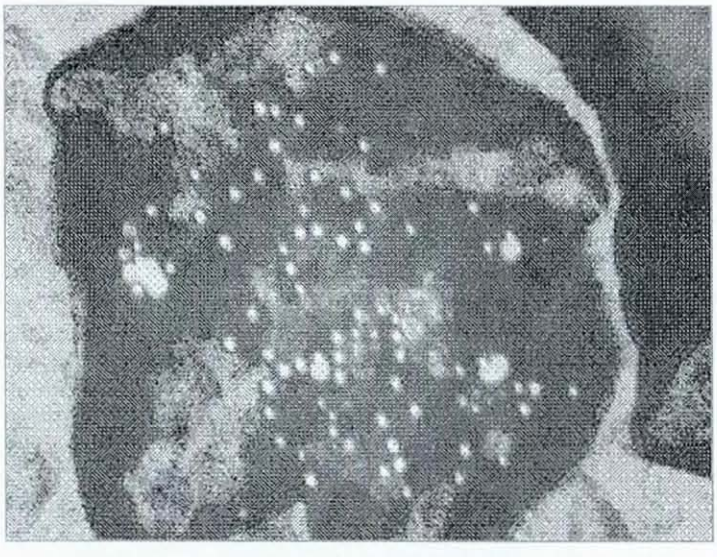

Figure 7.10: Micro photograph of an ITO transfer pad after assembly.

The laser processed displays were then tested using the procedures for high quality Automotive LCD panels. The customers of such displays require 100% test of every single display under varying temperature conditions, simulating the temperature changes in a car between winter and summer. During test, 157 panels out of the 160 laser processed passed the 100% electrical and optical final inspection at Optrex Europe GmbH. This was an excellent result and fully demonstrated the viability of this machine architecture within a production environment.

7.2.6 Applications in the Electronics Industry

Using scanners to manipulate UV laser radiation already has great potential in the electronics industry. Here applications are presented which involve the machining of copper and dielectric composites in printed circuit boards. The drilling of 35 µm thick copper foil as shown in figure 7.11a was carried out by trepanning the focussed laser beam in an outward spiral pattern. The wavelength was 355 nm, the pulse energy 2.5 mJ with a pulse repetition rate of 1 kHz. The system is capable of drilling 25 holes per second. In a multi-layer printed circuit board this technique is used to produce so called blind vias, where both the top copper layer and the dielectric under layer are removed.

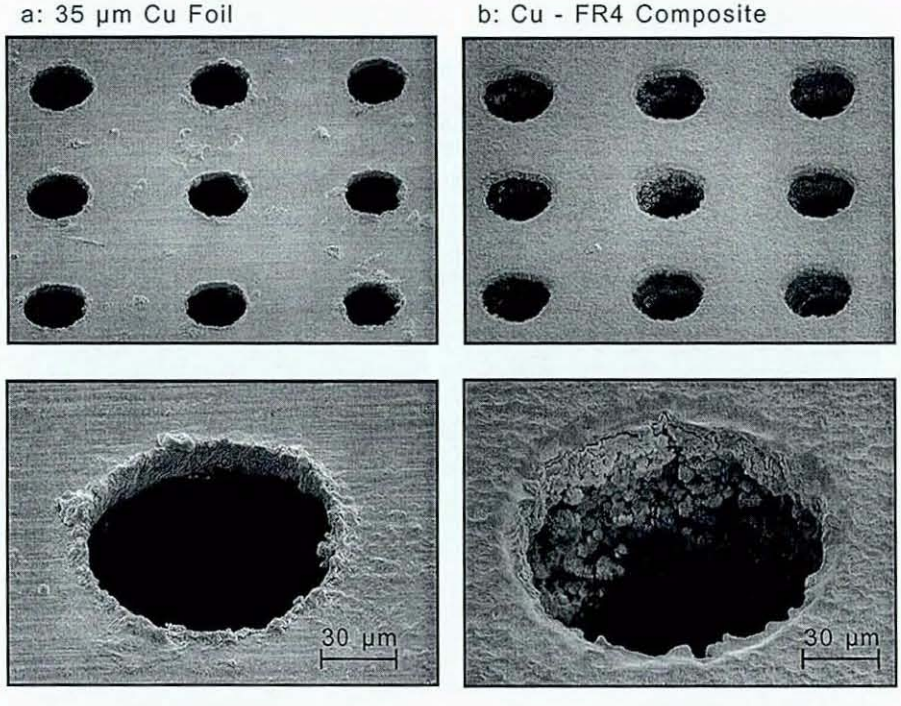

Figures 7.11 a,b,c,d Drilling of Copper and Copper-FR4 multi-Layer boards

Another potential application is the patterning of high resolution electrical interconnects. The example given in figure 7.12a shows a pattern, generating by ablation of 5 μm copper on an epoxy substrate. The lines of width 10 μm have been machined using a 56 mm focal length telecentric scan lens, which focuses the laser beam to a 4 μm spot. The laser source had an average output power of P_{AV} = 1.5 W at λ = 355 nm with a pulse repetition rate of f_P = 10 kHz. In Figure 7.12b samples were machined in 25μm thick polyimide on copper, they show 25 μm wide tracks. Polyimide is often coated onto copper to form a dielectric layer in the manufacture of multilayer printed circuit boards.

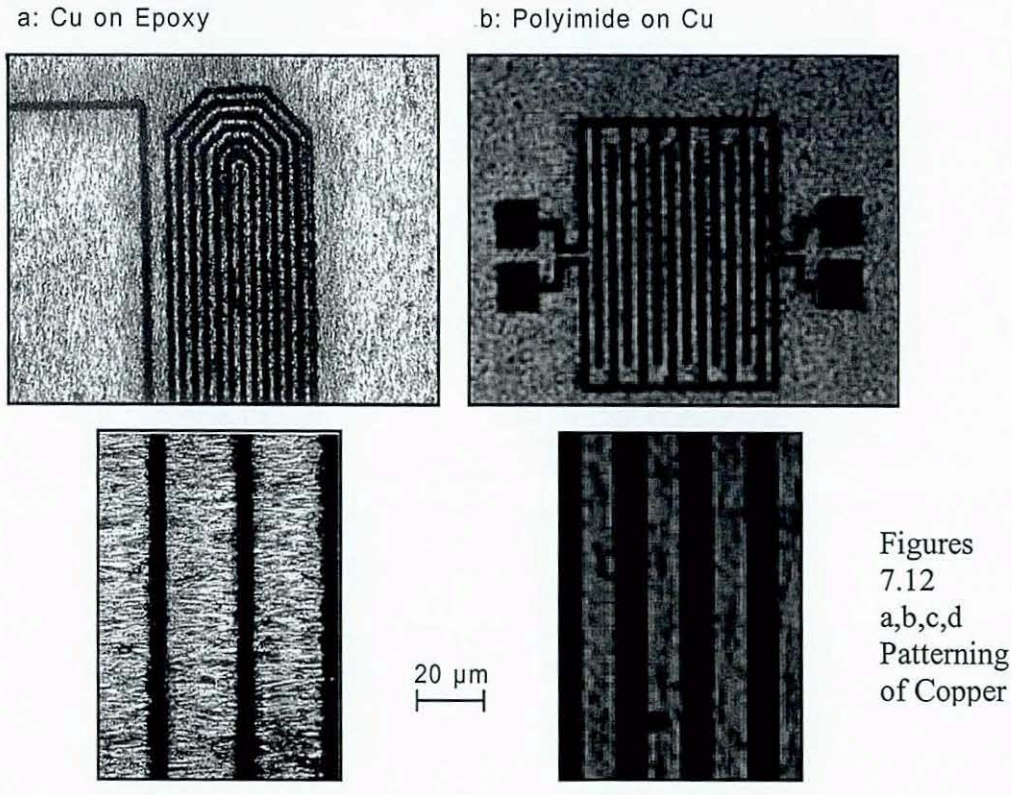

Figures 7.12 a,b,c,d Patterning of Copper

7.2.7 Discussion

This project demonstrated that a laser process and machine tool architecture could be successfully developed to meet requirements of a real production line. The positioning accuracy reached with this tool was better than 2 μm, with a maximum panel size of 450 x 600 mm. The laser machine tool was capable of ablating 2000 contact pads on one panel in 30 seconds, which is the current throughput of the existing production line.

By applying a laser based process, the printing of the contact pads with clichés screens can be replaced, leading to greater flexibility and reduced clean room storage requirements for the printing devices. The final test failure rate of these laser processed displays was 3 to 4% which is equivalent to the existing non laser process.

Besides the production of LCD displays, this machine tool has applications in micro and precision engineering. The machine architecture is very flexible and can be used to perform a wide variety of processes in organic and inorganic materials for volume production as well as for research. The implementation of auto-calibration and diagnostic systems gives the machine a high level of accuracy and reliability. The automatic work piece alignment and focusing system contribute to hands free operation. Potential applications for such a machine tool besides the patterning of displays are the drilling of printed circuit boards, the marking of chip substrates and rapid prototyping.

Importantly an in-chuck beam profiling system was used to characterise the laser beam intensity distribution at the laser process plane. This provided significant benefits in realizing accurate fluence control at the workpiece.

7.3 The M9000 Micro fabrication tool

excimer lasers and Nd:Yag lasers are now employed in many industrial systems and are widely regarded as a mature technology. These lasers are in use worldwide in many configurations and this section will address recent advances made with these systems. In particular, the use of high repetition rate Nd:Yag lasers to pattern large areas rapidly, and fabricate microstructures, will be described. A picture of the system is shown in figure 7.13

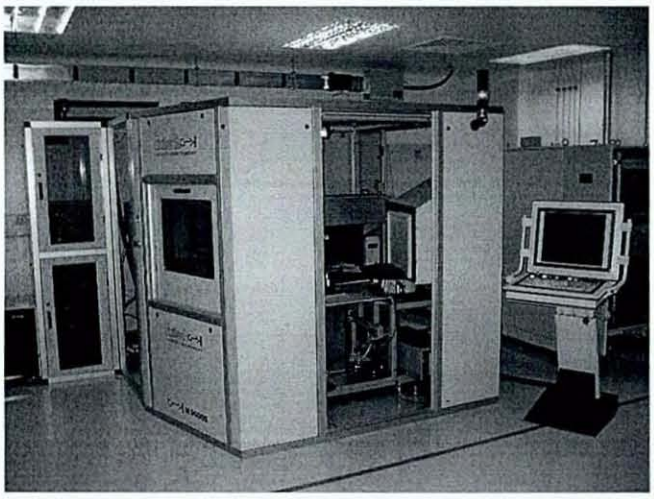

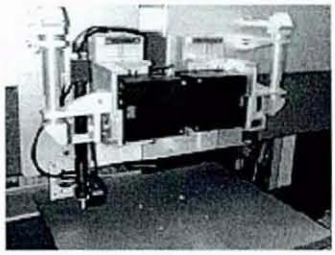

Fig 7.13
The Exitech M9000 micro-structuring system

7.3.1 Microvia fabrication and interconnect patterning

The current generation of solid-state lasers (e.g. Nd:Yag, Nd:YVO_3, Ti:Sapphire) and some gas lasers (e.g. CO_2 lasers) offer a large number of attractive benefits which include:

a). Large wavelength coverage (either directly tunable lasers or frequency-converted models).
b). High repetition rates (many tens to hundreds of kilohertz).
c). Different pulse durations.
d). Wide range of output powers.
e). High efficiencies (especially with diode-pumped lasers).
f). Relatively small sizes.
g). Relatively low running costs.

Mainly due to these reasons, many applications such as via hole drilling, solar panel scribing, display panel production and marking and cutting of devices or products use these lasers. In almost all cases, the technique of direct writing, or serial scribing, is used.

In direct write systems, the laser beam is focused to a small spot using a lens and either the beam or the sample (or both) is moved around to produce the desired pattern. In some cases, additional galvanometer-controlled scanning mirrors are also included. If

scanning mirrors are used, then a flat-field lens is required as this keeps the focal plane

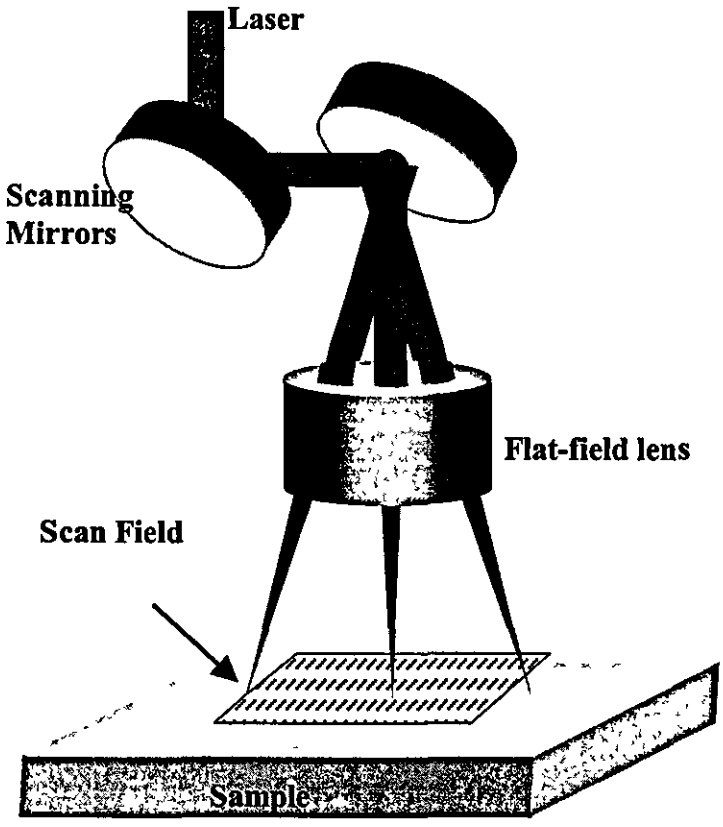

Figure 7.14. Direct writing using Galvanometer scanners.

position constant irrespective of the angle of the beam being deflected from the scanning mirrors. Beam spot sizes of a few tens of microns can be easily achieved with such systems and the combination of scanner mirrors and high repetition rate lasers means that very high processing speeds can be achieved. Such as system is shown in figure 7.14.

One drawback which has always existed with the type of system shown in figure 7.14 is that individual scan fields need to be joined (or "stitched") together to form a large area pattern. Hence, the process can be termed step-and-scan since the processing is performed for a scan field, the laser turned off, the sample moved to the position of the next scan field and the patterning re-started. This stepping aspect of this process, when no processing is taking place, obviously causes an increase in the total patterning time.

Even though the stepping time delay is only a few hundreds of milliseconds, it can produce significant cumulative effects on total processing times for large samples, which in turn can severely impact the economic attractiveness of the whole process.

7.3.2 Sync Scan

A solution to this step-and-scan approach is to move the sample continuously while the scanner scans the beam over the area in the scan field. This approach has been extended using sophisticated digital signal processing to synchronise the position of the sample and the scan field. Therefore, the sample can be moved continuously while the scan field of the scanner is continually updated to write a pattern continuously. This technique is called *Sync Scan.*

One of the main advantages of Sync Scan over mask projection techniques is the flexibility of not requiring a mask. The design of the pattern to be produced can be generated using CAD packages and the data file can be directly interfaced with the Sync Scan system. This also allows great freedom in assessing different designs quickly just by altering the code data.

Sync Scan operates by dividing the patterns into rectangular sections where the length of the rectangle is the size of the scan field. The width of the rectangle is typically a few hundred microns in size and the sample stages move along this direction. Therefore, the scanner mirrors scan along the length of the rectangle and the sample stages move orthogonal to this. During the motion, the scanner mirrors are supplied with continuously updated pattern data so that constant patterning can take place.

Typical scanning speeds of galvanometer mirrors are of the order of a few metres per second and the sample stages move at modest speeds of ~10-20mm/sec. The typical size of a scan field is currently between 20-100mm and this means that positioning accuracies of a few microns can be obtained.

The Sync Scan approach is also finding industrial applications in the laser drilling of via holes in PCB boards where speed of processing is also a key factor and where the positions of individual via holes are fed into the system through CAD data files.

Figure 7.15 shows an example of the output of the Sync Scan system where an electrode pattern for an inter-connect package has been written into a sample plastic (for demonstration purposes only). The width of the pattern is ~95mm and individual electrodes are ~55μm in width, as shown in the inset. The use of Sync Scan in the manufacture of display devices is likely to be a major application.

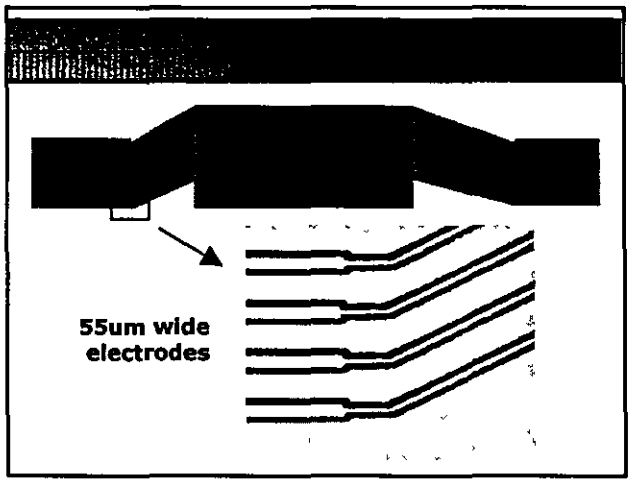

Figure 7.15. Electrical inter-connect structures for display devices patterned using direct writing with Sync Scan.

The technologies for the various types of displays planned for the next few years are all biased towards the development of larger areas, and this can impose severe limitations on their manufacture if only conventional lithography and etching techniques are to be used. The direct patterning of the various layers of the display panels is a very attractive and flexible option as it allows a variety of designs to be produced relatively easily with the same system and the size of the panels which can be processed is only limited by the size of the XY stages.

7.4 M9000S Solar cell scribing tool

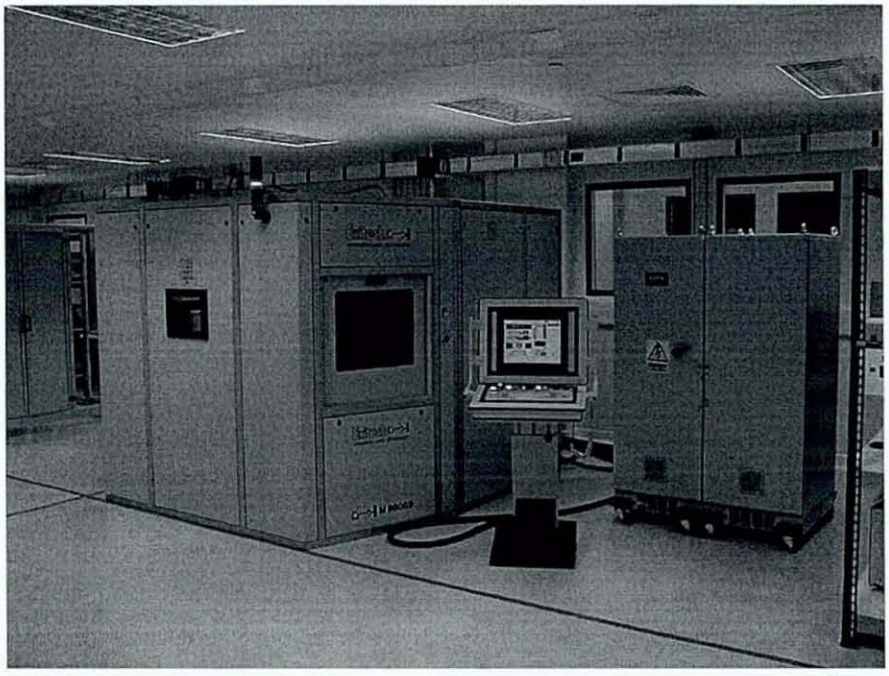

Figure 7.16 The M9000S Wafer scribing System

7.4.1 Description

The M9000S tool is designed for the high speed, high throughput processing of 6" silicon and poly silicon square and pseudo square wafers for the creation of solar cells using buried contact technology. The tool is suitable for both grooving and isolation processing. The grooving cutting is performed on the top surface of each wafer while isolation cutting is from the rear, followed by edge breaking.

The system uses a single high power high repetition rate Nd:Vanadate laser operating onto 2 wafers simultaneously. For grooving operations the beam from the laser is split into a total of 4 beams with two beams operating on each wafer. Both wafers are on chucks situated on a single set of high speed X, Y translation stages. A series of contact grooves are first cut in one direction following which the stages are moved in an orthogonal direction to create multi groove busbar structures.

Chuck loading and unloading is carried out automatically from (and to) dual cassettes of wafers using a dual arm robot. Pairs of cassettes are transferred into and out of the tool via 2 automatic turntable units.

The machines have been designed to meet the exacting requirements of multi shift production having high performance stages and highly stable optical systems. Beam power, position and profile diagnostics are integrated into the tool at appropriate locations to give the machine high levels of accuracy and reliability.

7.4.2 Scribing silicon

This machine is designed to scribe interconnect grooves into the top surface of mono crystalline Silicon solar cells [8]. The grooves are nominally 20 μm wide by 40 μm deep and the current system achieves a 650 mm per second cut speed using 8 W of diode pumped Nd:Vanadate laser power at 1064nm and 150 kHz repetition rate. Using an 8 μm diameter Gaussian focal spot this corresponds to 50 μJ per pulse, with a fluence in the region of 100 J/cm^2 at the focus. Examples of scribed groves are shown in figures 7.17.

A single 40 W laser is split into 4 separate beams using polarization splitting; two beams per wafer are then used to process two wafers simultaneously on the chuck. A fast dual arm wafer-handling robot is used to transfer wafers from the chuck to wafer cassettes. Beam profilers are integrated into the main beam lines to aid laser alignment. An In-chuck profiler is fitted to assist in the setting of beam offsets and focus, the process being sensitive to focus offsets of less than 10 μm.

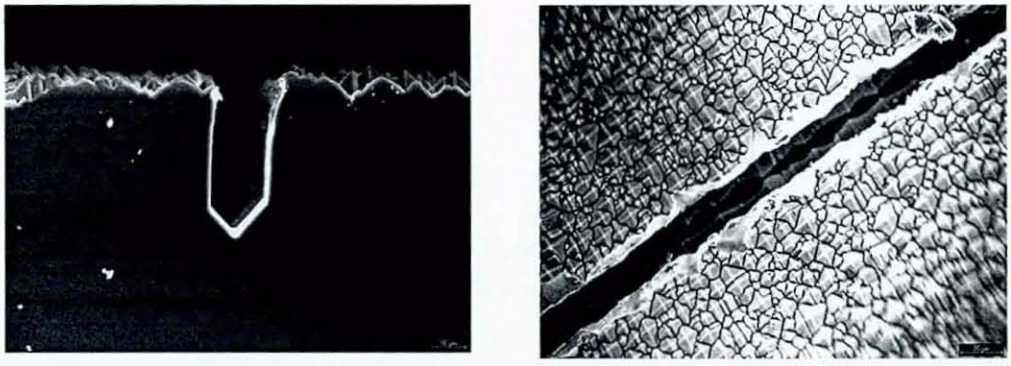

Figures 7.17 (a) & (b). 40 μm x 20 μm grooves scribed in Mono crystalline Silicon

7.4.3 Control System

The control system layout is shown in figure 7.18. The system control is via an Industrial PC running MS Windows NT4. The control system integrates motion control with machine vision and signal data acquisition. This allows single screen operation via a touch screen, fully integrated beam diagnostics and a simple user interface. The robot loader system has its own control unit that is linked via an RS232 interface to the main control PC. Beam profiling is implemented using a Matrox Orion Vision card, the same hardware as used in other systems described in this thesis. The layout of the in line beam profiling cameras is shown in figure 7.19.

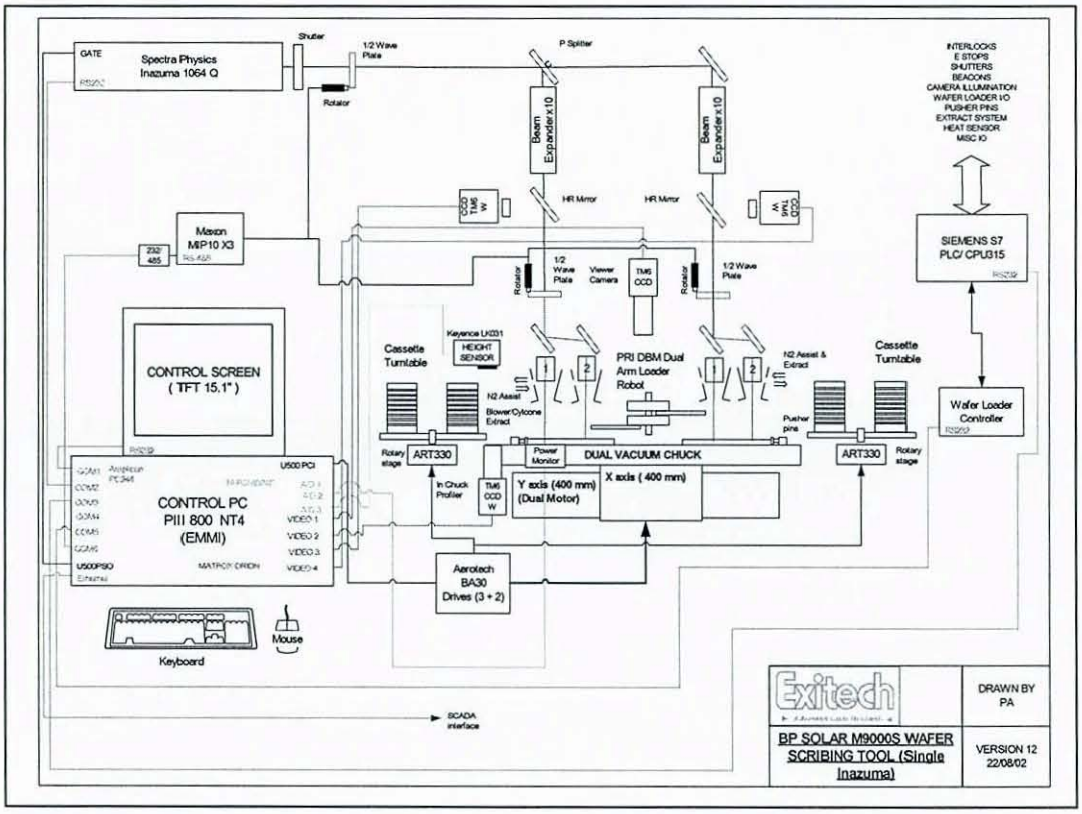

Figure 7.18. The M9000 S Control system

7.4.4 Optical system

Fig 7.20 shows the layout of the various optical components in the workstation. The beam from the laser is split into two near identical arms, using a beam splitter. The first wave plate rotator W1 is situated just before the 50 % splitter M1 (48% P Split). Beam expansion telescope T1 is situated after the splitter mirror. This telescope has variable expansion and collimation ratios, which is useful for making compensation adjustments if the laser divergence varies over time.

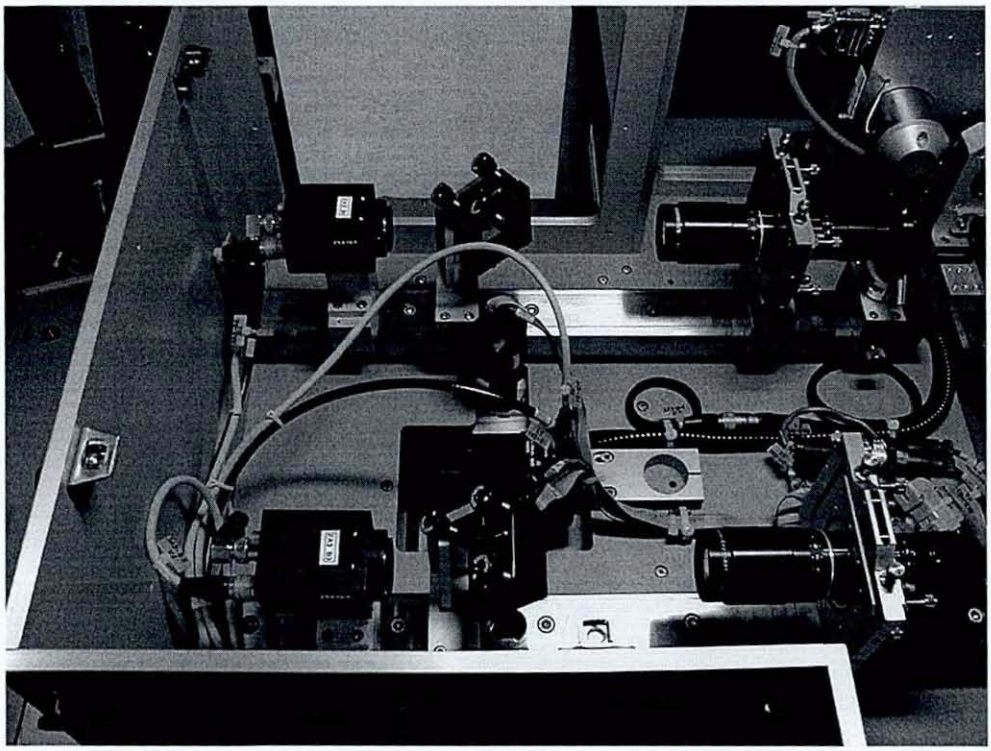

Figure 7.19. Optics box showing in line beam profiling cameras.

Beam balance is variable over a +/- 20 % range using the wave plate rotators. Mirror M3 steers the beam through the next wave plate rotator unit, and onto the final turning mirrors M4 (52% S Split) and M5 (99.9% HR), which split the beam into two again and direct it down through the focussing lenses, L1, L2 and onto the workpiece. Similarly, M2, T2, M6, M7, M8, L3 and L4 perform the same function for the left arm of the optical train. All optics are AR coated for use at 1.064um. The optics are as follows:

M1 = 45degree P splitter, 48%, with X-Y angle adjust
M2 = HR 99% S+P Mirror, with X-Y angle adjust
M4, M7 = 45 degree, S splitter, 52% with X-Y angle adjust
M3, M6 = HR 99% S+P Mirror, with X-Y angle adjust
M5, M8 = HR 99% S+P Mirror, with X-Y angle adjust

W1, W2, W3 = Half wave plates, multiple order, AR coated
T1, T2 = Beam expansion telescopes, variable zoom and collimation.
L1, L2, L3, L4 = Focussing lenses, AR, f=61mm, NA 0.19.

The internal layout of the optics within the workstation are shown in figure 7.21, all the components are mounted on precision optical rails within a sealed enclosure that can be purged with Nitrogen to avoid contamination and coating damage during prolonged operation.

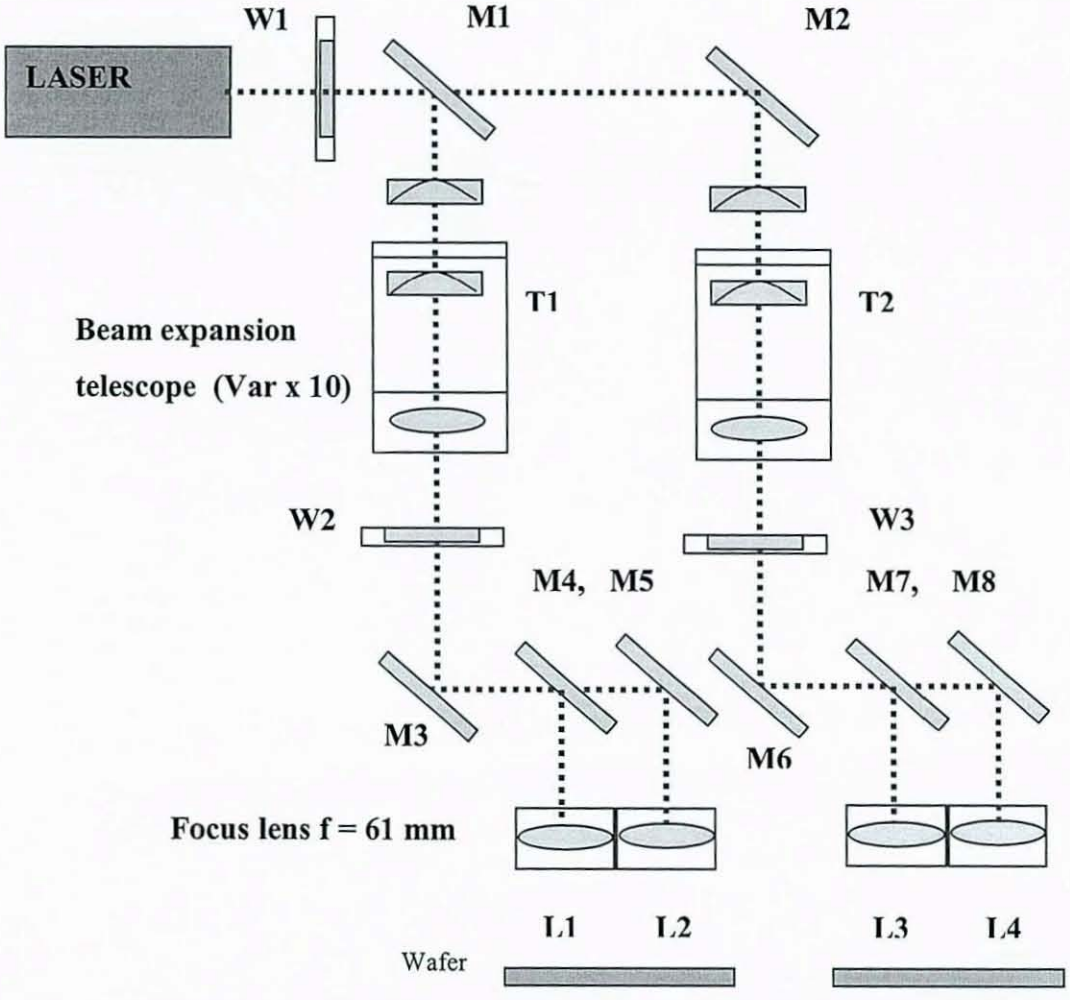

Fig 7.20. M9000S Schematic Optical layout.

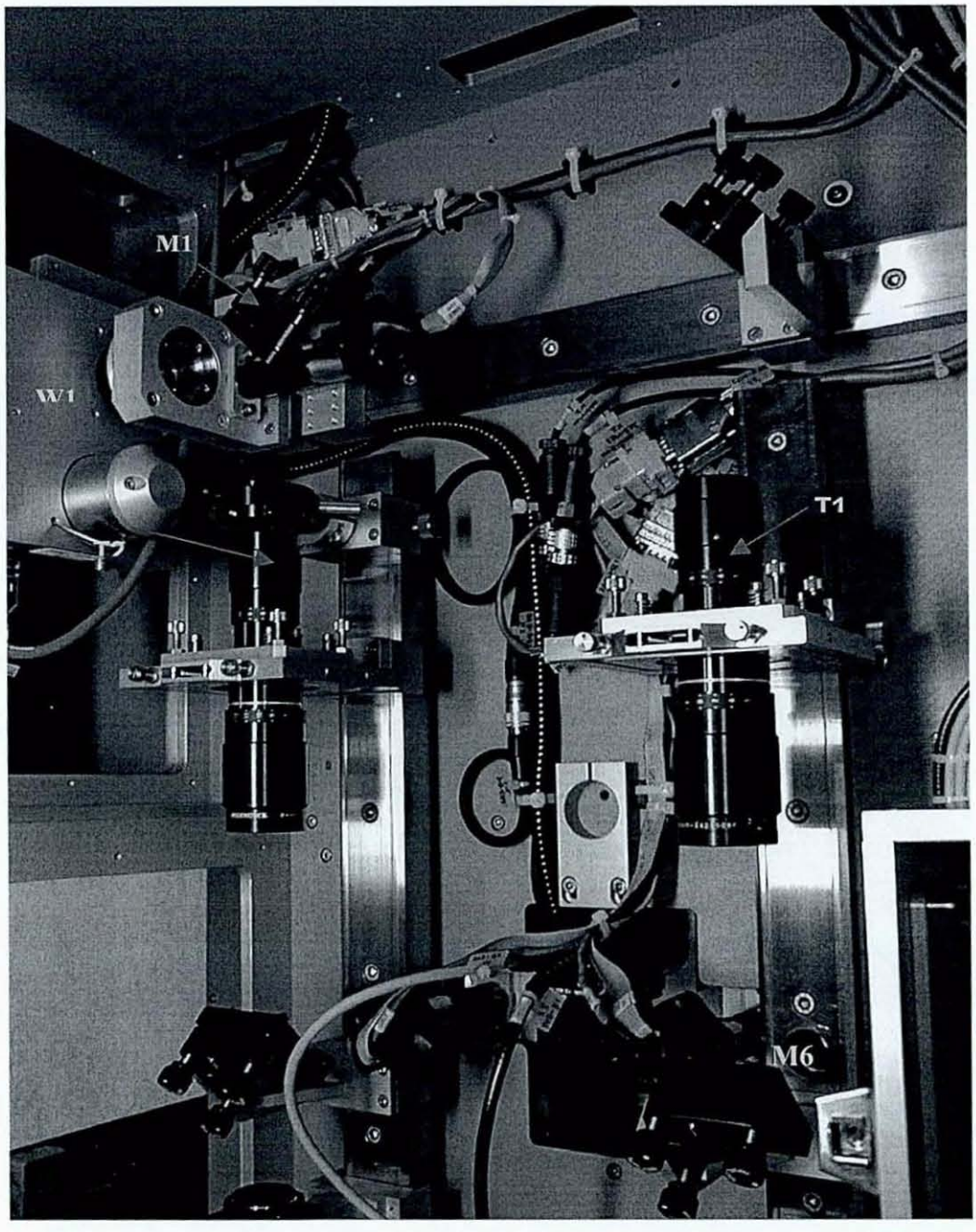

Fig 7.21 M9000S Internal optical layout

The beam expanders are made by Rodenstock and have variable beam expansion and collimation. They are fitted with 4 axis adjustable mounts. The focussing lenses are made by Linos Photonics. They are fitted with independently adjustable micrometer screws for focus adjustment.

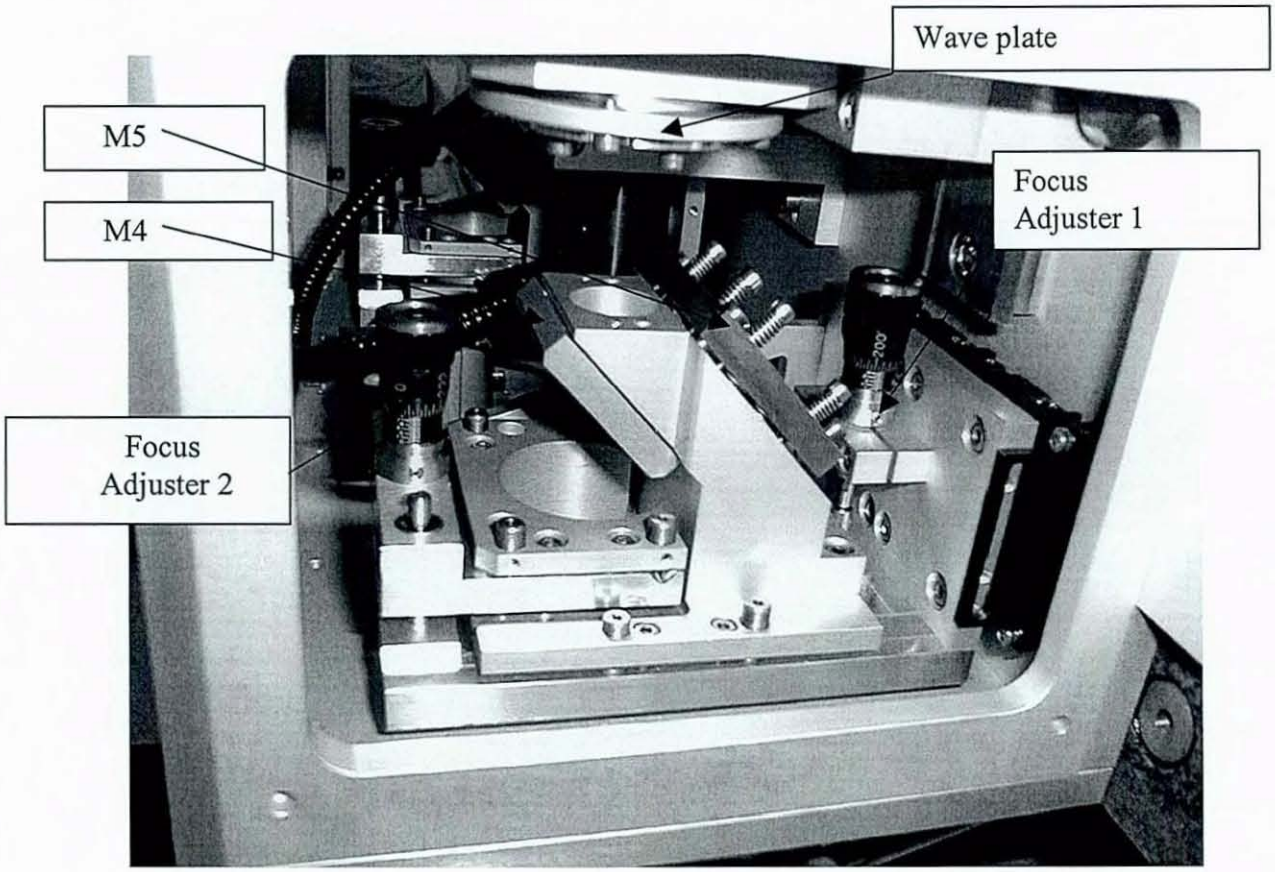

Fig 7.22 M9000S Focus adjustment

7.4.5 System Diagnostics

A Molectron power meter is mounted on the chuck to record the laser power at the workpiece, as shown in figure 7.23. This allows monitoring and setting of the correct process power and automatic beam balancing. A CCD camera and microscope are built into the chuck to form the in-chuck beam profiler, as shown in figure 7.24. This is used for setting beam offsets and finding coarse focus (to +/- 100 μm). A monochrome CCD camera is mounted in the microscope viewing optics above the chuck. This allows alignment and inspection of samples on the workpiece. The vision and profiler displays are integrated into the control touch screen. A Keyence laser diode based height sensor is fitted for chuck levelling and wafer thickness measurement

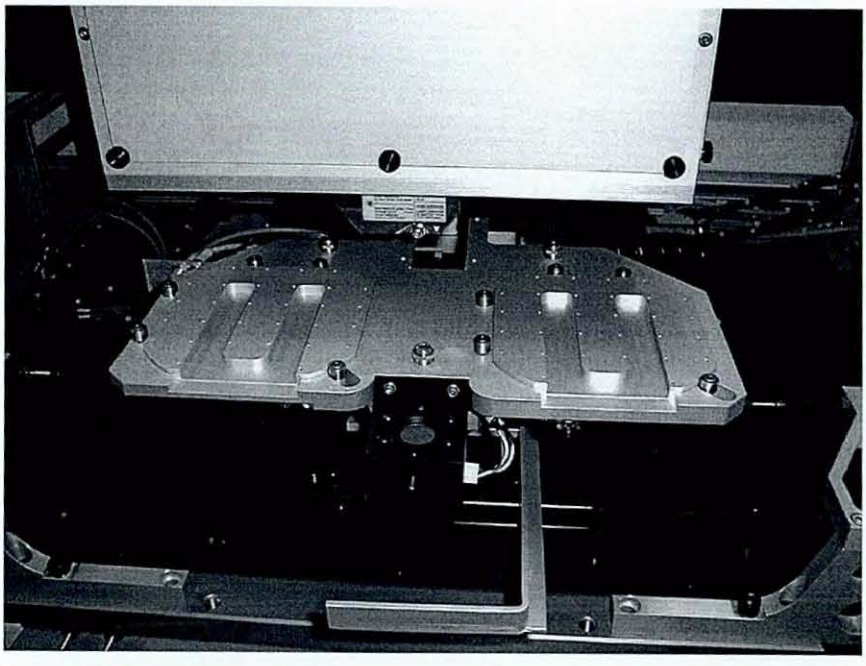

Figure 7.23. The chuck assembly showing integrated power monitor.

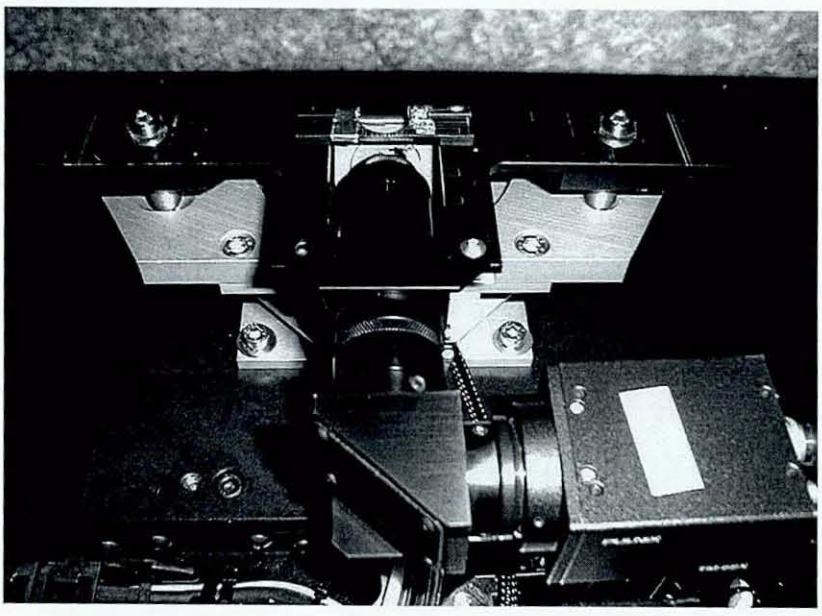

Figure 7.24. In-chuck beam profiling camera, mounted to the chuck.

7.4.6 Dust extract and assist gas

Coaxial dust extract and assist gas nozzles are integrated around the focussing lenses; this is attached to the bottom of the optics boxes. The extraction pipe is connected to the plant extraction system (> 100 m^3/Hr) and has an I/O port for a fire control sensor. The assist gas is compressed dry Nitrogen and the flow for all 4 nozzles can be set on a pneumatics panel by an adjustable flow meter (up to 28 l/min).

7.4.7.Translation stages

Figure 7.25 shows Aerotech ALS2020 (top stage X) and ALS5000W (Bottom stage Y) high-speed linear motor translation stages that are used to move the chuck assembly. These stages are capable of high accelerations (3G) and translation speeds in excess of 1 meter per second. They are forced air-cooled, to reduce thermal loading and prevent the ingression of Silicon dust.

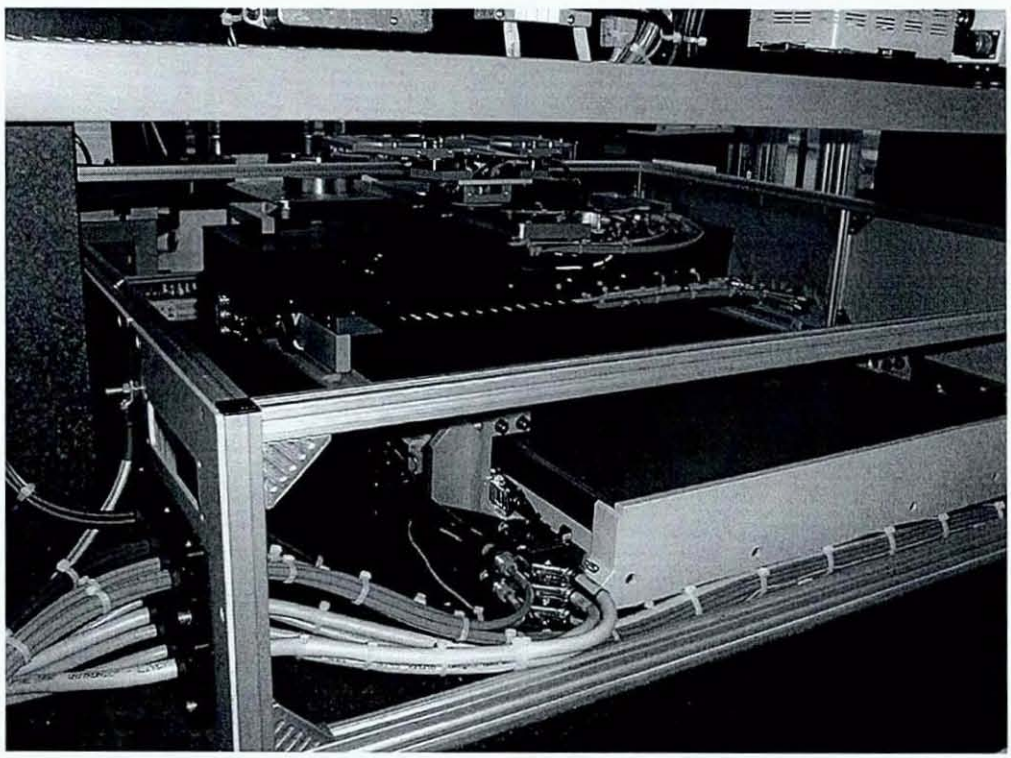

Fig 7.25. Linear XY translation stage assembly

7.4.8 Auto Loader systems

A PRI DBM 2400 Dual arm robot is used to load and place wafers on the process chuck. Custom designed end effectors are used to pick up and place both blank wafers for grooving and patterned wafers for isolation.

The loader turntables are driven by Aerotech ART 330 rotary stages. Adjustable mounts allow location of 25 or 50 wafer cassettes as required. The turntables are sealed against dust and laser light. The loader doors are locked under PLC control and interlocked to the system E Stop. Flashing buttons by the loader doors indicate that cassettes need to be changed (loaded or unloaded depending upon configuration).

Fig 7.26

Dual arm loader robot assembly

7.4.9 Process optimisation

The power in each beam can be automatically set using the power balancing system. This uses the embedded in-chuck power meter to measure the power of each of the four beams in turn and adjust the power balance using the wave plate rotators. Adjustment of the beam expanders and laser focus allows control over the scribe groove width and depth. The nominal groove parameters for this production system were 40μm deep by 20μm wide. These parameters were verified by examination under an interference microscope after the scribed wafers had been chemically etched.

7.4.10 summary

This tool has a number of new innovations that assist in reliable operation during production. It uses multi-beam optics in order to improve process throughput by scribing a single wafer with two beams simultaneously. For this to work reliably, the integration of an in-chuck beam profiler is essential to the setting of beam offsets and focus when using multi-beam optics. Other innovations include the implementation of automatic beam balancing using half wave plates and polarising beam splitters.

These machines are now being used for production and have a considerably higher throughput and reliability than previous generation Nd:Yag systems used for the same application.

7.5 Conclusions

Clearly there are many more applications for frequency converted solid-state lasers in micromachining and micro fabrication processes on an industrial scale. This is particularly true when these lasers are used with galvanometer scanners and high-speed translation tables. The machine tools described in this chapter demonstrate this well. Both tools serve practical micro fabrication applications on an industrial scale and both tools feature integrated beam diagnostics as an integral part of their design. They serve as good examples of state of the art laser processing tools and show how beam diagnostics are important to advanced manufacturing applications.

Further developments of these machine architectures continue, with even more advanced calibration and beam profiling systems. Indeed the next generations of wide screen flat panel displays could be fabricated using such machines.

7.5 References

1. M C Gower, "Industrial Applications of Pulsed Lasers to Materials Microprocessing", SPIE Conference on High-Power Laser Ablation, Santa Fe, New Mexico, Proc SPIE Vol. 3343, April (1998)

2. M C Gower, "Excimer Laser Micromachining: A 15 Year Perspective", SPIE Conference on Laser Applications in Microelectronic and Optoelectronic Manufacturing IV, San Jose, California, Proc SPIE Vol. 3618, January (1999)

3. F Dausinger, T Abeln, D Breitling, et al," Drilling of Ceramics With Short-Pulsed Solid-State Lasers", Laser Opto, 31(3), (1999)

4. A Ostendorf, K Körber, T Nether and T Temme, "Material Processing Applications for Diode Pumped Solid State Laser, Lambda Physik", Lambda Highlights May (2000)

5. H K Tönshoff, F von Alvensleben, A Ostendorf and C. Kulik, " Advanced Micro Machining with excimer Lasers", 1st International Conference and General Meeting of the European Society for precision Engineering and Nanotechnology, Bremen, Germany, Vol. 2, May (1999)

6. Scan Lab AG, Product information data sheet , SkanGine SK1010, Munich, Germany, (1999)

7. Sill Optics GmbH, Product information data sheet , Wendelstein, Germany, (1999)

8). J Perlin, "From Space to earth: The story of Solar Electricity", Harvard University press, October (2002)

CHAPTER 8

GENERAL CONCLUSIONS

Over the past 15 years there have been remarkable advances in computer and sensor technology. This has had a major impact on the development of laser beam diagnostics.

This thesis has described progress in the development of beam diagnostics from research instruments to industrial measurement tools. Improvements in computing power, algorithms, detectors and sampling optics have enhanced functionality and reduced implementation costs.

The availability of reliable, modular software and hardware has benefited systems integrators allowing the use of beam monitoring in a wider range of industrial laser applications. This has been further enhanced by the standardisation of analysis algorithms that now allow direct comparisons between lasers from different manufacturers. This in turn has lead to the improvement of laser systems reliability contributing to a wider take up within manufacturing industry. Powerful industrial computers can now implement real time image analysis for laser process control and monitoring, further enhancing process quality and repeatability.

To summarise the key conclusions of this thesis:

1). The concept of threshold beam uniformity is first introduced, a measurement now included in the ISO standard for beam profile analysis. Practical examples of its use were described, particularly in the measurement of line beam excimer laser profiles in machines used for the annealing of Silicon for LCD displays. This is now a major application for excimer lasers with the majority of compact TFT displays used in cameras and camcorders fabricated this way. All of the manufacturing systems used for this application have integrated line beam diagnostics.

2). Work has been presented that supports the ISO standards on laser beam characterisation. In general the ISO standards on beam profile measurement have been

widely accepted. The measurement of beam width is crucial to the accurate determination of beam propagation parameters and M^2 has become the standard now used by almost all laser manufacturers for specifying laser beam quality. The use of truncated moments in the measurement of the second moment beam width has been demonstrated, proving very useful for the suppression of noise in practical applications. Many of the instruments commercially available for measuring M^2 use moment truncation as a means for suppressing noise.

3). The first use of " in-chuck " beam profiling in an industrial system has been demonstrated. This technique is an invaluable aid to the alignment and calibration of laser materials processing machines for diverse applications. These devices are now in use in a number of critical applications, such as the calibration of galvanometer scanners and the alignment of multi beam optics. Indeed without these devices it would be impossible to align and service such machine architectures; as such in chuck profiling could be considered an enabling technology for these applications.

4). Descriptions have been given of two different industrial laser tools that incorporate integrated beam diagnostics. The first tool is used for the production of Fibre Bragg gratings using an excimer laser; the second tool is used for the scribing of electrical contact patterns on mono-crystalline Silicon solar cells. For both of these applications the use of integrated beam diagnostics is crucial to the reliable operation of the tool.

5). The development of a new machine architecture for micromachining applications, that combines linear stages with galvanometer scanners has been described. This new machine architecture has been the subject of several conference papers and magazine articles. Though the initial application for this machine was for the laser patterning of contact pads on LCD panels, it now has a wide range of uses for device fabrication in the microelectronics industry.

The author has developed beam analysis systems used in over 300 practical applications world wide, many of them to support new and novel processes. This includes the first use of an in-chuck profiling system for excimer lasers using a CCD camera. These have been a significant development for enhancing the performance of high precision laser processing machines.

8.1 Future outlook

Improvements in detectors are opening up some interesting new possibilities. The development of large-scale 2 dimensional pyroelectric and bolometer arrays is making accurate profiling of near and far infrared sources possible, which is of importance to the telecommunications market. The advent of low cost CMOS imaging arrays is also set to further increase the number of beam profiling applications. These devices offer high video frame rates and the possibility of making time resolved measurements in the order of ns. When coupled to the latest image acquisition hardware, these systems can process thousands of video frames per second.

The whole field laser micromachining for industrial applications looks set to grow at a considerable pace. New developments in telecommunications (fibre Bragg gratings), printed circuit boards (micro via technology) and ink jet nozzle production are driving the state of the art forward. Indeed more material could have been included on a variety of relevant topics during the preparation of this thesis.

It is pleasing that so much research and development work can be quickly transferred into real world applications, and be used in manufacturing industry worldwide. Indeed the equipment and techniques described in this thesis are already directly incorporated into machines that manufacture ink jet printer heads, CPU chips for super computers and even the marking of spectacle lenses, to name but a few. As long as mass production processes using lasers push further out the limits of speed, miniaturization and precision, the measurement and control of optical energy will remain an important topic of study.

8.2 A history of beam diagnostics development.

Table 8.1 lists the development history of the beam diagnostic systems developed by the author over a period of more than 15 years.

1984	Initial Video profiler development, using CCD cameras as part of final year project at Loughborough University for D.C.Emmony.
1987	Following on from final year project work at Loughborough and further work at the Rutherford Appleton Laboratory. PA joins Exitech Ltd to commercialise the instrument.
1988	Exhibit the world's first commercially available UV Beam analyser, the P256D at the Birmingham NEC laser show in March. Sell the first system to Japan, visit Tokyo and install the system at the Japanese atomic energy authority (NAIG) in August.
1989	Ship and install the second P256D system to Summit technology (Cambridge Mass) in February, the first ever use to characterise excimer lasers for corneal sculpting. Develop the P512 (higher resolution) using the Matrox PIP640 card.
1990	P256D production continues, develop the P256C and the EX1 CCD camera for use with visible to IR wavelengths. First sale in March to CEGB research. Develop the P1D spectrometer readout system
1991	P256C production continues. Last P256D sold in November (total 17 units). Now using UV sensitive CCD cameras. Exitech sells its first excimer laser processing tools, equipped with beam profilers.
1992	P256C production continues. Develop the P256NG using the Matrox IP8 card, first sale in October to Gillette in Berlin, used for aligning Lumonics Nd:Yag lasers on their ground breaking " Gillette Sensor" razor production line.
1993	P256NG production continues. Present paper on beam characterisation at the second LBC meeting in Madrid in July. Last P256C sold in March (total 66 units).
1994	P256NG production continues. Present paper on characterisation techniques at Berlin LBC in June. Develop Laser Sense software and

	integrate into a super computer chip repair system for Hitachi Kanagawa, the first ever fully integrated UV beam diagnostics in a commercial Laser tool. Exitech is now a world leader in manufacturing excimer laser micro machining tools.
1995	Develop the Exigrab PC card. Present a paper on ISO standards testing at SPIE Photonics West in February. Sell the first Exigrab system in June to IMEC in Belgium as part of a laser cleaning system. Develop M^2 measuring system for High power CO_2 lasers, install at GIMT in Singapore on a Trumpf laser-welding cell. Last P256NG sold in September (total 60 units).
1996	Exigrab PC card production continues. Present paper at Quebec LBOC in July on ISO standards testing; chair the session on Industrial beam diagnostics. Develop Laser Sense for Windows 95. Start work on Doctoral Thesis.
1997	Exigrab PC card production continues. Present paper at Munich LBOC in June on excimer line beam analysis. Develop a Labview beam profiler for a 193nm Lithography tool. Develop based Line beam analysis systems for Silicon annealing research using Matrox Pulsar vision cards.
1998	Last Exigrab PC system sold, (total to September 49 units). Continue development of integrated beam diagnostics using Matrox vision cards.
2002	Currently over 300 beam profiler systems in the field in over 17 countries, at least 100 of which are integrated into Laser processing systems. All Exitech Laser machines incorporate integrated Beam diagnostics and image processing. Submit Doctoral Thesis on laser beam characterisation.

Table 8.1 A history of beam diagnostics development

ACKNOWLEDGEMENTS

I would like to sincerely thank Dr Malcolm Gower and Dr Phil Rumsby for their support and permission to work on the studies described in this thesis and all my other colleagues at Exitech in particular Dr Nadeem Rizvi and Mr Bob Bann who have helped me in this work.

I would especially like to thank Professor David Emmony for his support and advice over a number of years.

Partial funding for this work was provided the European Commission, within the "Eureka programme " EU643 Laser safety in the workplace and the "Innovation Programme" (Project PURE, Patterning by UV-Laser Material Removal; Project No: IN 20668 I).

Publications and Conference presentations

1)."Characterising Beam quality for Laser Processing" P.Apte, M.Gower. P.Rumsby Proceedings of the 1st workshop on laser beam characterisation,, P.M.Mejias et al Madrid, Spain 1993.p359.

2)."Computational methods for beam Amplitude characterisation", P.Apte, M.C.Gower," Proceedings of the 2nd Workshop on laser beam characterisation, H.Weber et al eds,(FestKorper Laser Institut ,Berlin 1994),p57

3)."Experimental testing of integral truncation algorithms for the calculation of beam widths by proposed ISO standard methods". P.Apte,M.C.Gower SPIE Vol 2375,pg349,(1995).

4).".The Practical implementation of Test methods for the characterisation of Laser Beam Power and Energy density Distribution". P.Apte,M.C.Gower Proceedings of the 3rd Workshop on laser beam characterisation. Quebec city 1995.

5)."The measurement and characterisation of high aspect ratio line focus beam profiles for excimer laser applications" P.Apte, M.Gower. P.Rumsby. Proceedings of the 4th Workshop on laser beam characterisation. Munich 1997.

6)."Flexible Processing of Large Scale LCD Panels Using Scanner Deflected UV-Laser Radiation. ". A. Ostendorf et al. P.Apte et al . SPIE Vol 2375,pg349,(2000).

7)."Developments in Laser Micromachining Techniques" N.H. Rizvi , P.Apte Proceedings of the ICOPE conference , Singapore 2000.